Master's thesis

NTNU
Norwegian University of Science and Technology
Faculty of Natural Sciences
Department of Materials Science and Engineering

Lina Munkhaugen

The Effect of FEC and Water on NMC Cathodes for Li ion Batteries with LiFSI based Electrolytes

Master's thesis in Materials Chemistry and Energy Technology
Supervisor: Ann Mari Svensson
Co-supervisor: Camilla Lian

June 2022

NTNU
Norwegian University of
Science and Technology

Lina Munkhaugen

The Effect of FEC and Water on NMC Cathodes for Li ion Batteries with LiFSI based Electrolytes

Master's thesis in Materials Chemistry and Energy Technology
Supervisor: Ann Mari Svensson
Co-supervisor: Camilla Lian
June 2022

Norwegian University of Science and Technology
Faculty of Natural Sciences
Department of Materials Science and Engineering

NTNU
Norwegian University of
Science and Technology

Preface

This Master's thesis is a result of the subject TMT4900 - Material Chemistry and Energy Technology, Master's Thesis. The work related to the thesis was carried out at the Department of Material Science and Technology. The thesis builds on the project thesis "Stability of High Energy NMC Cathodes for Li-ion Batteries with LiFSI based Electrolytes", completed fall of 2021 by the same author. Parts of the theory and experimental sections of this project were used as the basis of this thesis, however the parts are extensively rewritten and extended. Both the project thesis and master thesis are affiliated with the NorGigaBatFact project with several industry partners including Freyr, Beyonder, Hydro, Equinor, Norsink and Nordic Mining.

I would like to express gratitude to my supervisor Ann Mari Svensson for valuable and readily available guidance and informative input from start to finish. Further, I would like to thank my co-supervisor Camilla Lian for training in the manufacture of pouch cells in addition to always being available for questions. In addition, I would like to express my gratitude to Philipp Schweigart for guidance in electrolyte preparation. I would also like to thank Johannes Ofstad for the training in the FTIR instruments, as well as Sergey Khromov for the training and valuable guidance in the GDOES instrument and analysis. Lastly, I would like to thank the entire battery group at NTNU for all your help with various lab techniques and valuable feedback on my results at our weekly meetings throughout the semester. The Research Council of Norway is acknowledged for the support to the Norwegian Micro- and Nano-Fabrication Facility, NorFab, project number 295864, for access and training in Scanning Electron Microscopy imaging and Energy-Dispersive X-ray analysis.

Lina Munkhaugen
Trondheim, 09.06.2022

Abstract

Lithium ion batteries are the current dominating battery technology, due to their superior energy density. The increasing demand for better and more efficient energy storage for portable electronics and electric vehicles not only requires increased performance, but also enhancements in safety and reduced flammability. Replacing the current market leader electrolyte, lithium hexafluorophosphate ($LiPF_6$), with lithium bis(fluorosulfonyl)imide (LiFSI) based electrolytes, improves the thermal stability, moisture sensitivity and overall safety of the batteries. However, the solute substitution causes new problems concerning corrosion of the aluminium current collector on the cathodes. This thesis investigates two additives, fluoroethylene carbonate (FEC) and water (H_2O), to see if these could alleviate this corrosion problem while still retaining the cell performance and cycling stability for $LiNi_{0.3}Co_{0.3}Mn_{0.3}O_2$ (NMC) cathodes. Cyclic voltammetry on aluminium and galvanostatic cycling on NMC_{111} cathodes were conducted, with four different LiFSI electrolyte compositions. Followed by several characterisation methods such as scanning electron microscopy (SEM) imaging, energy dispersive x-ray (EDX) analysis, glow discharge optical emission spectroscopy (GDOES) and Fourier transform infrared (FTIR) spectroscopy to analyse the aluminium and cathode surfaces and their respective compositions. The analysis shows that both FEC and water repress the oxidative currents on the aluminium current collector, both separately and combined. From the cyclic voltammetry, it is observed that the addition of FEC represses the corrosion further than the water, especially at higher potentials. The surface morphology observed from SEM shows that FEC causes thicker surface layers than the water, but that the combined additives result in the most evenly distributed passivating layer. No large distinction in surface layer composition can be observed, only a higher content of the elements for the FEC containing electrolytes. The galvanostatic cycling of the NMC cathodes shows that FEC degrades the cell performance and cycling stability, this is not observed for the water containing electrolytes. For the combined electrolyte superior discharge capacities are observed, however poor coulombic efficiencies and poor cycle stability are still observed. The surfaces of the cathodes show no large differences in surface composition and appearance. From this analysis, it can be concluded that the addition of

10 wt% of FEC results in poor cell performance, but combining it with 1000 ppm of water increases the poor cell performance. However, poor coulombic efficiencies, poor cycling stability and leak currents can still be observed. This leads to the suggestion that further work should focus on optimising the FEC content together with the 1000 ppm of H_2O, by investigating if a lower FEC content could cause an increase in the beneficial performance of the Li ion batteries.

Sammendrag

Litium ion batterier er den nåværende dominerende batteriteknologien på grunn av deres overlegne energitetthet. Den økende etterspørselen etter bedre og mer effektiv energilagring for bærbar elektronikk og elektriske kjøretøy krever ikke bare økt ytelse, men også forbedringer i sikkerhet og redusert brennbarhet. Ved å erstatte den nåværende markedsledende elektrolytten, litiumheksafluorfosfat ($LiPF_6$), med litiumbis(fluorsulfonyl)imid (LiFSI)-baserte elektrolytter, forbedres den termiske stabiliteten, fuktighetsfølsomheten og sikkerheten til batteriene. Imidlertid forårsaker substitusjonen av saltet nye problemer angående korrosjon av aluminiums strømkollektoren på katodene. Denne oppgaven undersøker to tilsetningsstoffer, fluoretylenkarbonat (FEC) og vann (H_2O), for å se om disse kan lindre korrosjonsproblemet samtidig som de beholder celleytelsen og sykling stabiliteten for $LiNi_{0.3}Co_{0.3}Mn_{0.3}O_2$ (NMC) katoder. Syklisk voltammetri på aluminium og galvanostatisk syknling på NMC_{111} katoder ble utført med fire forskjellige LiFSI elektrolytt sammensetninger. Etterfulgt av flere karakteriseringsmetoder som elektronmikroskopi (SEM), energidispersiv spektroskopi (EDX), optisk emisjonsspektroskopi (GDOES) og infrarød spektroskopi (FTIR) for å analysere aluminium- og katodeoverflatene og deres komposisjon. Analysen viser at både FEC og vann demper de oksidative strømmene på aluminiumsstrømkollektoren, både separat og kombinert. Fra den sykliske voltammetrien er det observert at tilsetning av FEC demper korrosjonen mer enn vann, spesielt ved høye potensialer. Overflatemorfologien observert fra SEM viser at FEC gir tykkere overflatelag enn vann, men at å kombinere tilsetningsstoffene gir det mest jevnt fordelte passiverende laget. Ingen store forskjeller i overflatelagsammensetning kan observeres, kun et høyere innhold av de ulike elementene for prøvene syklet i den FEC-holdige elektrolyttene. Den galvanostatiske syklusen til NMC katodene viser at FEC degraderer celleytelsen og syklusstabiliteten, dette observeres ikke for de vannholdige elektrolyttene. For den kombinerte elektrolytten observeres overlegne utladningskapasiteter, men dårlige coulombiske effektiviteter og dårlig syklusstabilitet er fortsatt et problem. Overflatene på katodene viser ingen store forskjeller i overflatesammensetning og utseende. Fra denne analysen kan det konkluderes med at tilsetning av 10 vekt% FEC resulterer i dårlig celleytelse, men å kombinere det med 1000 ppm

vann forbedrer celleytelsen. Imidlertid kan dårlige coulombiske effektiviteter, dårlig syklusstabilitet og lekkasjestrømmer fortsatt observeres i batteriene. Dette fører til forslaget om at videre arbeid bør fokusere på å optimalisere FEC-innholdet sammen med 1000 ppm av H_2O, ved å undersøke om et lavere FEC-innhold kan føre til en økning i den fordelaktige ytelsen til litium ion batteriene.

Contents

Chapter 1

Introduction

As technology is developing and leading to larger energy consumption, the demand for more effective energy sources is increasing. The global climate crisis the world is facing demands a more renewable solution to replace the fossil solutions used today. To allow effective utilisation of today's state of the art renewable energy sources, devices that can store and effectively release the energy that these sources capture are highly necessary.

Today's market leader within battery technology, Li ion batteries, outperforms other technologies due to their superior energy density [1]. However, to meet the increasing demand for energy storage for portable electronics and electric vehicles advancements are necessary. Rechargeable Li ion batteries are currently one of the most researched power sources, searching for solutions to improve the volumetric energy density, cyclability, stability and safety [2, 3]. Currently, the main obstacle to increasing the performance lies at the cathode component. Since the anodes have much higher capacity and thereby outperform their positive counterpart [4]. This predicament establishes the need for more research to be put into promoting the properties of the cathode. This cannot be done by only focusing on the cathode itself, but also by examining the impact other components have on the cathode performance. The most relevant field to further research into is the electrolyte and its components, including the solvent, solute and possible additives.

In the current state of the art batteries, the electrolyte is based on lithium hexafluorophosphate, $LiPF_6$, salt. The main drawback with these electrolytes is that they are

thermally unstable and sensitive to moisture [5]. The latter leading to HF formation, which is detrimental in terms of safety as it makes the batteries highly flammable [3]. Consequently, a substantial amount of research has been put into finding a replacement. Salts that have attracted attention recently are lithium imides, these contain anions with a large electron-withdrawing force which is beneficial for the electrolyte performance [6]. One prosperous candidate is lithium bis(fluorosulfonyl)imide, LiFSI. The salt results in higher solubility and better thermal stability than the current $LiPF_6$ electrolytes [7]. Still, some obstacles have to be alleviated for LiFSI to work as a realistic substitution. The decrease of HF in the battery, which is positive with regards to safety, leads to corrosion issues inside the cell. The HF created from $LiPF_6$ reacts with the Al current collector on the back of the cathode, creating a passivating layer that prevents corrosion at higher voltages. Since the LiFSI electrolyte only contains trace amount of HF, this passivating layer is not formed causing the current collector to corrode during operations above 4 V [8, 9].

The great opportunities the properties of this salt provides gives rise to research on other possibilities to alleviate the corrosion occurring. This thesis focuses on the effect that the fluoroethylene carbonate, FEC, additive has on the cathode component in LiFSI based electrolytes. Its effect on the anode is widely researched and has shown to have a positive effect on cycling performance, by increasing the stability and conductivity of the SEI layer [10]. Its effect on the cathode, especially NMC cathodes, has been far less researched [11]. For this reason, it is of interest to further investigate this, as all components are influential on the battery performance. In addition, water can also be treated as an additive. Batteries are currently manufactured in very dry environments, which is very costly and energy demanding. Further investigating the effects small additions of water have on the battery performance could help alleviate the large energy demands, if the negative effects are reasonable.

Aim of Work

This master thesis aims to investigate the effect fluoroethylene carbonate, FEC, has as an additive on NMC_{111} cathodes in electrolytes based on LiFSI salt. This was examined by electrochemically testing pouch cells using galvanostatic cycling, in electrolytes both with and without FEC, to study if the additive had an impact on the cycling stability. In addition to NMC_{111} cathodes, cells with Al foil replacing the cathode were also tested with cyclic voltammetry to closer inspect the corrosion on the aluminium current collector. In addition, the effect of water was also analysed. Both the NMC_{111} cathodes and Al foil were tested with water containing electrolytes, both with and without FEC. The water is added to investigate the possibility of cell manufacture in a less dry atmosphere, as this would reduce both the energy demand and the cost of the battery production. After electrochemical testing, the surfaces of the cathodes and Al foil were characterised using a variety of different methods. The cathodes were analysed using both SEM imaging and EDX analysis. While the Al foils were, in addition to the SEM imaging, analysed using GDOES and FTIR analysis for a wider elemental analysis of the surface composition.

Chapter 2

Literature Review

2.1 Fundamentals of Li-ion Batteries

2.1.1 Working Principle

Lithium ion batteries are electrochemical devices that convert stored chemical energy into electrical energy. The batteries are rechargeable, meaning that by applying electrical energy the chemical reactions reverse and charge the battery. Consisting of two electrodes, a cathode and an anode, the batteries charges and discharges their energy by passing Li ions and electrons between these electrodes. The electrons, which create the electrical energy, are pushed through an external circuit due to the electrolyte in which the components are soaked in. The electrolyte has high ionic conductivity allowing ions to migrate between the electrodes, but a low electronic conductivity. Therefore, the electrons are not able to move through the electrolyte but are instead forced through an external circuit which allows for the extraction of electrical energy. The separator is soaked in an electrolyte and placed between the electrodes to prevent physical contact, as this would cause the battery to short circuit [12]. However, the separator still has to allow the ions to pass through as they migrate between the electrodes. Therefore its important that the separator is compatible with the electrolyte so that the electrolyte can completely wet the separator ensuring ionic contact between the electrodes [13]. Lastly, current collectors are attached to each electrode, Cu to the anode and Al to the cathode, to provide the electrical contact between the external source and the active materials in the battery. The structure of the Li ion batteries is shown in Figure 2.1, which also illustrates the fundamental

principle of the moving charges inside the battery. The illustration is inspired by Goodenough and Park's illustration [14].

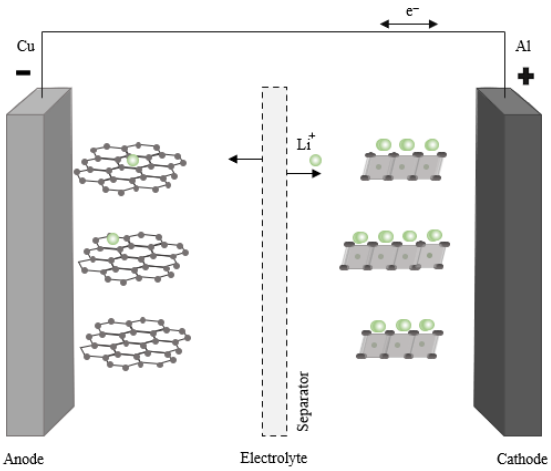

Figure 2.1: Illustration of a Li ion battery showing the movement and intercalaction of lithium between the anode and cathode during charge and discharge. The electrodes are separated by the electrolyte and the separator, with an external circuit connecting the anode and the cathode [14].

How the Li ions are stored in the electrodes depends on the type of electrode. There are three ways of classifying electrodes depending on the storage mechanism: intercalation electrodes, alloying electrodes and conversion electrodes [3]. These mechanisms are further explained in Section 2.1.3.

The most common anode material is graphite, which is classified as an intercalation electrode. The cathode is usually some category of lithium metal oxide, these are also commonly intercalation electrodes. During charge, an external voltage is applied to the batteries. This allows the cathode to be oxidised according to Reaction 2.1, where M is one or several transitional metals.

$$\mathrm{LiMO_2} \underset{\text{discharge}}{\overset{\text{charge}}{\rightleftharpoons}} \mathrm{Li_{1-x}MO_2} + \mathrm{xLi^+} + \mathrm{xe^-} \tag{2.1}$$

The Li ions released from this oxidation reaction migrate through the electrolyte

towards the anode, where they eventually intercalate into the structure. The reaction also generates free electrons which, due to the electronically insulating properties of the electrolyte, pass through the external circuit generating an electrical current. The intercalation of Li ions into the layers of the anode material follows Reaction 2.2.

$$\mathrm{xLi^+ + xe^- + 6\,C} \underset{\text{discharge}}{\overset{\text{charge}}{\rightleftharpoons}} \mathrm{Li}_x\mathrm{C}_6 \tag{2.2}$$

The process of incorporating the Li ions into the electrode structure is called lithiation, while the removal of Li ions is called delithiation. The lithiation of anodes increases the electrochemical potential while it decreases during delithiation. It is this difference in potential that is used to perform the work of moving the electron through the external circuit, generating the electrical current. The lithium ion batteries are secondary batteries, meaning they are rechargeable. This is because of the electrodes' ability to be both reduced and oxidised depending on if they are in a charged or discharged state. By definition, the cathode is reduced during the discharge of the batteries, while the anode is oxidised. During charge the electrodes switch, meaning the cathode is oxidised while the anode is reduced [12]. Despite the electrodes switching roles, the denomination of the electrodes stays consistent.

2.1.2 Parameters and Terminology

The *open circuit potential* ,V_{OC}, of a battery is defined as the difference in the electrochemical potential between the cathode and the anode when no current is drawn. The potential can be determined by Equation 2.3 [12].

$$V_{OC} = -\frac{1}{nF}(\mu^i_{anode} - \mu^i_{cathode}) \tag{2.3}$$

$\mu^i_{cathode}$ and μ^i_{anode} are the electrochemical potentials of the cathode and anode, respectively. The number of electrons participating in the electrochemical reaction, n, and Faradays constant, F, are also factors included in the equation.

In batteries the *c-rate* relates to the time it takes to completely charge or discharge the cell, i.e. it states the discharge current relative to its maximum capacity [12]. By

definition, a c-rate of nC completes a full charge or discharge in $1/n$ hours.

The *capacity*, Q, is defined as the amount of charge that can be stored in a battery. It depends on the current, I, and the time, t, it takes to pass as can be seen by Equation 2.4. .

$$Q = \int_0^{\Delta t} I dt \tag{2.4}$$

The *irreversible capacity losses*, ICL, that happens during the cycling of batteries leads to a reduction of the cell voltage during discharge, and an increase during charge. This loss is a result of reaction between the electrodes and electrolyte, volume changes in the electrodes and electrode decomposition [14].

In batteries the *coulombic efficiency*, CE, is commonly used to describe battery performance. The parameter is defined as the ratio between the capacities at the charge and discharge step at each cycle, as stated in 2.5 [12].

$$CE = \frac{Q_{discharge}}{Q_{charge}} \cdot 100\% \tag{2.5}$$

In batteries as much *energy* as possible should be stored. The available energy in a battery, in Wh, can be found by Equation 2.6.

$$energy = \int_0^{Q} V(q) dq \tag{2.6}$$

Where V(q) is the potential of the battery at a certain state of charge. The *energy density* in batteries states how much energy that a battery can store per unit of mass or volume. These are denoted as gravimetric energy density (Wh kg^{-1}) or volumetric energy density (Wh L^{-1}), respectively [14].

Cyclability of batteries is defined as the number of times a battery can be charged and discharged without large energy losses. This indicates the reversibility of the Li ion insertion and extraction in the electrodes [3].

2.1.3 Li ion Storage Mechanisms

The three mechanisms for storing Li ions in the electrodes of a Li ion battery are as previously mentioned are intercalation, alloying or conversion.

Electrodes that use the intercalation mechanism store Li ions in between the layers of its structure [12]. The mechanism follows Reaction 2.7, with a layered Li oxide as an example [3].

$$MO_x + yLi^+ + ye^- \longleftrightarrow Li_yMO_x \tag{2.7}$$

As mentioned, graphite is among the most common intercalation electrodes. Graphite incorporates one Li ion per six carbon atoms, resulting in a reversible capacity of 372 mAh g^{-1} [15].

The alloying mechanism utilises the following reaction mechanism to store Li ions, described in Reaction 2.8 [3].

$$M + zLi^+ + ze^- \longleftrightarrow Li_zM \tag{2.8}$$

The mechanism causes large volumetric expansion of the electrode which leads to a capacity fade as the battery cycles [3].

The last mechanism, conversion, stores the Li ions according to the mechanism described in Reaction 2.9 [3].

$$M_xO_y + 2\,yLi^+ + 2\,ye^- \longleftrightarrow xM + yLi_2O \tag{2.9}$$

This mechanism is typically seen for transitional metal oxide electrodes. Due to its ability to incorporate several Li ions for each transitional metal cation, the mechanism usually provides high theoretical capacities [3]. However, a problem with this mechanism is that it can cause sloped voltage resulting in poorer energy density. In addition, the formation of the alloys can cause large volume changes and cause cracking of the material during cycling [12].

2.2 Electrode Materials

Electrodes are the components which Li ions migrate between when a battery charges and discharges. During charge, Li ions are extracted from the cathode structure, migrate and intercalate into the anode structure, and oppositely during discharge [16]. Several materials have been tested for both the anode and the cathode, but still new and better possibilities are being explored. Materials that provide higher energy densities, longer cycle life, are cheaper and have higher safety are highly desirable [13]. To develop such materials a broad understanding of how the material properties influence the battery performance is required. As many factors influence the performance of the battery, finding the optimal solutions often leads to compromising some of the performance requirements.

An overview of several of the anode and cathode materials tested for Li ion batteries with their respective capacities and voltage is shown in Figure 2.2, adapted from Osiak et al. [16].

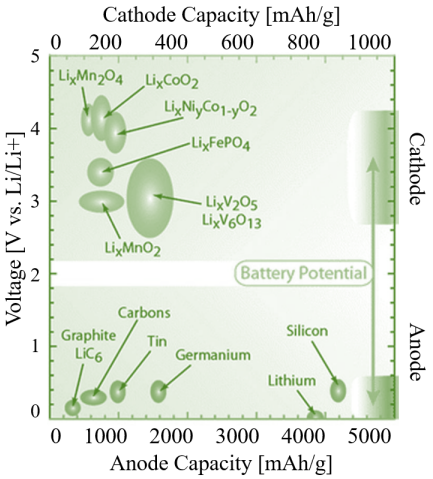

Figure 2.2: Illustration of different materials tested as anode and cathode materials for Li ion batteries, with their respective theoretical capacities and electrochemical reduction potentials vs Li/Li^+ [16].

2.2.1 Anode

Though anodes are not the focus of this thesis some key properties should be discussed as their compatibility with the cathode and electrolyte is crucial for optimal battery performance. Anodes are the Li ion receivers during charge. In addition to storing Li ions, several other properties are important for anode materials. To be eligible as an ideal anode material the following requirements, inspired by Julien et al. [12], should be met:

1. The material should store large amounts of Li ions per weight to enhance the gravimetric capacity.
2. The material should have a low redox potential with respect to Li/Li^+ to allow a high cell voltage.
3. The material should have good electronic and ionic conductivity allowing faster movement of Li ions and thereby higher power density.
4. The material should be inert in terms of contact with solvents and lithium salt in the electrolyte.
5. The material should be safe, light, cheap and environmentally favourable.

An example of an anode material that fulfils a substantial amount of these requirements is graphite. Graphite is one of the most used anode materials in conventional Li ion batteries. They classify as intercalation electrodes, meaning that during the charging the lithium ions intercalate between the graphite layers, forming LiC_6. In secondary batteries the graphite anodes cycle between C and LiC_6, for discharge and charge respectively. This reaction leads to a theoretical capacity of 372 mAh g^{-1} for the graphite anodes. This capacity is adequate for the current state of the art batteries, as cathode materials are currently the limiting component in terms of capacity [12].

Recently another material has gained attention for its suitable anode properties, silicon. The material is an abundant element, which is beneficial in terms of keeping the cost low. Silicon anodes are classified as alloying electrodes, these typically have very high capacities. The theoretical capacity of silicon anodes is 4200 mAh g^{-1}, which

is very high compared to graphite [12]. With regards to the requirements of ideal anode materials, silicon has some drawbacks. The main problem is the materials' large volume change during cycling, which is detrimental to the battery performance as it causes large capacity losses during cycling [17].

2.2.2 Cathode

Cathodes are the source of lithium ions in Li ion batteries. Over the years, extensive research has been put into finding better cathode materials, as it currently is the limiting electrode. This is due to the materials' low theoretical capacity compared to the currently used anode materials [4]. Finding an ideal cathode material has proven to be challenging, as there are many factors influencing the performance. To be eligible as an ideal cathode material the following requirements, inspired by Whittingham [18], should be met:

1. The material should have a high oxidation potential with regards to Li/Li^+.
2. The material should have a good electronic and ionic conductivity.
3. The material should reversibly react with lithium, allowing for large amounts of lithium to be inserted/extracted without changing the structure of the material.
4. The material should, in a reaction with lithium, have a high free energy of reaction since this gives rise to high capacity, high voltage and high energy storage.
5. The material should rapidly insert/extract lithium, giving rise to high power density.
6. The material should be chemically stable, cheap and environmentally favourable.

As mentioned, finding materials that fulfil all of these requirements is challenging. Currently, the most common cathode materials are metal oxides. These either have a layered or a spinel structure [16]. The layered cathode materials have a more compact structure than the spinel materials. The higher density in the structure gives the

material higher capacity per volume, which is desirable as the cathode component can be made smaller [18].

Of the layered structures the transition metal oxides, LiM_xO_y with M being one or several transition metals, are great candidates as cathode materials. A common transition metal oxide is $LiCoO_2$, which has previously been the dominating cathode material for Li ion batteries [19]. Several capacity intervals have been listed for the theoretical capacity of these electrodes, such as 135-150 to 120-140 mAh g^{-1} [19, 20]. Though the material possesses remarkable properties including high thermal stability and high capacity, the material also faces some issues [21] . The cobalt content gives rise to ethical issues in addition to toxicity and structural stability in the batteries. The material also suffers from rather large volume changes during cycling [20].

Another transitional metal oxide used in Li ion batteries is $LiNiO_2$. The material shows a theoretical capacity 274 mAh g^{-1} [19], which is higher compared to $LiCoO_2$. In addition to a higher theoretical capacity, the material does not contain Co, reliving the toxicity and ethical issues tied to cobalt. However, the material is not extensively used. This is due to the high nickel content of the electrode, which prevents the flow of Li ions between its layers and diminishes its electrochemical properties [19, 22].

2.2.3 NMC Cathodes

A cathode material showing great potential is NMC, short for $LiNi_xCo_yMn_zO_2$. The material is a solid solution of the transitional metal oxides $LiCoO_2$, $LiNiO_2$ and $LiMnO_2$ and was first synthesised by Liu, Yu and Lee in 1999 [12, 23]. The material has been extensively researched in hopes of producing a material with enhanced thermal and structural stability as well as an increased capacity [12]. NMC can be synthesised with different compositions depending on the Ni, Co and Mn content. The different compositions are often written as NMC_{xyz}, where x,y,z subsequently indicates the Ni, Co and Mn content. Some of the more common compositions are NMC_{442}, NMC_{622} and NMC_{333}, the latter often also denoted as NMC_{111}.

Research shows that NMC_{111} has a rechargeable capacity of more than 200 mAh g^{-1} when operated between 2.5 - 4.6 V. The material displays great capacity retention,

in addition to preserving its coulombic efficiency during cycling [20]. The material also displays little to no volume expansion during charging, contradictory to the previously mentioned $LiCoO_2$. Initially, the $LiCoO_2$ has a smaller lattice, but due to this volume change the material reaches a lattice volume equivalent to that of the NMC_{111}. Causing the gravimetric and volumetric densities of the NMC_{111} to be equal or greater than the $LiCoO_2$ [20]. From the same study by Yabuuchi and Ohzuku, it was also reported that the thermal stability is better for NMC_{111} than for both the $LiNiO_2$ and $LiCoO_2$. In summary the NMC_{111} performs as good, or even better than $LiNiO_2$ and $LiCoO_2$ [20].

In a study by Li et al., various composition of NMC, $LiNi_yMn_yCo_{1-2y}O_2$, is researched to find the optimum composition. NMC_{442} obtained the highest theoretical capacity while keeping the Co content low and retaining its rate capabilities and capacity to a level comparable to NMC_{111} material [21]. The study by Li et al. also found that the open circuit potential for NMC_{111} was higher than NMC_{442} and NMC_{992} when more than 55 % of the Li was extracted from the cathode. The increase in voltage lead to a slightly lower capacity for the NMC_{111} compared to the NMC_{442} and NMC_{992} when the materials were charged above 4 V [21].

When NMC was first synthesised by Liu et al., it was concluded that the Mn doping needs to be kept moderate for the material to show good capacity values and long cycle life [23]. In terms of cobalt content, increasing content increases the rate performance [21]. As previously mentioned, it's desired to keep the Co content low due to toxicity and ethical issues, but removing it completely is still unattainable. This can be seen from the research done on NMC_{550}, where the absence of Co leads to problems with a slow charging rate [21]. The nickel content is of importance as the specific capacity of the NMC cathodes increases with increasing nickel content, as can be observed from the increase to 190-200 mAh g^{-1} for NMC_{811} from 160 mAh g^{-1} for NMC_{442} [24]. Conversely, the higher nickel content also decreases the thermal stability of the material. This decrease is a consequence of the phase transitions happening when a notable amount of the nickel ions are reduced and oxygen is released [25]. The impaired thermal stability increases the probability of thermal runaway and may cause the battery to ignite [26]. Measures to improve the thermal stability by the

addition of Mg or Zr dopants to the structure have been successful, though it reduces the capacity to some extent [27].

2.3 Electrolyte

The role of the electrolyte is to conduct the migration of the Li ions between the electrodes. This task is of major importance as the mobility of the ions determines the rate of the electrochemical reactions and hence the power output of the battery [11, 28]. In addition, the lifetime of the electrodes and overall cell is dependent on the electrolyte and its components [29]. There are several classes of electrolytes; aqueous, nonaqueous, ionic liquid and solid [11]. Nonaqueous electrolytes are currently dominating the Li ion battery market and are also the focus of this thesis. Nonaqueous electrolytes can be divided into two main components, the solute and its solvent. The solute is a salt, while the solvent is one or possibly several nonaqueous liquids, often carbonate based [28]. Other components can also be added to the solution to achieve desired properties, these are called additives and are a cheap and effective way of modifying the electrolyte without changing the main components [28].

Inside the battery the electrolyte is in contact with both electrodes, therefore requirements for compatibility with the different electrode materials are important. For the electrolyte to fulfil its role the following requirements, stated by Xu [28, 30] , have to be satisfied:

1. The electrolyte should be a good ionic conductor and an electronic insulator.
2. The electrolyte should have a large electrochemical window.
3. The electrolyte should be inert in terms of contact with the electrodes, separator and other cell components.
4. The electrolyte should withstand electrical, mechanical and thermal abuses/damages.
5. The electrolyte should be environmentally favourable.

In addition to conducting the Li ions through the separator, the electrolyte has to force

the electrons that part from the lithium through the external circuit. Therefore, it is important that the electrolyte is electronically insulating while remaining ionically conductive. The electrochemical window, i.e. the energy gap between the lowest unoccupied molecular orbital (LUMO) and the highest occupied molecular orbital (HOMO), should preferably be larger than the difference in energy levels between the cathode and the anode. An illustration of this electrochemical window is shown in Figure 2.3, inspired by Goodenough and Parks illustration [14]. If the electrochemical potential of the anode is not higher than the LUMO or the electrochemical potential of the cathode is not lower than HOMO, the electrolyte will be reduced rather than the electrodes [16, 31].

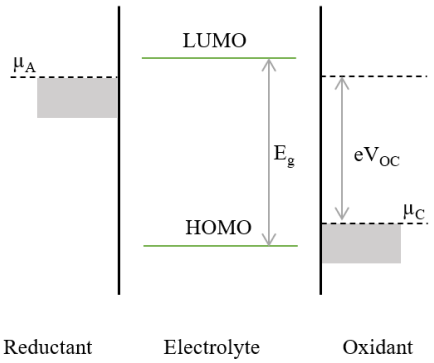

Figure 2.3: Illustration of the electrochemical window, E_g, and the electrochemical potentials of the anode, μ_A, and cathode, μ_C. The schematic energy diagram illustrates how the electrochemical window of the electrolyte has to exceed the difference in electrochemical potentials between the anode and the cathode for the electrolyte not to be reduced or oxidised [14].

2.3.1 Solvent

The main function of the solvent is to dissolve the salt and conduct the Li ions generating the ionic current flow inside the batteries [32]. Still, the solvent has to possess several other characteristics to constitute a functional electrolyte for Li ion batteries. For the solvent to function as an ideal solvent the following requirements, inspired by Schmitz et al. and Xu [11, 28, 32], should be fulfilled:

1. The solvent should have a high dielectric permittivity to enable complete dissociation of the solute.
2. The solvent should have a low viscosity to encourage ion transport.
3. The solvent should be chemically inert with regards to the other cell components, both during storage and cycling.
4. The solvent should preserve its liquid state over a broad temperature range, meaning it should have a low melting point and a high boiling point.
5. The solvent should have a consistent electrochemical inertness over a broad voltage range.
6. The solvent should be nontoxic and have a high flash point, while being cost effective.

Finding a single solvent that fulfils both high dielectric permittivity so that it can dissolve the salt and has a low viscosity to promote the transport of ions has been proven to be difficult. Therefore, the current solution has been to combine several solvents that together accommodate all of these properties [11, 30].

The requirements of high dielectric permittivity reduce the range of possible solvents, narrowing the nonaqueous solvents down to solvents containing polar groups or an ether linkage [28]. Such solvents are mainly organic esters or ethers. Esters either have a poorer dielectric permittivity and a low viscosity, or a higher dielectric permittivity but a higher viscosity, depending on if they are cyclic or acyclic, respectively [28]. Ethers have high ionic conductivity due to their low viscosity and also demonstrate the ability to repress dendrite formation during cycling. However, ether based electrolytes show poor capacity retention during cycling and also decompose at the cathode surface [28, 33, 34].

A cyclic carbonate ester that is used in most electrolytes is ethylene carbonate (EC). The solvent has a sufficient viscosity and a high ability to dissolve the salt [12, 28]. The solvent successfully forms stable SEI layers on graphite anodes which can improve the performance and conductivity of the electrolyte at lower temperatures [32]. However, the solvent has a high melting point of 36 °C which makes it less favourable

when working in ambient temperatures [28]. This issue led to the search for other solvents that could be used together with EC, as the solvent fulfils a lot of the requirements. Expanding the solvent range to linear carbonates has been the solution to the main problems for EC. These linear carbonates, such as dimethyl carbonate (DMC), have low viscosities and a large liquid range making them great cosolvents [28, 35]. Compared to the previously discussed cyclic carbonates, DMC has a lower viscosity correlating with high ionic conductivity, but a poorer dielectric permittivity [28, 36]. Therefore, combining EC and DMC shows great solvent properties due to the contribution from both the low viscosity of the DMC and the high dielectric constant of EC. This can be seen relative to the mole fraction of a LiFSI salt in Figure 2.4 (a) and (b), adapted from Wang et al. [36].

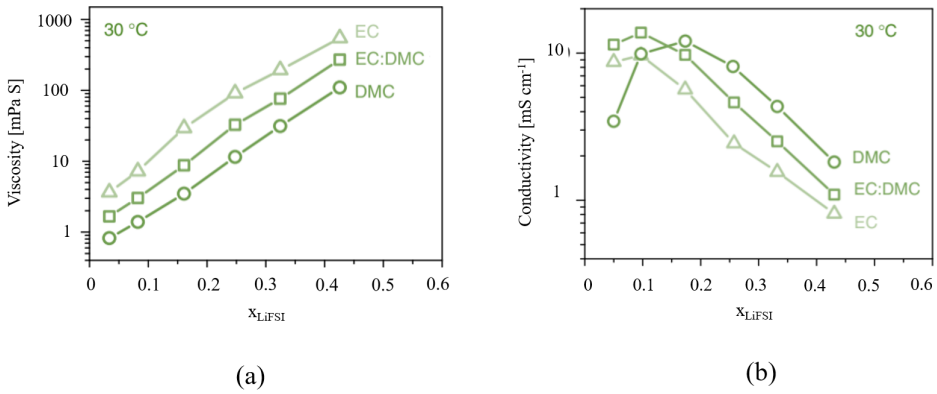

Figure 2.4: Illustration of how the a) viscosity and b) conductivity of the EC, DMC and EC:DMC is dependant on the mole fraction of the LiFSI salt, X_{LiFSI} [36].

2.3.2 Solute

Finding a solute that is compatible with the solvent is imperative for the electrolyte to obtain the desired properties. In lithium ion batteries the solute is, as previously mentioned, a category of lithium salt. The salt should fulfil the following requirements, inspired by Julien, Richard et al. and Xu [12, 28, 37], to perform as an ideal solute in the electrolyte:

1. The solute should completely dissolve in the solvent at adequately high concentrations.
2. The solute should allow the Li cation to move with high mobility.
3. The solutes anion should withstand the oxidation reaction at cathode while also being inert with regards to the solvent.
4. The solutes ions should be inert to all other components in the cell.
5. The solute should be thermally stable in terms of overheating of the battery while also being non toxic.

Finding a solute that satisfies all these requirements is a major challenge in battery research. Since lithium ions have such a small ionic radius, most of the simpler salts have issues with low solubility in dielectric solvents [28]. Another condition that requires consideration is the salts' ability to passivate the current collector, preventing the aluminium from corroding. In addition, the anions of the salt can be sensitive to water exposure since this leads to hydrolysis which can cause the formation of hydrogen fluoride, HF, in the electrolyte [37]. The HF causes dissolution of the transitional metals inside the battery, which can affect the performance [38]. All these requirements make it difficult to find suitable candidates and the options are limited compared to the options for solvents [30].

In commercial Li ion batteries there has been one dominant solute since the Li metal anode was replaced with carbon based anodes, lithium hexafluorophosphate, $LiPF_6$ [37]. Combined with organic solvents, such as the previously discussed DMC and EC, these electrolytes obtain valuable properties such as high ionic conductivity, electrochemical stability and passivation of the aluminium current collector [39, 40]. $LiPF_6$ is in fact one of the salts with the highest conductivity in nonaqueous solvents, due to the combination of good ionic mobility and dissociation constant [28]. Though other salts on the market outperform $LiPF_6$ in single requirements, the reason for its dominance is its combination of well balance properties as it meets all the diverse requirements to some extent [28]. However, the solvent also shows some less favourable properties. Electrolytes based on $LiPF_6$ show poor thermal stability, this causes decomposition of the salt at elevated temperatures creating HF which is destructive

for both the environment and the battery performance. On the other hand, the HF also leads to the passivation of the current collector preventing corrosion and thereby increasing the stability of the batteries [41]. This causes the batteries to have a limited operating temperature window of -20 to 50 °C, where cycling outside of this range causes a reduced capacity and power [28]. This mechanism is further explained in Section 2.4. In addition, the thermal instability leads to the formation of harmful decomposition products that accelerate the degradation of the electrolyte [42]. Another limiting factor of this salt is its sensitivity to water. A study showed that a water concentration of merely 300 ppm lowers the salts' decomposition temperature and thereby reduces the already limited operating temperature window [43]. This sensitivity to moisture also causes problems at ambient temperatures [28]. Therefore it's desirable to minimise the water impurities in these $LiPF_6$ based electrolytes, as reported in a study by Campion et al. that minimising these impurities will maximise the thermal stability [42].

Other salts that has been thoroughly research is $LiClO_4$, $LiBF_4$ and LiFSI. $LiClO_4$, lithium perchlorate, demonstrates a decent solubility together with high conductivity. Using this salt in the electrolyte also forms a SEI layer with a low impedance, lower than both $LiPF_6$ and $LiBF_4$. $LiClO_4$ is also reasonably stable to moisture in the cell. A drawback is that the chlorine present in the perchlorate is highly oxidising and will consequently react with most organic solvents [28]. This highly reactive property causes hazardous behaviour when used in secondary cells. As reported by Newman et al. cells with this salt detonated and caught fire when discharged at high current densities and elevated temperatures [44]. $LiBF_4$, lithium tetrafluoroborate, only demonstrates a moderate conductivity which is a significant impediment for these electrolytes [28, 32]. The conductivity is, as previously mentioned, dependent on the anions' mobility and the salts' dissociation constant which often are inversely proportional. This is the case for $LiBF_4$, which anion has one of the highest mobility, but has a dissociation constant that is quite low [28]. This salt, however, has a higher safety than the previously discussed $LiClO_4$ and has shown enhanced performance at temperatures both higher and lower than the operating window of $LiPF_6$ [45].

A candidate that has gained interest more recently is lithium bis(fluorosulfonyl)imide,

LiFSI. The salt shows great promise to replace the current market leader. Comparatively, the LiFSI shows a higher ionic conductivity, higher solubility and most importantly higher thermal stability. The latter lowers the probability of HF formation due to thermal decomposition, which could diminish the performance of the battery [39]. According to a study by Li et al. LiFSI displays thermal stability up to 180 °C, surpassing the thermal operating range of $LiPF_6$ [9]. From the same study, it can be seen that the ionic conductivity exceeds its contender over a broad temperature range of -50 to 50 °C. These prominent properties is a result of the anions' low binding energy and their strong interaction with the oxygen's lone pairs [9]. The salt also shows a reduction in flammability and thereby increases the safety of the batteries containing LiFSI based electrolytes [36]. The absence of HF also leads to some negative effects. Since the HF contributes to the formation of the passivating layer on the aluminium current collector at high potentials, its absence causes the current collector to corrode during cycling at potentials above 4 V [8, 9]. This mechanism is further explained in Section 2.4.

The chemical structures of both the current market leader, $LiPF_6$, and its contender, LiFSI, is illustrated in Figure 2.5.

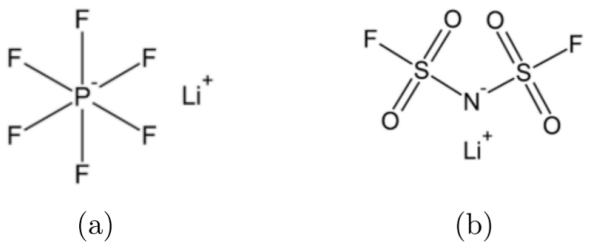

(a) (b)

Figure 2.5: Illustration of the chemical structure for the a) $LiPF_6$ and b) LIFSI salts.

2.3.3 Additives

Additives are supplementary components added to the electrolyte to enhance or achieve certain desired properties, such as increased performance and stability, without changing the major components [28, 32]. This approach is an economical and efficient method that also preserves the electrolytes' bulk properties. The additives are often sacrificial, meaning they are consumed during operation [11]. Additive containing

electrolytes are often denoted as functional additives where the additives are often added in small amounts in the range of 5-10 wt% [28].

Additives can be categorised depending on their function. They are usually added to either expand the electrochemical operating range or the thermal stability, modify the SEI layer or improve the safety [28]. Additives used to improve the electrolyte interface layers on the electrodes should be oxidised or reduced before the electrolyte, for the cathode and anode respectively. In addition to preventing a further decomposition of the interface layer [10]. By stabilising the interface layers the batteries can achieve a higher coulombic efficiency and a longer cycle life [46, 47, 48]. With regards to the additives that increase the safety of the batteries and flame retardant additives, a multitude of factors should be fulfilled. Not only should their radical cations be stable, but they should also be able to pursue other radicals to terminate possible reactions [10]. However, to achieve the best performance, combining several additives into the electrolyte can be beneficial as the combination can lead to synergistic effects [10, 49]. Thereby increasing the battery performance further than what the single additives would. Additives that are commonly used are vinylene carbonate (VC) and fluoroethylene carbonate (FEC), which are mainly used to enhance the interface layers. The latter is the focus of this thesis.

The effect of FEC on the anode has been widely researched. The additive shows a positive influence on the formation of the SEI layer and increases the cycling performance, for both silicon and graphite anodes [10]. In terms of its effect on the cathode, less research has been done. Recently, more effort has been put into this research as the cathode is the limiting component of the Li ion batteries. Improvements in cycling stability have been reported for some cathodes. However, limited research has been done on NMC cathodes cycled in a FEC containing electrolyte [11]. The SEI layer on the anode formed in FEC containing electrolytes is less porous and more stable [50]. Comparatively, interface layers formed without the additive are more porous which causes them to be more permeable and less protective. The additive also causes the interface layer at the anode to have a smaller impedance and a better capacity retention [30, 50]. The structure of the FEC additive can be seen in Figure 2.6.

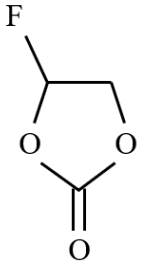

Figure 2.6: Illustration of the chemical structure of the FEC additive.

For the effect of FEC on the cathode, especially NMC cathodes, the research is limited [11]. However, some studies have been performed on FECs' effect on these. For NMC_{523} in LiFSI salt based electrolytes the FEC improves the capacity retention compared to the cells without FEC, to such an extent that they show similar performance to cells with FEC and $LiPF_6$ [29, 30]. This improvement in cycling performance and capacity retention due to the addition of FEC has also been seen for Li rich LNMO cathodes [51]. In addition, the additive has been shown to increase the threshold voltage at which the Al current collector corrodes from 4.0 V to 5.5 V [52]. For the NMC cathodes, some negative effects of the additive have also been reported. In cells where not all the FEC is consumed during the formation of the SEI layer in the initial cycles, the remaining FEC can defluorise. This leads to the formation of HF causing transitional metal dissolution of the NMC cathode resulting in a reduction in capacity [53].

To further understand the impact these additives have on the performance, their decomposition products have to be investigated. If there is remaining FEC in the system after SEI formation, the additive will be reduced to form LiF and VC. The VC further decomposes to polycarbonates such as HCO_2Li, $Li_2C_2O_4$ and Li_2CO_3 [54]. The presence of LiF together with Li_2CO_3 has shown to increase the ionic conductivity [55]. The reasons for the increased stability of the electrolyte interface layer differ. Some suggest that the reason is the high LiF presence, which contributes to a higher Li ion conductivity [56]. However, it is also reported that the LiF contributes to a slower Li^+ conductivity and that its the polycarbonate decomposition products that are the main contributors to the stability of the interface layer [57, 58].

VC is an additive that has shown to be of great importance for the SEI formation at the anodes, resulting in stable cycling in $LiPF_6$ electrolytes [30]. Also in LiFSI based electrolytes, VC has shown to result in superior performance, decreasing the impedance and improving the capacity retention for NMC_{532} containing cells [29]. For the silicon anodes, the additive causes a much more flexible film compared to FEC. The increased flexibility ensures that the interface layer can withstand the volume changes that the Si anodes go through during cycling. However, the drawback is the reduction in conductivity for Li ions through the film, as the addition of VC increases the impedance [55, 56]. Xu states that a drawback of the VC additive is that it forms undesired species during cycling, which decrease the amount of LiF, lithium fluoride, inside the batteries [30]. However, researchers are conflicted on the effect of the LiF presence [11]. A study by Krause et al. argues that the presence of LiF causes higher porosity and disorder of the protective film on the surface of the current collector. Which distorts the passivating effect of the film, causing corrosion of the current collector. Thus, electrolytes containing VC showed a decreased stability during cycling [8].

A problem in Li ion batteries is the dissolution of Mn from the cathode surfaces. Mn dissolution causes major problems in Li ion batteries as it limits the cycle life. This is a result of the Mn ions depositing on the electrode surfaces, causing a destabilisation of the electrode-electrolyte interfaces both for the anode and the cathode. To prevent this both FEC and VC have been researched. The addition of FEC and VC has little to no effect on preventing the Mn dissolution from the cathode. However, VC was found to decrease the Mn deposition on the surface of the anode [59]

Another compound that can be treated as an additive is water. As the Li ion batteries are manufactured in a dry atmosphere, the water content inside the cell is kept at a minimum. However, trace amounts of water may still be present. This water content has been denoted as unwanted, as Li is very reactive and will upon contact with water form LiOH, as seen in Reaction 2.10 [12]. LiOH, lithium hydroxide, appears white when it crystallises and attracts water from the surroundings making it very corrosive [12].

$$Li + H_2O \longrightarrow LiOH + \frac{1}{2}H_2 \tag{2.10}$$

In addition, for batteries containing a $LiPF_6$ based electrolyte the presence of water could accelerate the decomposition of the salt at elevated temperatures, larger than 40 °C, and at high potentials, above 4 V [5]. As the salt decomposes, HF is formed. This will upon reactions with the cathode material forms more H_2O and further decompose the $LiPF_6$ salt resulting in deterioration of the cell performance [5].

Recently, the addition of water has been more heavily investigated as this could allow for a reduction in energy consumption during manufacture. The combination of water together with other additives has also been researched. A study showed that in combination with VC small amount of water, 100 ppm, affected the anode more than the cathode. But the addition of larger amounts, 1000 ppm H_2O, had a larger impact on the cathode [60].

2.3.4 Electrolyte Interface Layers

On the surfaces of the electrodes, interface layers form due to reactions between the electrode and electrolyte. These layers, the cathode electrolyte interface (CEI) on the cathode and the solid electrolyte interface (SEI) on the anode, influence the performance of the batteries. The SEI layer forms on the anode during the initial cycles from species formed during the decomposition of the electrolyte and prevents further decomposition in the subsequent cycles. This results in an enhanced reversible capacity, and overall better cycling performance [10, 16]. Compared to the SEI layer, the CEI layer has not been a major subject of research. As a result, there is a lack of information on this layer and its effect on the battery performance, even for the most common cathode materials [61].

The similarity of these layers is uncertain, i.e. if the CEI layers have properties similar to the SEI, like being electrically insulating while still maintaining its ionic conductivity towards Li ions [61, 10]. However, research has shown that the composition and thickness of the CEI layer has a substantial influence on the electrochemical performance of batteries with NMC_{111}, NMC_{442} and NMC_{76} [61, 62, 63].

A study by Niehoff and Winter thoroughly investigated the CEI layers effect and composition on NMC_{111} cathodes in $LiPF_6$ based electrolytes. The study showed that the elements from the decomposition of the electrolyte created a layer on top of the carbon on the surface, and not on the actual NMC material. These CEI layers mainly consists of LiF, but also rather large amounts of Li_2CO_3 and RCO_3 [64]. The presence of LiF in the cathode electrolyte interface layer is beneficial as it increases the coulombic efficiencies of the battery. The increase is mainly owed to LiF's ability to block electrons from leaking through and into the electrolyte solution. Preventing this electron leakage is important as it prevents decomposition of the electrolyte and dendrite formation [65, 66]. The addition of $LiBF_4$ together with the common $LiPF_6$ salt results in a decrease of the CEI layer thickness on the NMC_{442} surface, causing an increase in the performance at higher operating voltages compared to using the salts alone [62]. Another mixed salt electrolyte, lithium bis(oxalate)borate (LiBOB) and $LiPF_6$, showed an increase in the cycling performance, rate capability and stability in the operating voltage [63]. For LiFSI based electrolytes studies show that higher concentrations, 3.6 M LiFSI, can be beneficial in terms of a more stable CEI layer [67]. A similar study was conducted for NMC_{622} cycled in superconcentrated electrolytes, 10 M LiFSI. These show that the high concentration leads to the formation of not only a more stable layer but also a thinner and LiF rich layer which has shown to be beneficial for battery cycling [68].

Not all cathode electrolyte interface formations have favourable effects on the battery performance. For batteries with LNMO cathodes cycled in $LiPF_6$ based electrolytes, the formation of an unstable film was observed on the cathode surface. The film was a result of the operating voltage exceeding the oxidation potential of the electrolyte and caused poor coulombic efficiencies for the batteries [69].

Additives can also influence the interface layers. LiDFOB has been shown to create a SEI layer that has lower interfacial resistance and that is more stable during cycling [70]. A combination of several salts, LiTFSI, $LiPF_6$ and LiBOB, have also been shown to enhance battery performance factors like discharge capacity and capacity retention, due to the improved stability of both the anode and the cathode for NMC_{76} and Li metal [71]. Some additives have been reported to influence these layered negatively,

such as LiBOB. This additive makes a dense and resistant CEI layer in the initial cycles, which degrades during the cycling [71]. The addition of LiBOB together with LiTFSI creates interface layers containing large amounts of carbonates, polycarbonates and borates which contribute to preventing the dissolution of transitional metals on the cathode for both NMC_{622} and NMC_{811} [71]. FEC has also been shown to have a positive effect on the CEI layer in $LiPF_6$ based electrolytes. The addition of small amounts of FEC, 2 wt%, has shown to produce the previously discussed thin and LiF rich CEI layers that are beneficial for the performance of NMC_{111} cathodes due to their ability to inhibit capacity loss [61].

2.4 Corrosion of the Aluminium Current Collector in Li-ion Batteries

The current collector on the cathode side in Li ion batteries is, as previously mentioned, made of aluminium. When Al is exposed to air or an aqueous solution, an oxide layer, Al_2O_3, forms on the surface which prevents further oxidation [5]. Aluminium has one of the lowest reduction potentials, causing it to easily be oxidised. This aluminium oxidation varies in different electrolytes, due to its dependency on the electrolyte salt. This dependency is related to the solubility of the aluminium complexes in the electrolyte solutions [72]. When the current collector is immersed in the electrolyte the Al will polarise in the anodic direction [41]. This causes the oxide layer on the surface to oxidise according to Reaction 2.11. This reaction will continue until the aluminium surface below is exposed causing the Al to oxidise as described in Reaction 2.12 [39].

$$Al_2O_3 \longrightarrow 2\,Al^{3+} + \frac{3}{2}\,O_2 + 6\,e^- \tag{2.11}$$

$$Al \longrightarrow Al^{3+} + 3\,e^- \tag{2.12}$$

The Al ions that form are unstable causing them to form complexes with surrounding ligands in the electrolyte solution, according to Reaction 2.13. Since the complexes that form on the Al surface often are soluble in the electrolyte they desorb from the surface and migrate into the solution. This exposes the bare Al again, causing a continuous loop of the described reactions and continuous corrosion of the Al surface. Contrarily, if these complexes are not soluble they will not desorb but rather deposit on the Al surface. This protects the underlying Al and stops the continuous corrosion of the aluminium [39].

$$Al^{3+} + \text{ligand} \longrightarrow Al^{3+} - \text{complex} \tag{2.13}$$

The passivation mechanism for a) $LiPF_6$ based electrolytes and the corrosion mechanism for b) LiFSI based electrolytes are illustrated for in Figure 2.7, adapted from Yamada et al. [39].

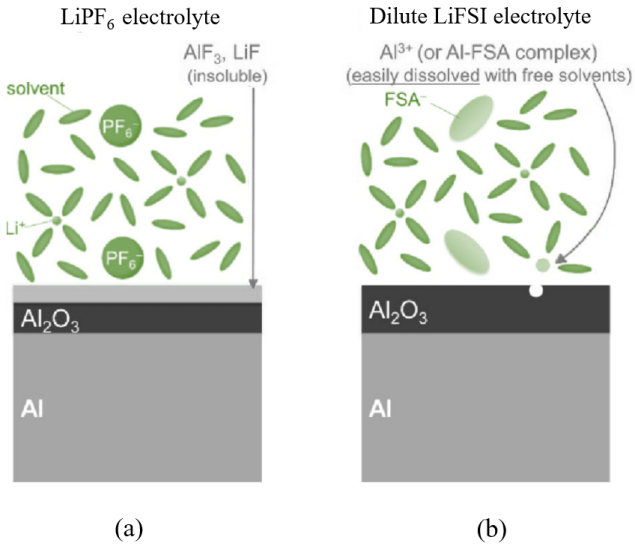

Figure 2.7: Schematic illustration of the corrosion prevention mechanism for the aluminium current collector in batteries containing a) $LiPF_6$ based electrolytes together with the corrosion mechanism for b) LiFSI based electrolytes [39].

$LiPF_6$ based electrolytes have high stability against pitting corrosion of the aluminium

current collector [73]. The salt decomposes due to reactions with small amounts of water present in the electrolyte, forming HF [39]. The fluoride anions, F^-, react with aluminium cations forming AlF_3, creating a thin surface layer on the current collector. The strong ionic bonds in AlF_3 prevent the layer from desorbing from the surface, forming a stable layer that will prevent corrosion of the aluminium current collector [39]. In addition to the AlF_3, there is also reported that Al_2O_3 is present in the surface film [5]. This layer forms during air exposure before battery manufacture, so that the previously discussed AlF_3 layer forms on top of the Al_2O_3 layer [74].

In electrolytes based on LiFSI salt, only trace amounts of HF is present due to the salt's superior thermal stability. As the aluminium cations form complexes with free solvent molecules in the electrolyte, they desorb from the surface due to their solubility [39]. This causes continuous corrosion of the current collector, which is harmful to the performance of the battery. For the current collectors in batteries with LiFSI based electrolytes, the onset potential for this corrosion is 4.0 V vs. Li/Li^+ [9, 52]. This is problematic as this voltage lies within the operating voltage of these batteries. For a slightly higher LiFSI concentration of 1.25 M, passivation of the aluminium current collector has been reported up to 4.3 V [7].

2.5 Electrochemical Measurement

2.5.1 Cyclic Voltammetry

Cyclic voltammetry is an electrochemical method commonly used to study the oxidation current on the aluminium current collectors in Li ion batteries. This is done by applying potentials that are increased linearly between a minimum and a maximum potential at a set sweep rate.

The measurement is done by applying a potential to see how the current changes as a response to the potential increase. At low scan rates, the current will be determined by the kinetic limitation, and not the diffusion limitation, causing the current to increase steadily as the voltage increases. At high scan rates, the Nernst diffusion layer on the electrode surface has linear concentration gradients. As the potential increases, the

surface concentration of reactant displays a continuous decline. This causes a rise in the concentration gradient, which increases the current in the system [75]. Eventually, the concentration almost reaches zero, and the mass transfer rate of surface reactant and concentration gradient reaches its maximum. This causes the increase in current to halt and the current to reach its maximum value, subsequently the current will then reduce due to the depletion effect [76]. During the current increase the surface chemistry changes, which results in a different path as the current decreases.

This method causes a peak current-potential curve illustrated in Figure 2.8 together with the linear potential change, inspired by Bard and Faulkner [76].

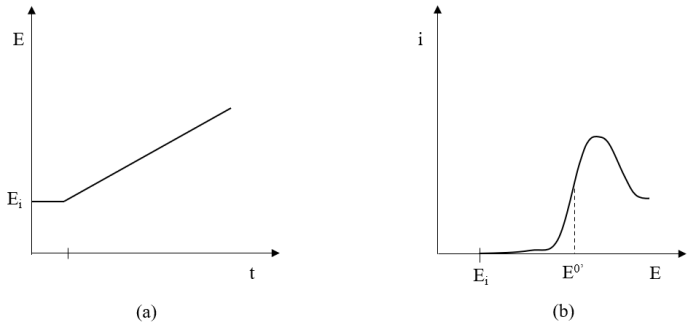

Figure 2.8: Illustration of a) linear potential change and b) the corresponding current-potential diagram during cyclic voltammetry

For cyclic voltammetry, the current path as the voltage returns to its initial value usually has a similar shape as it did for the voltage increase. However, the measurements performed in this thesis were done for reactions that are not reversible. This causes a steady decline in the current, as the voltage returns to its initial value and the cycle is completed.

2.5.2 Galvanostatic Cycling

Galvanostatic cycling is an electrochemical method used to determine the performance of batteries. From the method a wide range of different parameters that can illustrate the battery performance can be found, such as coulombic efficiency and discharge capacity. How these are obtained from the potential-time diagrams is discussed in Section 2.1.2. In comparison to linear sweep voltammetry where the potential is

varied, in galvanostatic cycling it's the applied current that is varied to determine the potential as a function of time. The applied current is selected based on the capacity of the electrode used [76].

The applied current is shown in Figure 2.9 together with the resulting potential-time diagram, inspired by Bard and Faulkner [76].

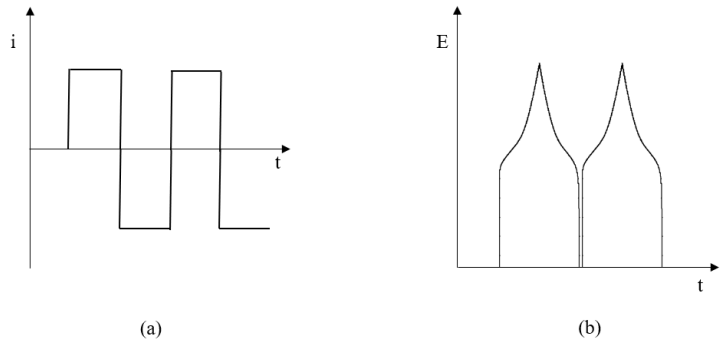

Figure 2.9: Illustration of a) applied current and b) the corresponding potential-time diagram during galvanostatic cycling.

2.6 Characterisation Techniques

2.6.1 Scanning Electron Microscopy Imaging

Scanning electron microscopy (SEM) is a common imaging technique that utilises electrons to produce an image. This is done by focusing a thin electron beam on the specimen that generates multiple different signals i.e. secondary electrons, backscattered electrons, characteristic x-rays, Auger electrons and photons. Each signal has distinct energies that can be detected by the instrument. Most frequently used are the secondary electrons, backscattered electrons and x-rays [77].

The instrument has different parameters that can be adapted and effects image resolutions. The acceleration voltage controls the beams' penetration depth into the sample. A higher acceleration voltage causes the electrons to scatter further into the sample, which leads to a larger primary excitation region. This volume increase causes some of the surface information to dissipate and entails a decrease in resolution

[78]. The working distance also affects the image resolution. If the objective is at a shorter working distance, this leads to a higher resolution but at the expense of a reduction in the depth of field [77].

Energy-Dispersive X-ray Analysis

Energy-dispersive x-ray (EDX) spectroscopy is an analytical surface technique used to identify elemental components on the surface of a sample. The elements are detected from the characteristic x-ray emitted from the sample as the electron beam hits the surface. These characteristic x-rays contain different energies depending on the elemental composition of the surface and result in peaks on an electromagnetic spectrum. The spectrum works as a fingerprint and can distinguish the different elements on the sample surface [79].

2.6.2 Glow Discharge Optical-Emission Spectroscopy

Glow discharge optical-emission spectroscopy (GDOES) is an analysis technique used to identify the elements on the surface of a sample [80]. The method is highly sensitive to all solid materials which makes it an optimal analysis technique with regards to identifying unknown elements [81].

The device creates an electric field between the anode and cathode, where the sample is the cathode. The system creates plasma by applying this electric field to the low pressure argon gas. Plasma is a weakly ionised gas, that glows as the voltage reaches its threshold value. The free electrons are balanced with positively charged argon ions so that the atmosphere remains electrically neutral. The analysis method works by sputtering electrons onto the sample. As the sample elements are sputtered they travel into the plasma where they collide with the ionised argon or the free electrons causing them to enter an excited state. The following deexcitation of these atoms emits light in the form of photons, with characteristic wavelengths allowing the species to be detected [80, 81].

2.6.3 Fourier Transform Infrared Spectroscopy

Fourier transform infrared spectroscopy (FTIR) is an analysis method that can be used to detect molecular bonds present in a sample [82]. FTIR utilises the principle that molecular vibration absorbs infrared radiation. Each vibration holds a unique frequency depending on the type of chemical bonds and the atomic masses [83]. The method obtains an infrared (IR) spectra by measuring an interferogram of the sample surface which is Fourier transformed into the IR spectrum. The peaks in the Fourier transformed spectrum are a result of the reduction of the amplitude in the interferogram as the sample absorbs light at a certain wavelength [82]. The absorption of radiation causes vibration of the chemical bonds of the sample molecules [84]. IR radiation is electromagnetic radiation with frequencies of 14 300 - 20 cm^{-1}, while only the mid range of 4000 to 400 cm^{-1} is of importance for classifying organic molecules [83].

Attenuated total reflectance FTIR (ATR-FTIR) is a sampling technique that enhances the ability to analyse only the surface of a sample by utilising the contact surface between a crystal and the sample surface. Through these contact surfaces the sample absorbs infrared light and due to the set-up of the ATR this infrared light has low penetration depths allowing only surface molecules to be detected [82]. There are several kinds of crystals that can be used for this analysis, such as ZnSe, Si, Ge and diamond. Each of these has different ranges for which wavenumbers they can detect, with diamond having the largest range. Additionally, diamond is very durable and hard but at the expense of being expensive [82].

However, not all bonds are applicable to be measured with infrared radiation. As not all vibrational modes are IR active and can absorb infrared radiation. This causes homonuclear diatomic molecules to be invisible during FTIR measurements. Another noteworthy component that can not be detected by FTIR is LiF, due to it being IR inactive [85]. An exert of molecules that can be detected that are relevant for the analysis performed in this thesis are listed in Table 2.1.

Table 2.1: FTIR

Component	Vibration [cm^{-1}]
Aldehyd, ketone	1725-1650 [86]
C=C	1700-1600 [87]
C−H	2928(EC) [88] , 2900-2800 [89], 1394 [90]
CH_2	1481(EC) [91], 1391(EC) [91], 774(EC) [88]
CH_3	1454(DMC) [91, 92], 1433(DMC) [91]
CH_2(EC),CH_3(DMC), combined	3003 [92], 3002 - 2850 [90]
CH_3−O	916(DMC) [92]
C−O	1069 [90]
C=O	1769(EC) [91], 1750(DMC) [91], 1642 [90], 1342 [90]
C−O−H	1050-1000 [93]
Carboxyl	1725-1650 [94]
EC	1870(liquid) [95], 1810(solid) [95], 1782(solvated) [90]
H_2O	5400-4800 [96]
Li_2O	609 [97]
LiOH	3675-3660 [98]
Li_2CO_3	1435 [97], 875 [99], 857 [97]
LiFSI	1365 [100], 1177 [100], 1209 [100]
Li-oxalate	1300-1350 [101]
OCO_2	797(DMC) [92]
O−H	3800-3000 [96], 1075-1050 [102]
Polycarbonates(EC/DMC)	1765 [90], 1196 [90]
$ROCO_2Li$	2900 [97], 1668 [103], 1650 [97], 1450-1400 [99], 1350 [98], 1300 [97], 1115 [98] , 1090 [88], 855 [98], 840-800 [99], 820 [97]
ROLi	2963 [104], 2900-2700 [105], 1100-1000 [97], 600 - 500 [105]
S−H	2550 [106]
S=O	1375-1300[106], 1350-1140[106]
SO_2	1380 + 1360 [107, 108], 1211 [109], 1184 [109], 570 [109]
SO_2−N−SO_2	1100 [107, 108]
S−F	897 [110], 827 [109]
S−N−S	870 [109], 759 [109]

Chapter 3

Methods

This section presents an overview of all steps completed to manufacture the pouch cells with regards to this thesis. This includes electrode manufacture, electrolyte mixing, pouch cell manufacture and assembling. The section also provides cycling parameters used during electrochemical testing with cyclic voltammetry and galvanostatic cycling. Lastly, the parameters for post mortem characterisation using SEM, EDS, GDOES and FTIR are given.

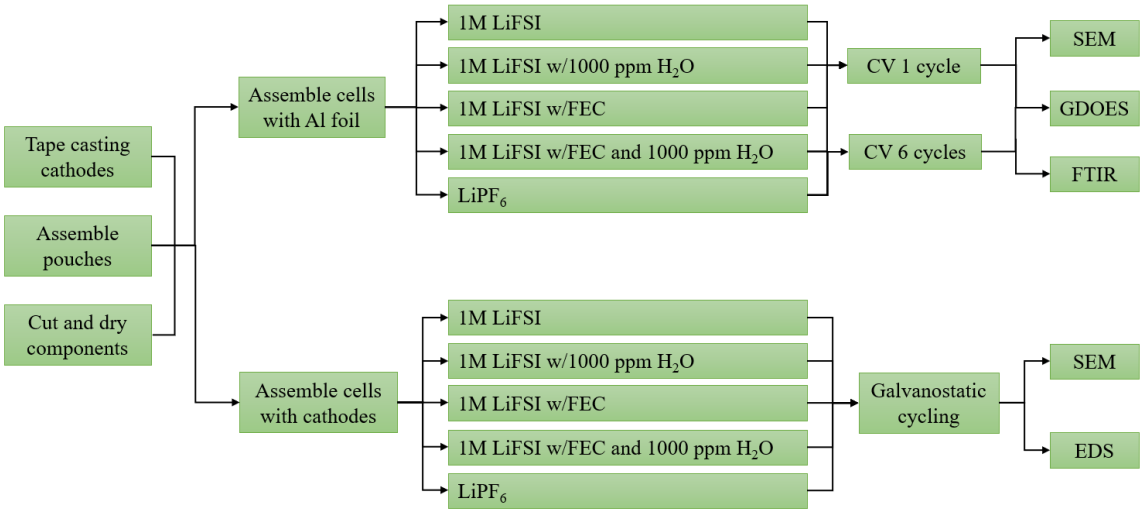

Figure 3.1: Flow chart providing an overview of all the experimental steps performed.

3.1 Electrode Manufacture

A binder solution of 5 wt% of PVDF in NMP was created by mixing 0.5039 g of PVDF with 8.5633 g of NMP, before stirring overnight. Carbon black was dried overnight at 120 °C before being mixed with the binder solution in ZrO containers containing ZrO pellets. The solution was mixed using the RETCH mixer mill for 10 min with a frequency of 25 sec^{-1}. After mixing the NMC powder was added together with additional NMP to obtain the correct viscosity. The final solution was mixed in RETCH mixer mill for a minimum of 25 min. The exact amounts used for the different components are listed in Table 3.1.

Table 3.1: Amounts of components used in manufacture of NMC_{111} electrodes

	NMC_{111} [g]	Carbon Black [g]	Binder Solution [g]	NMP [g]
Calculated amount				
80:10:10	1.2	0.15	3	1.1
Added amount				
Batch 1	1.2072	0.1532	3.0288	1.1044

The solution was cast on top of Al foil. Before casting the foil was secured onto a plastic film for stability. The mixed solution was spread on top of the foil using an RK K Control Coater 101 tape caster with a gap height of 200 μm and a speed of one. After casting the cast was dried for 30 min at 60 °C before drying in a vacuum oven at 120 °C for 12 h. Finally, the cast was cut into 12 mm circles. An overview of c-rates and loading for the cathodes used and which electrolyte they were combined with is given in Table 3.2.

Table 3.2: Properties of manufactured NMC_{111} cathodes, denoted after the cells they were used for.

Cathode	C-rate, 1C [mA]	Loading [mg cm^{-2}]
LiFSI 1	0.599168	3.417951
LiFSI 2	0.602888	3.439172
Water 1	0.628928	3.587717
Water 2	0.630168	3.594790
FEC 1	0.616528	3.516981
FEC 2	0.526008	3.000610
FEC and Water 1	0.645048	3.679673
FEC and Water 2	0.636368	3.630158
Old FEC 1	0.596688	3.403804
Old FEC 2	0.585528	3.340142
Old FEC and Water 1	0.659928	3.764556
Old FEC and Water 2	0.641328	3.658452
$LiPF_6$ 1	0.581808	3.318921
$LiPF_6$ 2	0.581808	3.318921

3.2 Electrolyte Mixing

Several electrolyte solutions was created, exact amounts of each component for all solutions are given in Table 3.3.

Table 3.3: Amounts of the different components used in electrolytes.

Electrolyte	DMC [g]	EC [g]	LiFSI [g]	Water [g]	FEC [g]
1M LiFSI	10.074	10.065	3.275	-	-
1M LiFSI w/FEC	2.00432 g *extracted from 1M LiFSI*				0.20022
1M LiFSI w/water	10.004	10.005	3.251	0.02261	-
1M LiFSI w/FEC+water	2.43683 g *extracted from 1M LiFSI w/water*				0.24618

All solutions were created with a 1:1 ratio of EC:DMC in a controlled argon atmosphere with 0.1 ppm of water and oxygen. This was done by first melting the EC at 50 °C, before combining it with an equal amount of DMC. LiFSI salt was dried at 80 °C for a minimum of 10 h before it was weighed out and added to the DMC:EC

solution. After addition, the mixture was stirred overnight. For the solutions containing additional water, the solution was taken out of the controlled argon atmosphere. The water was added to the solution using a syringe and a cap with a membrane in the lid. This membrane seals itself after the syringe was extracted, ensuring that no additional water or other species from the atmosphere entered the electrolyte. In case this membrane did not properly seal, the electrolyte was covered if it was taken out of the glove box. To create the FEC containing electrolytes an amount of the LiFSI and the LiFSI with water electrolyte was extracted before 10 wt% of FEC was added to the solutions.

The water amount for all solutions was measured using Karl-Fisher titration, with values listed in Table 3.4. Due to inconsistent values are given by the measurements, average values of 2-3 measurements were calculated and the water amounts may therefore deviate from the actual values. As the FEC was added to the preexisting LiFSI and LiFSI with water electrolytes, the amounts of water would realistically be smaller. However, the same average values are used for the FEC electrolytes as approximate water contents.

Two electrolytes, LiFSI with FEC and LiFSI with FEC and additional water, from the previous semester was also used. These were manufactured with the same method, both containing 10 wt% of water. The FEC with additional water had a water content of 1004 ppm, while the FEC electrolyte had a water content of 111 ppm.

Table 3.4: Water amount in the different electrolyte solutions determined by Karl-Fisher titration

Electrolyte	Water [ppm]
1M LiFSI	97
1M LiFSI w/water	960
1M LiFSI w/FEC	97
1M LiFSI w/FEC+water	960

3.3 Separators, Al foil and Counter Electrode

Solupor 3P07B from Lydall made of Ultra High Molecular Weight Polyethylene was cut into 18 mm circles and used as the separator in all cells. While 16 mm lithium

metal circles was used as the anodic counter electrode. Al foil used for these cells was cut into either 12 or 16 mm circles. Where 12 mm is the standard, but as the GDOES instrument requires samples to have a minimum diameter of 15 mm, this lead to the use of larger 16 mm Al foils.

3.4 Pouch Cell Manufacture

To create the pouches Al foil laminated with polyethylene was used as the outer layer. On the coated side of the Al foil a clear strip of tesa® copolyester-based thermoplastic bonding film was placed leaving a small gap on top of the Al foil. On top of the bonding film, a strip of white electrical tape was placed, leaving about half to be folded over onto the other side of the foil. Two current collectors, Al and Cu, was placed in a triangle formation inside the pouch before the pouch was folded and sealed twice with an Audion 421 MGMIDS-2 Magenta Motor sealing machine. An illustration of the placements and relative sizes of the components is shown in Figure 3.2.

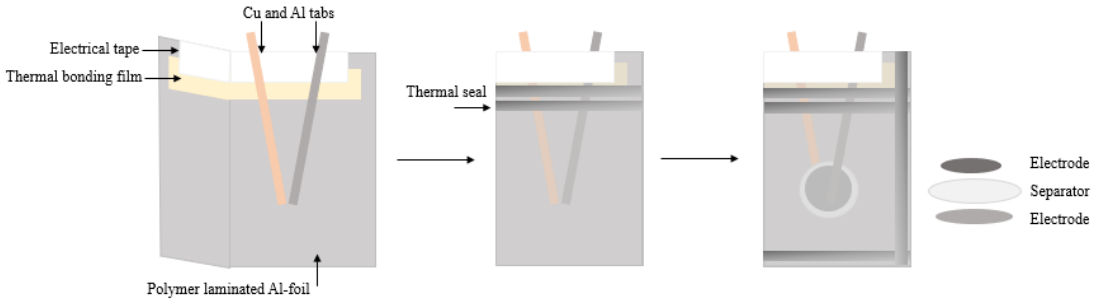

Figure 3.2: Schematic illustration of the different steps of pouch cell manufacture, including the placement of the electrodes and separators inside the pouch.

3.5 Pouch Cell Assembly

Before assembling the cells all components was brought into the argon filled glove box through a vacuum chamber. The components have different requirements, which are listed in Table 3.5.

Table 3.5: Method for introducing the different components into the glove box.

Component	Method
Pouch and Al foil	3x1min of evacuation, refilling with Ar in between
NMC_{111} cathode	3x1 min of evacuation as above then 120 °C under constant evacuation for at least 12 h
Separator	3x1 min of evacuation as above then 80 °C under constant evacuation for at least 12 h

The cells were then assembled by the following procedure. The first step was creating the electrode-separator stack. The stack consists of a Li metal counter electrode, a separator and a cathode or Al foil. The Li metal was brushed with a bristle brush to remove the oxide layer from the surface. When the Li metal surface was clean the electrolyte was pipetted on. The separator was then placed on top, soaking in the electrolyte. Before the cathode or Al foil was placed on the separator the remaining electrolyte was pipetted onto the separator. Different electrolyte amount was used for different cells. For cells containing electrolytes with no additional water, 50 μL of electrolyte was used. The cells with water containing electrolytes the electrolyte had to be extracted using a syringe, which did not allow for exact measurements of such small volumes. But an estimate of 40-60 μL was attempted extracted. When the stack was completed it was placed inside the pouch, where the cathode or Al foil was connected to the Al current collector and the Li metal connected to the Cu current collector. The cells were completed by sealing both open sides as illustrated in Figure 3.2, using a AudionVac VMS 53 vacuum sealer.

3.6 Electrochemical Testing

Post assembly the cells rested in ambient conditions for a minimum of 5 hours, to allow the electrolyte to soak into the cell components before the electrochemical testing. The cells were cycled using BioLogic MSC-805 battery cycler, applying different programs depending on if a cathode or Al foil was used. Cells with Al foil was cycled using cyclic voltammetry, while for the cells containing the cathode material a galvanostatic cycling program was utilised. Both cycling programs are specified in Table

3.6.

Table 3.6: Steps for the galvanostatic cycling program and the cyclic voltammetry program, where C is the capacity for the cathode.

Step	Current	Voltage range	Number of cycles
Galvanostatic cycling			
1	C/10	4.2 - 3 V	2
2	1C	4.2 - 3 V	20
3	1C	4.3 - 3 V	20
4	1C	4.4 - 3 V	20
Cyclic voltammetry			
1	-	4.9 - 3 V	6
Cyclic voltammetry, 1 cycle			
1	-	4.9 - 3 V	1

3.7 Characterisation of Cells Post Mortem

After cycling the pouch cells were disassembled inside the glove box where the cathode or Al foil was extracted for further analysis. The collected component was cleaned with DMC, approximately 50 μL for a total of three times.

3.7.1 Scanning Electron Microscopy (SEM) Imaging

The collected cathode and Al foil was imaged with the scanning electron microscope SEM APREO in the cleanroom at NTNU Nanolab. The cleanroom is ISO grade 6 containing below 1000 particles larger than 0.5 μm per ft^3 and has a stable temperature at 19 °C ± 1 °C and relative humidity of 43 % ± 5 %. The imaging was done at a working distance of 4 mm, using an acceleration voltage of 5 kV and an emission current of 0.8 nA. Images were taken at different magnifications, including 1200 X for the cathodes and 200 X for the Al foils.

3.7.2 Energy Dispersive X-ray (EDX) Analysis

Elemental analysis was performed on the cathodes using the EDX Oxford Xmax 80 mm^2 Solid angle (10mm WD, 0.03409 srad, 127 eV) detector on the SEM APREO.

For this analysis, the parameters was changed to a working distance of 10 mm and an acceleration voltage of 10 kV, while the emission current was kept at 0.8 nA.

3.7.3 Glow Discharge Optical Emission Spectroscopy (GDOES)

Elemental analysis was performed on Al foils using the GD-Profiler 2™. For the analysis the flushing time was set to 100 seconds, pre-integration time was set to 100 s, background acquisition of 5s and bulk acquisition of 10 s. Using an RF excitation mode the pressure was set to 600 Pa with a power of 32 W.

The Al foils analysed with the GDOES had a diameter of 16 mm, as the instrument requires the sample to cover the o-ring to create the plasma. To load the samples onto the instrument the samples need to be more sturdy. Therefore, the Al foils was taped onto steel plates using double sided Cu tape. This method is illustrated in Figure 3.3. However, the Cu tape did not provide sufficient hold of the samples, resulting in stability issues for the analysis.

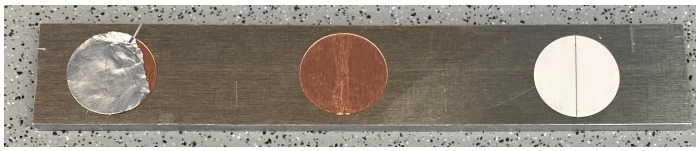

Figure 3.3: Method used to attach the Al samples onto the steel plate. Where the entire procedure of sticking the Cu tape to the plate, exposed Cu tape and the attached sample can be seen from right to left.

A brief introduction of the general signal is included. The GDOES measurement works by etching through the surface, meaning that the measurements start at the surface at 0 s and etch inwards in the sample as the time increases. From the width of the peaks, the time interval it takes to etch through, and the relative thickness of the surface film present on the Al surface can be compared. Each element reaches certain voltages for each sample, represented by the height of the peaks, comparing these heights of the same element one can compare the relevant amount of each element on the different samples.

3.7.4 Fourier-Transform Infrared (FTIR) Spectroscopy

Elemental analysis was performed on Al foils using the Bruker Vertex 80V ATR-FTIR with a diamond crystal. A scanner velocity of 10 kHz with an aperature of 6mm was used for the room temperature detector. A scan range of 350-4000 $^{-1}$ was used together with a resolution of 4 cm^{-1}, for a total of 100 scans.

To prevent the samples from being exposed to air before the measurements the samples were mounted on the ATR disk inside the glove box. The samples were sealed with contact paper to prevent air exposure and ensure proper contact between the sample and crystal, as is illustrated in Figure 3.4. The background measurements are subtracted from the sample measurements by the instrument, while an additional subtraction of a pristine sample was also done.

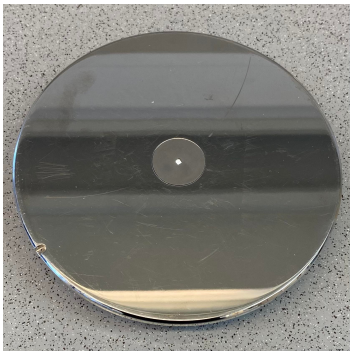

(a) ATR disk with diamond crystal.

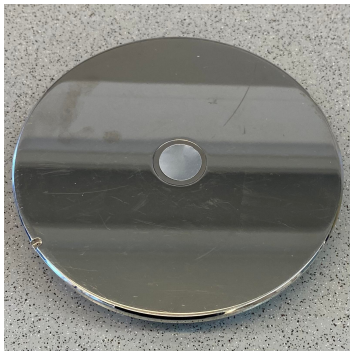

(b) Al foil sample placed on top of the diamond crystal.

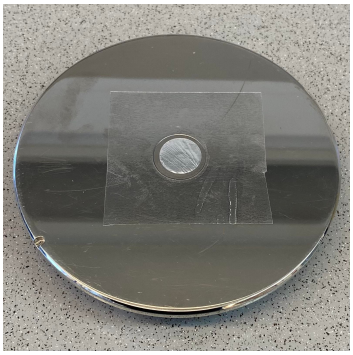

(c) Contact foil added on top of the foil prevent air exposure.

Figure 3.4: Method for bringing samples in to the FTIR instrument to prevent air exposure.

Chapter 4

Results

This section presents all the results obtained for NMC_{111} cathodes and Al foils cycled in the four different electrolytes, in addition to $LiPF_6$ electrolyte used for reference. The sections first provide an overview of the cycling performance before the characterisation results are presented. The electrolytes utilised are LiFSI, LiFSI with 1000 ppm of H_2O, LiFSI with 10 wt% of FEC and LiFSI with 10 wt% of FEC and 1000 ppm of H_2O. Further, these electrolytes are referred to as LiFSI, water, FEC and FEC with water.

4.1 Effect of FEC and Water on NMC Cathodes

4.1.1 Cell Performance during Galvanostatic Cycling

Figure 4.1 shows the discharge capacities in mA g^{-1} for each cycle during galvanostatic cycling of NMC_{111} in electrolytes a) without FEC and b) with FEC. In each of the figures two cells are included, one with an additional water content of 1000 ppm of H_2O and one without. In both of the figures, a reference cell cycled in $LiPF_6$ is added for comparison to the current market leader electrolyte. These figures are also divided into voltage sections with vertical dashed lines. The sections, from left to right, are 4.2 V, 4.3 V and 4.3 V, respectively. All cycles are cycled at a c-rate of 1C, except the two initial cycles which are cycled at C/10.

In Figure 4.1a the discharge capacity for each cycle for the NMC_{111} cathode cycled in electrolytes without FEC is presented. The electrolytes without FEC show discharge capacities higher than the $LiPF_6$ reference throughout the entire 4.2 and 4.3 V regions.

The cell cycled in LiFSI shows discharge capacities of 114 mA g^{-1} for the two initial cycles with the lower c-rate. The increase of c-rate to 1C leads to a decline in the average capacities to 101 mA g^{-1}. Increasing the voltage up to 4.3 V causes the capacities to increase up to an average value of 111 mA g^{-1}. For the last voltage range, up to 4.4 V, a capacity fade occurs. Starting at 120 mA g^{-1} the capacity gradually decreases, reaching a final value of 117 mA g^{-1} which is slightly lower than the $LiPF_6$ reference cell. This indicates a capacity fade of 2.83 mA g^{-1}. The water containing electrolyte, with 1000 ppm of H_2O, also obtains discharge capacities above the $LiPF_6$ reference. The initial cycles show capacities of 113 mA g^{-1}. The following cycles at 1C show average capacities of 100 mA g^{-1}. For the increased voltage range up to 4.3 V average capacities of 111 mA g^{-1} are obtained. For the final voltage range, 3.0 - 4.4 V, an average capacity of 119 mA g^{-1} is observed. A small capacity fade of 0.86 mA g^{-1} is observed. However, this is much smaller than the fade observed for the cell without the water and the final capacity value is larger than both the LiFSI and the $LiPF_6$ cells.

The cells presented in these results are the cells that obtained the most stable potential profiles and cycling performances. However, several of the cells produced for this thesis show very unstable performance often causing the cycling program to stop completely. This is observed for several of the water containing electrolytes. In Appendix A all cells produced are provided together with details on if they completed cycling, if not the exact cycle number the cycling stopped is included. Also provided in the appendix, in Figure A.2a, is the average discharge capacities calculated for two parallels of the cells containing electrolytes without FEC. In general, the addition of a second parallel to the cycling performance values shows more deviations in capacity values compared to those shown in Figure 4.1a. Most notable is the much larger capacity fades observed for the water containing electrolytes.

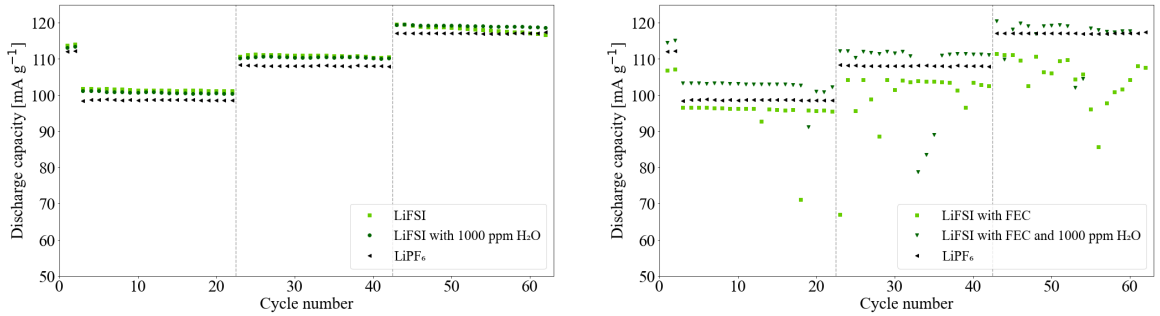

(a) Discharge capacity without FEC

(b) Discharge capacity with FEC

Figure 4.1: Discharge capacity for NMC_{111} cycled electrolytes a) without FEC and b) with FEC.

The discharge capacities of the FEC containing electrolytes are presented in Figure 4.1b. Compared to the capacities for the electrolytes without FEC, in Figure 4.1a, these show larger variation for the capacity values. For the cell containing the FEC electrolyte, the average capacities of the two initial cycles are 107 mA g^{-1}, which is lower than the reference. The lower capacities continue as the c-rate increases, with average values of 96 mA g^{-1} for 1C at 4.2 V. These values are relatively stable throughout the voltage range, except for the drops at cycle 13 to 93 mA g^{-1} and at cycle 18 to 71 mA g^{-1}. As the voltage range increases more variations in capacity can be seen, with the general trend lying around 103 mA g^{-1} for the 4.3 V voltage range. Drops are observed for cycles 23, 25, 27-28, 30, 38-39, with the minimum capacity at cycle 23 of 57 mA g^{-1}. A capacity fade of 1.84 mA g^{-1} can be observed for this voltage range. At the largest voltage range up to 4.4 V, another capacity fade of 3.87 mA g^{-1} is observed. In addition, several large drops in capacity can be seen with the largest drop observed at cycle 56 with a capacity of 86 mA g^{-1}. The cell containing the FEC and water electrolyte shows higher capacity values than the cell containing just FEC. The initial cycles at lower c-rate show average capacities of 115 mA g^{-1}, while the increased c-rate to 1C results in average capacities of 103 mA g^{-1}. For all cycles at the 4.2 V range, except cycle 19, the capacities are higher than the $LiPF_6$ reference. The drop at cycle 19 is relatively large, reaching a capacity of 91 mA g^{-1}. As the voltage range increases up to 4.3 V, the majority of the capacity values are above the reference cell values at 111 mA g^{-1}. A small drop is observed at cycle 25 to 110 mA g^{-1}, while a major drop is observed at cycle 33 to 79 mA g^{-1}. This is the

lowest capacity value of all cycles. In addition, a small fade of 1.02 mA g^{-1} can be observed for this voltage range. At the largest voltage range a capacity fade of 2.69 mA g^{-1} is observed. The final cycles are not included due to the cycling ending at cycle 60.

Figure A.2b in Appendix A.1 presents the average discharge capacities for the two parallels of cells cycled in the different FEC containing electrolytes. Similar to the discharge capacities for the cells without FEC, these also show more deviations in capacity values. Notable is that the additional parallels added for the FEC containing cells did not complete the cycling. This is a result of the FEC containing cells having the same problem with the stop in cycling as the water containing cell without FEC, as can be seen in Table A.1.

Figure 4.2 shows the coulombic efficiencies achieved for each cycle during cycling of NMC_{111} cells in LiFSI electrolytes a) without FEC and b) with FEC. Both figures show one parallel without additional water and one with a water content of 1000 ppm. In addition, a NMC_{111} cathode cycled in the commercial market leader electrolyte, $LiPF_6$, is also added to the figures as a reference. The figures are divided into voltage sections, as explained previously.

In Figure 4.2a the electrolytes without FEC show stable coulombic efficiency values. At the initial cycles of the C/10 at 4.2 V, 1C at 4.2 V and the 4.3 V region, drops in the coulombic efficiencies can be seen for both electrolytes. The cell with LiFSI electrolyte cycles 1 and 3 has efficiencies of 87.41 % and 90.15 %, respectively. These cycles for the cell with the water containing electrolyte show similar efficiencies of 87.00 % and 89.62 %, for cycles 1 and 3, respectively. The drop at cycle 23 is the largest for LiFSI with efficiencies of 81.17 %, smaller for the water containing electrolyte with 84.80 % and smallest for the $LiPF_6$ electrolyte, 87.29 %. This drop does not occur during the initial cycle in the 4.4 V region. The remaining cycles at these voltage ranges show coulombic efficiencies equal to the $LiPF_6$ reference, with values in the range of 99.1-98.8 % for LiFSI and of 99.1-98.5 % for the water containing electrolyte. However, at 4.4 V a gradual decline in efficiency is observed for the LiFSI cell. The decrease stops at 97.67 %, causing an efficiency loss of 1.03 % for the 4.4 V range.

The average coulombic efficiencies are presented in Appendix A.1 in Figure A.1a. Similar to the discharge capacity results, these also present more deviations in efficiency values due to the poorer performance of the additional cycle.

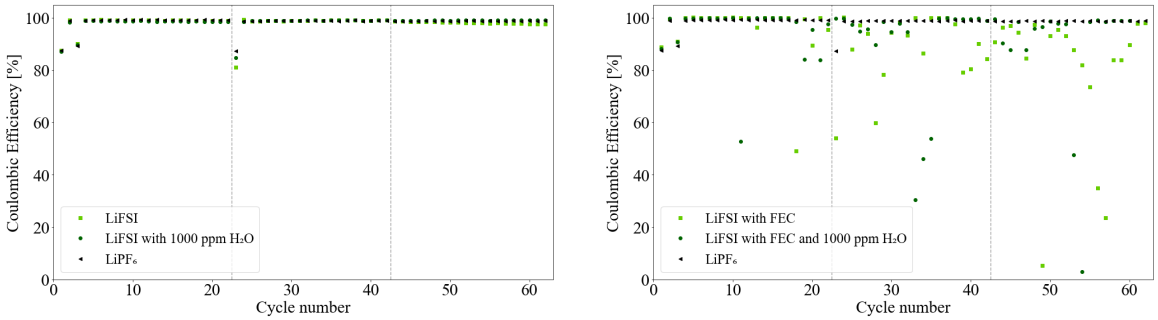

(a) Coulombic efficiency without FEC

(b) Coulombic efficiency with FEC

Figure 4.2: Coloumbic efficiency for NMC_{111} cycled electrolytes a) without FEC and b) with FEC.

The coulombic efficiencies for the cells cycled in the FEC containing electrolytes are presented in Figure 4.2b, plotted together with the same $LiPF_6$ containing cell for reference. Easily observed by comparing these with the cells not containing FEC is that these have much more deviations of efficiencies and larger drops. The initial drops for cycles 1 and 3 are observed for the FEC containing electrolytes as well, with drops to 88.72 % and 91.06 %, respectively for the FEC containing electrolytes and to 88.17 % and 90.76 % for the FEC and water containing electrolyte. These drops are similar to the equivalent drops for the electrolytes without FEC. For the FEC containing cells, the efficiencies in the first cycles are similar to that of the $LiPF_6$ reference, with values that are slightly larger at 100.12 % to 99.8 %. The first deviation can be seen at cycle 13, with a drop down to 96.30 %. Then, at cycle 18 a large drop down to 49.11 % is observed which can be marked as the beginning of a continuous deviation in the efficiencies that lasts throughout the remaining cycles. These drops for the efficiencies are quite large, with a minimum value at cycle 49 at 5.29 %. For the cell with FEC and water containing electrolyte, the deviations from the reference cell values are smaller compared to the electrolyte without water. In addition to the drops in cycles 1 and 3, this cell also shows a rather large drop in cycles 11 to 52.81 %. Then until cycle 18, the cell shows efficiencies just above the reference value of the $LiPF_6$ cell around 99.8 %. From cycle 18 in 4.2 V to cycle

36 in 4.3 V, a large variation of coulombic efficiencies is observed. The majority of the drops are not that large, with values between 10-15 %. However, at cycle 33 a large drop down to 30.48 % is observed before the cell gradually reaches the reference values. Throughout the last part of the 4.3 V range until cycle 44, the cell shows stable efficiency values. A deviation can be seen from cycle 44 to 49, with a minimum of 87.64 %. At cycle 53 the largest drop starts, ending at a coulombic efficiency of 2.91 % at cycle 54. This is the lowest efficiency obtained for all of the cells listed in these results. However, after this drop, the values again reach the reference values which hold steady until the cycling is complete.

In Appendix A.1 Figure A.1b, the average coulombic efficiencies of the FEC containing cells is shown. These efficiencies are similar to those presented for the parallels in Figure 4.2b. Note that the additional parallels used for the average efficiencies stopped cycling during the galvanostatic cycling program. Information on the exact cycles are presented in Table A.1.

4.1.2 Potential Profiles from Galvanostatic Cycling

This section provides the potential profiles for NMC_{111} cathodes produced by galvanostatic cycling in the different electrolytes, in addition to the $LiPF_6$ reference cell. These profiles are the most steady ones for each electrolyte, an additional parallels are provided in Appendix A.2. The cycling program used is stated in the experimental section of this thesis.

In Figure 4.3 the potential profile of an NMC_{111} cathode cycled in $LiPF_6$ electrolyte is presented. In the potential profiles no slow charges or other discrepancies can be observed.

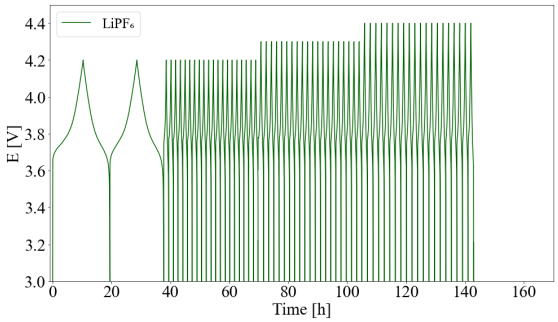

Figure 4.3: Galvanic cycling of NMC_{111} in $LiPF_6$

In Appendix A.2 a plot including an additional parallel of the $LiPF_6$ cycled cell is presented in Figure A.3. As observed the additional cell shows equally stable cycling, completing the cycling program at similar times.

In Figure 4.4 the potential profiles obtained during galvanostatic cycling of NMC_{111} in a) LiFSI and b) LiFSI with 1000 ppm of H_2O is shown as cell potential versus time. For the LiFSI electrolyte, the potential profile shows no delay of charging or discharging during the cycle program. However, as the potential range increases with voltages up to 4.3 V the transition appears irregular. This is not due to any instabilities in the cycling, but due to the cycling being performed in two portions and the two potential profiles added together afterwards.

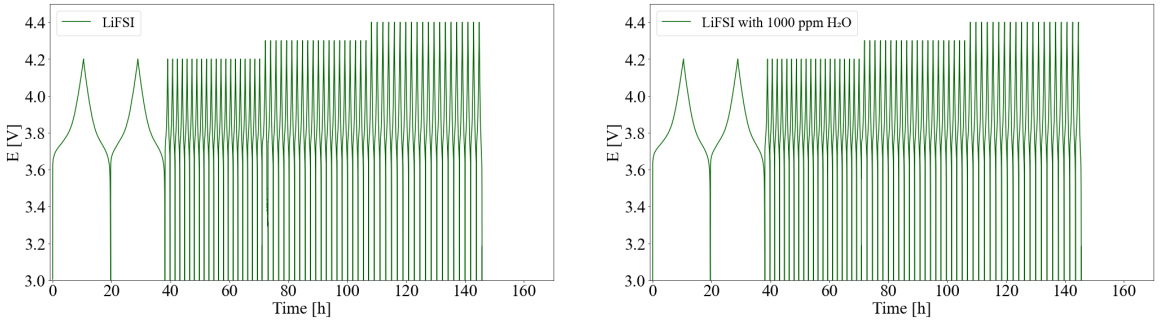

(a) LiFSI

(b) LiFSI with 1000 ppm H_2O

Figure 4.4: Galvanic cycling of NMC_{111} in electrolytes without FEC

The potential profile of the water containing cell is shown in Figure 4.4b. Also in this potential profile, no delays in charging or discharging are observed. The same two

cycling programs were used for this cell as for the LiFSI. However, no mismatch can be observed in the transition from 4.2 V to 4.3 V for this cell. Overall the electrolytes with no FEC complete the cycling program in times similar to the $LiPF_6$ reference cell with charging and discharging times only slightly longer than the reference, reflecting the similar capacities obtained.

Additional potential profiles for the additional parallels used in the average calculations for the discharge capacity and the coulombic efficiencies are presented in Appendix A.2. In Figure A.4 these are shown for cells cycled in a) LiFSI and b) water electrolytes. For the LiFSI electrolyte in Figure A.4a the potential profile for the second parallel is relatively similar to the first, except for some small deviations in charging times causing the poorer average cell performance observed. For the water containing electrolyte, in Figure A.4b, the second parallel completes the cycling program in a much shorter time. This could cause poor capacity retention observed for the average discharge capacities.

In Figure 4.5 the potential profiles for the NMC_{111} cathodes cycled in the FEC containing electrolytes are shown with the potential as a function of time. Figure 4.5a shows the cycling for the FEC containing electrolyte. An abnormal potential profile is observed upon charging at cycles 18, 49, 56 and 57. The cell fails to charge, indicating leak currents inside the cells. These abnormal profiles lead to abnormal coulombic efficiency values.

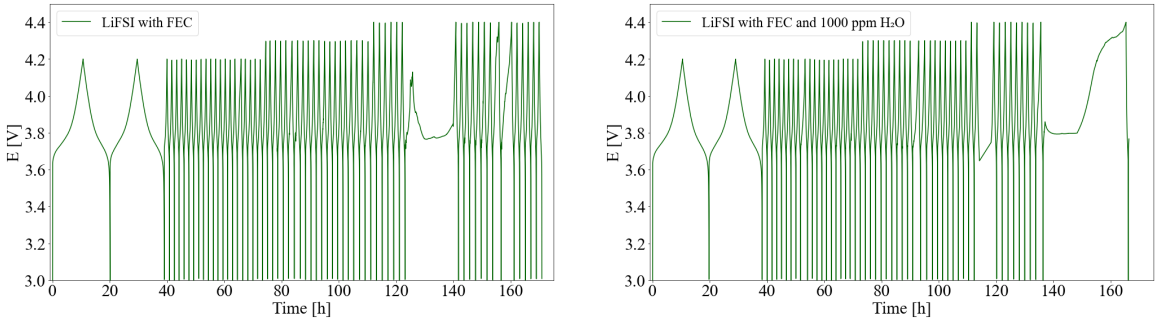

(a) LiFSI with FEC

(b) LiFSI with FEC and 1000 ppm H_2O

Figure 4.5: Galvanic cycling of NMC_{111} in electrolytes with FEC

In Figure 4.5b the potential profile for the electrolyte containing both FEC and

1000 ppm of H_2O is presented. The cell does not complete the galvanostatic cycling program but stops cycling after cycle 54. In addition to the very slow charging at cycle 54, slow charges can be observed at cycle 11, cycle 33 and cycle 45. Where the delay in charging time increases for each of the cycles.

For easier visualisation of the problematic cycles for the FEC containing electrolytes, the discussed cycles have been put into a common plot in Figure 4.6 for both the a) FEC and b) FEC and water containing electrolytes. Each of the cycles has been marked with its respective cycle numbers.

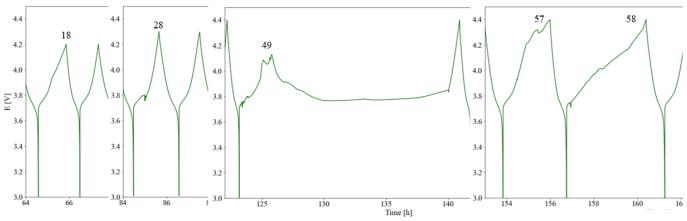

(a) LiFSI with FEC

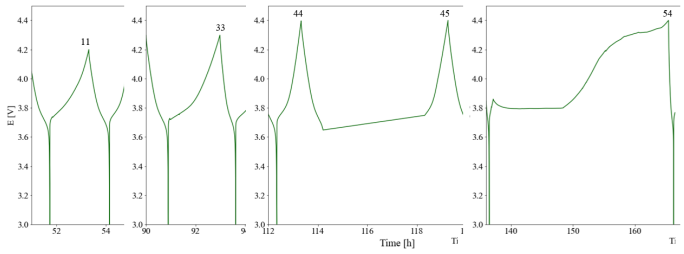

(b) LiFSI with FEC and 1000 ppm H_2O

Figure 4.6: Outcuts of galvanic cycling of NMC_{111} in electrolytes with FEC

The additional parallels for the FEC containing cells are presented in Figure A.5 in Appendix A.2. These also fail to charge sufficiently causing the cell to stop during the cycling program. In Table A.1, the cycle numbers this occurred at is provided.

Leak Currents during Galvanostatic Cycling

As mentioned previously, a large amount of the cells manufactured did not complete the galvanostatic cycling program. As observed from Table A.1, this was mainly an issue for the cells containing either the water or the FEC, or both. As observed from

Figure 4.6, the issue occurred during the charging of the batteries, i.e. as the Li is drawn out of the cathode. Also observed from the potential profiles of the FEC containing cells, is that the charging of the subsequent cycle caused no abnormalities in the potential profiles. This suggests that the charging problems are a result of leak currents in the battery. Cause if these were used for something else, this could impact the cycling performance of the cell on the subsequent cycle. Eventually, the insufficient charging continued for such a large time interval causing the potential to drop and the cycling program was stopped.

4.1.3 Post Mortem Characterisation

SEM Imaging

Figure 4.7 shows the SEM images obtained for four NMC_{111} cathodes each cycled in one of the four LiFSI electrolytes, a) LiFSI, b) LiFSI with 1000 ppm of H_2O, c) LiFSI with FEC and d) LiFSI with FEC and 1000 ppm of H_2O. All images are taken with similar magnifications.

The images are quite similar, with no major differences between the cathodes cycled in the different electrolytes. On the surfaces, lighter spheres can be observed together with a darker more porous background. Cracks are observed in all samples to some extent. However, these can also develop due to the handling of the cathodes both before and after cycling. So as no major differences in the number of cracks were observed, these are not considered.

The SEM imaging for the uncycled cathode and the $LiPF_6$ reference cell can be seen in Figure 4.8 a) and b), respectively. These are taken at the same magnification as the cathode cycled in the different LiFSI electrolytes. The surfaces are quite similar to the SEM images in Figure 4.7. Therefore, no major differences in the surface morphology can be observed after the cycling of the cathodes in either the LiFSI or the $LiPF_6$ electrolytes as they are indistinguishable from the uncycled cathode surface.

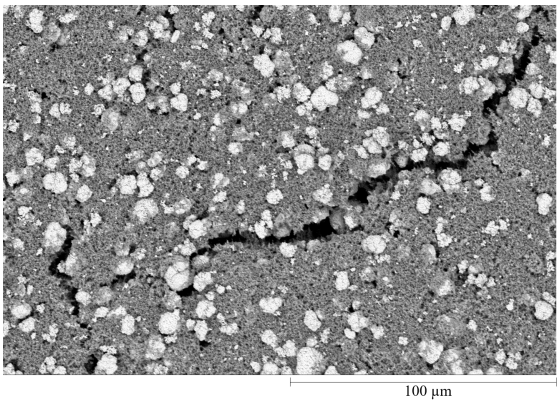

(a) LiFSI

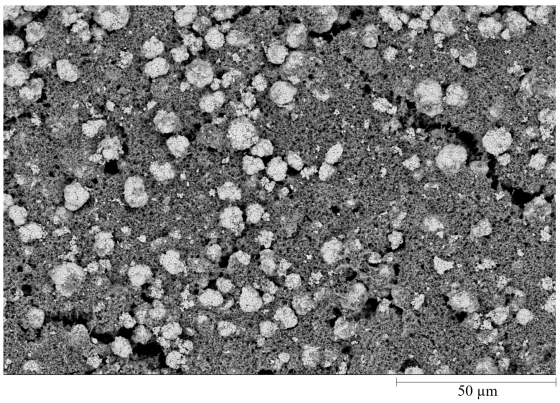

(b) LiFSI with 1000 ppm of H_2O

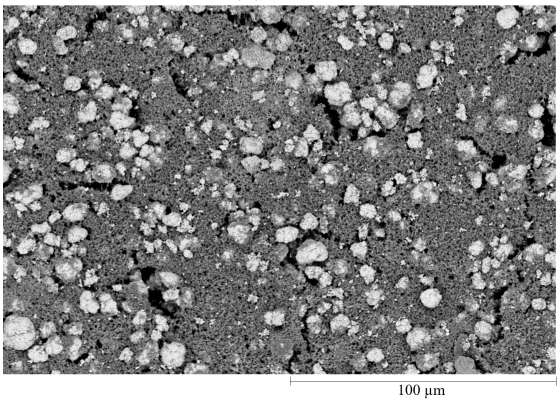

(c) LiFSI with FEC

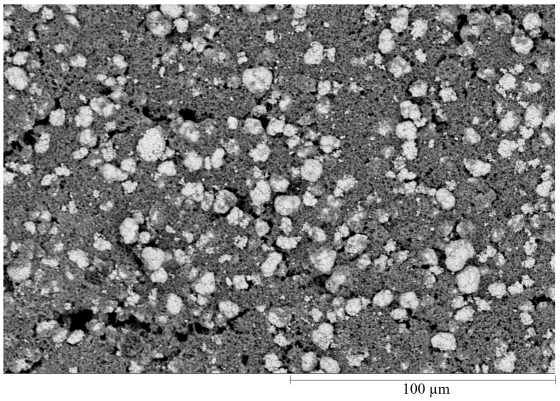

(d) LiFSI with FEC and 1000 ppm of H_2O

Figure 4.7: SEM images of NMC_{111} cathodes cycled in the galvanostatic cycling program in the different electrolytes.

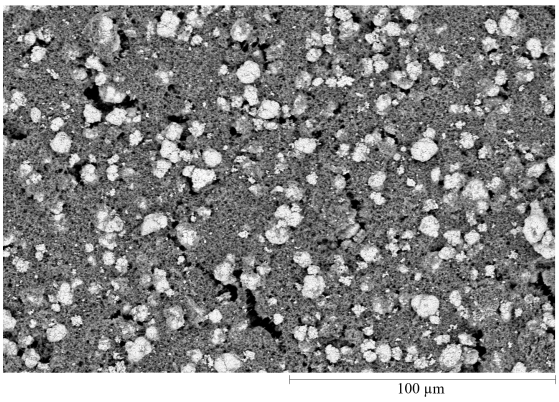

(a) Pristine

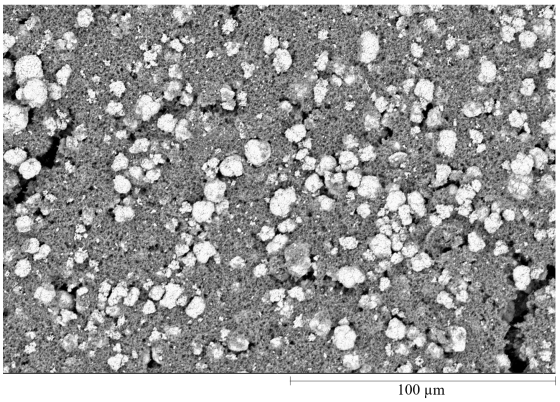

(b) LiPF6

Figure 4.8: SEM images of a) pristine NMC_{111} cathode and b) NMC_{111} cathode cycled in a $LiPF_6$ electrolyte.

EDS Analysis

The following figures show the EDS analysis performed for NMC_{111} cathodes cycled in the four different LiFSI electrolytes for the following elements b) Carbon, c) Chlorine, d) Cobalt, e) Fluorine, f) Manganese, g) Nickel, h) Oxygen and i) Sulphur. Figure a) shows the image of the surface with the EDS images layered on top.

The EDS analysis of a pristine NMC_{111} cathode is shown in Figure 4.9.

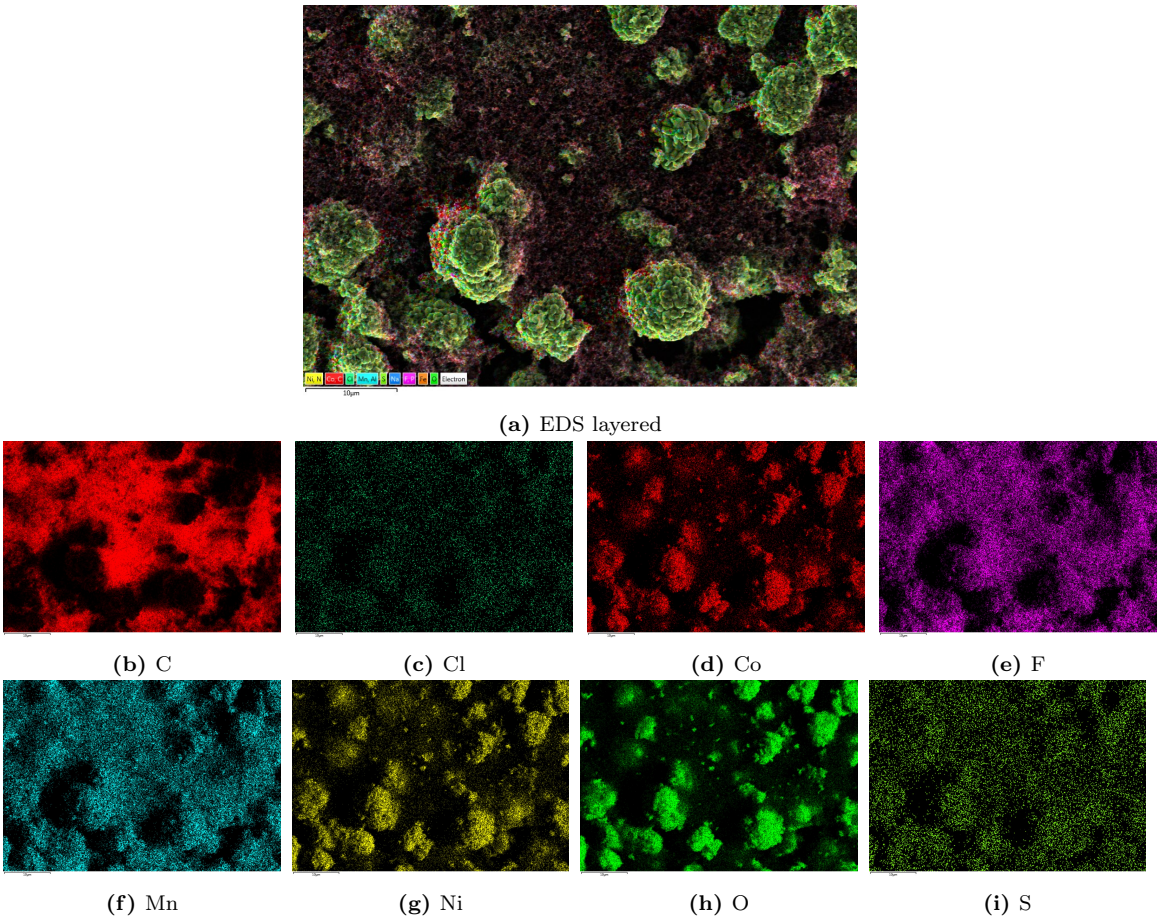

(a) EDS layered

(b) C **(c)** Cl **(d)** Co **(e)** F

(f) Mn **(g)** Ni **(h)** O **(i)** S

Figure 4.9: SEM with EDS uncycled NMC_{111} cathode

The analysis shows that the previously mentioned spheres consist of Co, Mn, Ni and O, from Figure 4.9 d), f), g) and h). This composition correlates with the composition of the active material in the $LiNi_xMn_yCo_z$ cathodes. The Li in the cathodes are not

detectable in EDS analysis. From both the Co, Ni and O figures it can quite clearly be seen that the majority of the elements are found in the spheres. However, the Mn content can be seen in the background as well. Some areas have no Mn content, these areas are mainly the craters around the spheres and not on the spheres. The more porous background consists mainly of C and F from the carbon black and PVDF used in the binder. The Mn content is as mentioned observed on the entire surface, the same can also be seen for the S and Cl content but at lower concentrations.

EDS analysis was also performed on the surfaces of the NMC cathodes cycled in the different LiFSI electrolytes, shown in Appendix A.3. From these, no significant differences in the surface composition can be observed compared to the analysis of the pristine cathode surface.

4.2 Effect of FEC and Water on Al foils

4.2.1 Cyclic Voltammograms of Al foils

Cells made from an Al current collector as a working electrode were cycled using cyclic voltammetry. The cyclic voltammograms for 6 subsequent cycles for Al foil cycled in the electrolytes without FEC are shown in Figure 4.10, for a) LiFSI electrolyte and b) 1000 ppm of H_2O electrolyte.

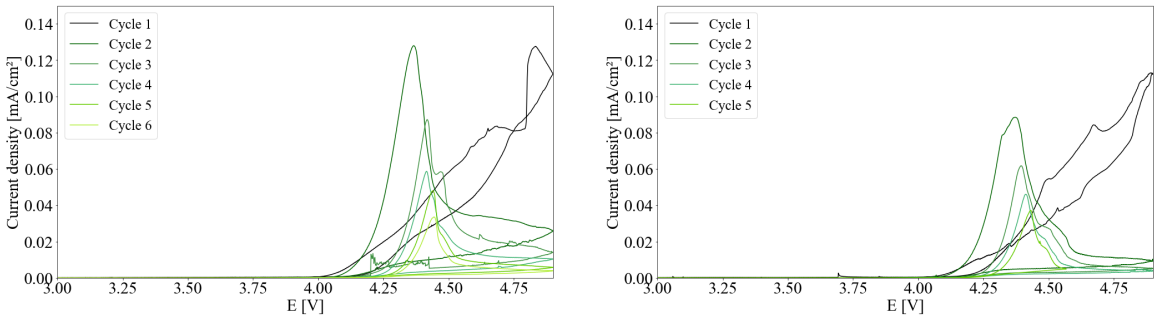

(a) LiFSI

(b) LiFSI with 1000 ppm of H_2O

Figure 4.10: Cyclic voltammetry of Al foils cycled in electrolytes without FEC for 6 cycles.

Figure 4.10a shows the current densities achieved as potentials are applied to the Al

foil cell with LiFSI electrolyte. The maximum current densities of each cycle from cycle one to six are summarised in Table 4.1. These values show that the current densities fade as the cycle number increases from cycle 2 to 6. However, a small increase in the current density can be seen from cycles 1 to 2. The onset potentials are also summarised, shown in Table 4.2. In this thesis, the onset potential is defined as the potential in which the current density exceeds 0.001 mA cm^{-2}, which is the average maximum current densities of the Al foils cycled in the $LiPF_6$ electrolyte. For the Al foil cycled in the LiFSI electrolyte the onset potential is 4.273 V. The current densities for the Al foil cycled in the LiFSI electrolyte containing water are shown in Figure 4.10b. Note that the cell failed after 5 cycles, the reason for this sudden stop in cycling is unknown. The maximum current densities are listed in Table 4.1 for cycle 1 to 5. The current densities fade as the cycle number increases. Compared to the LiFSI electrolyte, the current densities of the water containing electrolyte are slightly lower. The onset potential is 4.296 V, which is only slightly higher compared to the LiFSI electrolyte. Higher onset potentials indicate that the surface tolerates higher applied potentials before the Al surface starts corroding. However, the differences here do not have a significant impact. For both the Al foils cycled in the non FEC electrolytes the first cycle differs largely in shape compared to the other cycles. For the LiFSI, the second cycle has a slightly higher current density, while for the water containing electrolyte the second cycle has a significantly lower current density.

In Figure 4.11 the current-potential profiles for the Al foils cycled in the FEC containing electrolytes are presented. For both the a) FEC containing and b) FEC and 1000 ppm H_2O containing electrolyte, the shapes of all cycles are fairly similar.

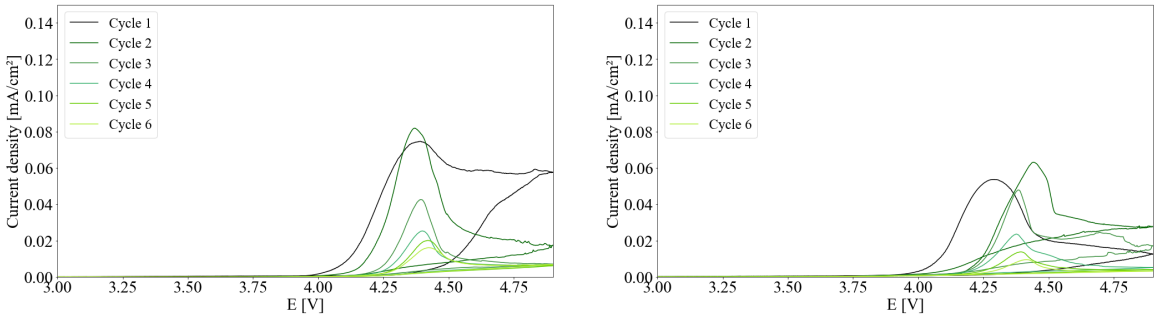

(a) LiFSI with FEC

(b) LiFSI with FEC and 1000 ppm of H_2O

Figure 4.11: Cyclic voltammetry of Al foils cycled in electrolytes without FEC for 6 cycles.

For the FEC containing electrolyte in Figure 4.11a current densities for cycle 1 to 6 are listed in Table 4.1. Compared to the electrolytes without FEC the current densities are lower in the equivalent cycles. The highest current density of the FEC containing electrolyte is similar to the current densities of cycle 3 for the LiFSI electrolyte and cycle 2 for the water containing electrolyte. The onset potential for this electrolyte is 4.28316 V, this is fairly similar to the non FEC electrolytes. The voltammograms of the FEC containing electrolyte with a water content of 1000 ppm H_{20} are shown in Figure 4.11b. The current densities of cycles 1 to 6 are listed in Table 4.1. These current densities are even lower than the current densities of the FEC containing electrolytes, with the highest value corresponding to that of cycles 4 and 3 of the non FEC electrolytes, without and with additional water respectively. The onset potential for the Al foil cycled in the FEC and water containing electrolyte is 4.228 V, which is the lowest onset potential of all the four electrolytes. However, the onset potentials for the four electrolytes do not differ significantly for all values in the 4.2 V range. For both the FEC containing electrolytes, the second cycle has a higher maximum current density than the first cycle. From cycles 2 to 6 the current densities fade as the cycle number increases.

Compared to the previous testing of similar electrolytes for the project work, presented in Figure D.1 in Appendix D.1, these have lower current densities. The shapes of the new FEC figures also have slightly deviating shapes. This can be related to the time after manufacture the electrolyte was utilised, as the degradation of FEC can have an impact on the cycling. This will be further elaborated in Section 4.3.

Figure 4.12 shows cycling of the Al foil in the $LiPF_6$ reference electrolyte. Where the maximum current density of the first cycle 0.001 mA cm^{-2}, observed in the zoomed plot, is used as the reference value for the onset potentials.

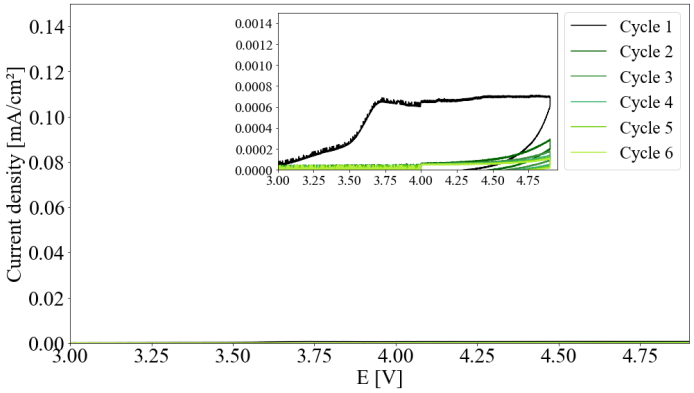

Figure 4.12: Cyclic voltammetry of Al foil in $LiPF_6$ electrolyte

Table 4.1 summarises the maximum current densities of each cycle for all four electrolytes in mA cm^{-2}.

Table 4.1: Maximum current density [mA cm^{-2}] of each cycle for Al foil cycled in the different electrolytes for 6 cycles.

Electrolyte	Cycle 1	Cycle 2	Cycle 3	Cycle 4	Cycle 5	Cycle 6
LiFSI	0.128	0.128	0.087	0.058	0.040	0.034
LiFSI H_2O	0.113	0.088	0.062	0.046	0.037	-
LiFSI FEC	0.075	0.082	0.043	0.025	0.020	0.016
LiFSI FEC+H_2O	0.054	0.063	0.0479	0.024	0.014	0.009

Additional first cycle voltammograms for all electrolytes are plotted together in Figure 4.13. In addition, a cycle for a $LiPF_6$ electrolyte is plotted together as its maximum current density is used to find the onset potentials. To mark the onset potentials of the different electrolytes, dots in similar colours as the cycles are placed.

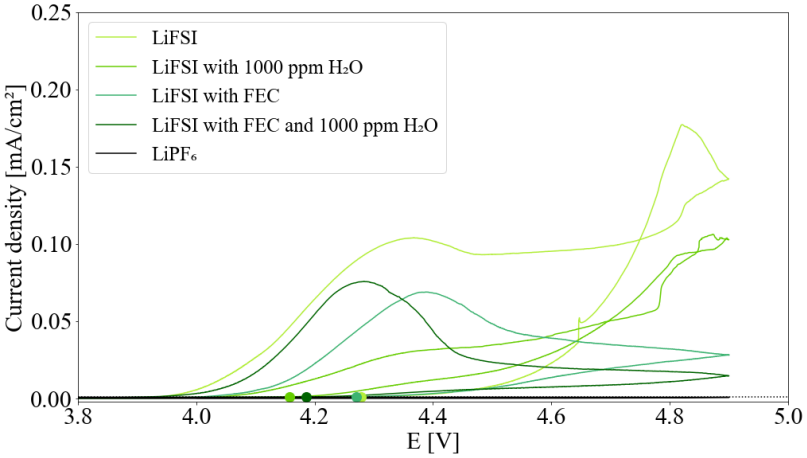

Figure 4.13: Cyclic voltammetry of Al foils cycled in all electrolytes for only 1 cycle.

Table 4.2 the onset potential for corrosion of the aluminium current collector for all four electrolytes are presented, for parallels in Figures 4.10, 4.11, 4.13, B.1. As there is no standard method for determining the onset potential, it was done based on a current density of 0.001 mA cm^{-2}. This is the average maximum current density of two Al foil cells cycled in $LiPF_6$ achieves in the first cycle. The calculated average onset potentials are also included. These show that the water containing electrolyte has the lowest onset potential, followed by the FEC and water containing. Both the electrolytes without water have higher onset potentials, with the FEC electrolyte having the highest.

Table 4.2: Onset potentials for Al foils cycled in the different electrolytes.

	Onset potentials [V]			
Electrolyte	*6C*	*1C p1*	*1C p2*	*Average*
LiFSI	4.273	4.279	4.233	4.262
LiFSI H_2O	4.296	4.163	4.157	4.205
LiFSI FEC	4.283	4.293	4.270	4.282
LiFSI FEC+H_2O	4.228	4.185	4.246	4.220

The maximum current densities for the first cycles in Figures 4.10, 4.11, 4.13, B.1 are listed in Table 4.2. In the table the parallels are denoted as 6C for the cell cycled six

times, 1C p1 for the cell cycled once presented in the results and 1C p2 for the cell cycled once presented in the Appendix. From these values average maximum current densities are also included in Table 4.2, for better comparability. These averages show that the FEC and water containing electrolyte achieves the lowest current density, with only a slight increase for the FEC electrolyte. The cells without FEC have the highest current density values, with the pure LiFSI electrolyte showing the highest oxidative currents on the aluminium current collector.

Table 4.3: Onset potential and the maximum current density of Al foils cycled in the different electrolytes for 1 cycle.

	Current density [mA cm^{-2}]			
Electrolyte	*6C*	*1C p1*	*1C p2*	*Average*
LiFSI	0.128	0.177	0.132	0.145
LiFSI H_2O	0.113	0.106	0.094	0.105
LiFSI FEC	0.075	0.069	0.079	0.074
LiFSI FEC+H_2O	0.054	0.076	0.057	0.064
$LiPF_6$	-	0.001	0.001	0.001

4.2.2 Post Mortem Characterisation

SEM Imaging

Figure 4.14 shows the SEM imaging of the Al surfaces cycled in the electrolytes without FEC, for both one and six cycles. The LiFSI electrolyte is shown in the first two images, showing the cell cycles for a) 1 cycle and b) 6 cycles. Distinct differences can be seen from one to six cycles. In Figure 4.14a a large abundance of pits can be observed on the surface due to the Al corrosion. Small areas with darker spots can be observed as well. For the 6 cycle cell in Figure 4.14b the area that these dark spots have increased. Additionally, darker spots can be observed within these areas. The amount of pitting occurring on the surface is relatively equal to that observed on the Al surface only cycled once. For the LiFSI electrolyte containing 1000 ppm of H_2O the cells cycled for one and six cycles can be seen in Figure 4.14 c) and d), respectively. On the aluminium surface of the cell only cycled once, in Figure 4.14c, pits are observed in addition to a larger amount of the darker spots on

the surface. Compared to the Al cycled once in the LiFSI electrolyte the amount of pits on the Al cycled in the water containing electrolyte is less. However, the area covered by the darker spots is larger. The surface of the Al foil cycled in the water containing electrolyte for 6 cycles, in Figure 4.14d, shows the same tendency as the LiFSI electrolyte. The additional cycles have led to an increase in the darker areas over the surface however the amounts of pits observed are also larger. Note that the magnification for the surface cycled for 6 cycles is slightly larger than for the three other images. Also notable is that the striped surface texture observed on all of the surfaces is a result of the polishing of the Al foil during manufacture.

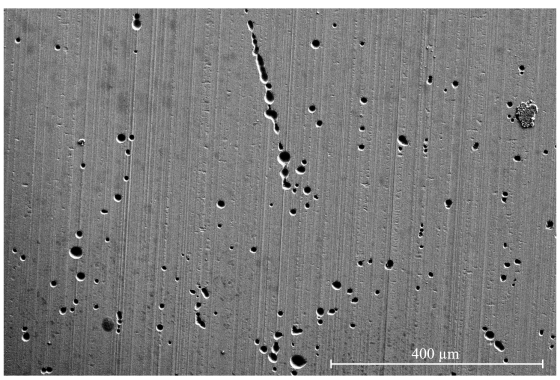

(a) LiFSI 1 cycle

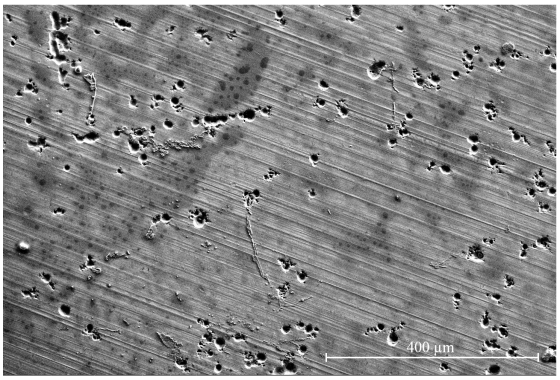

(b) LiFSI 6 cycles

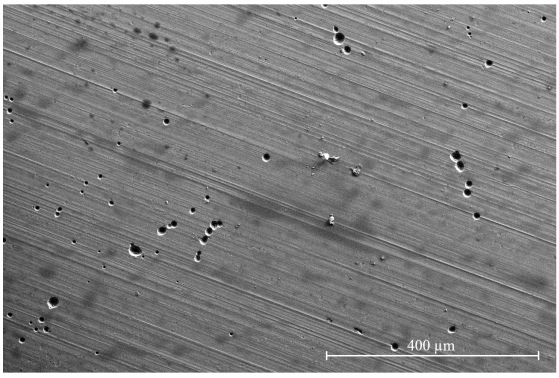

(c) LiFSI with 1000 ppm H_2O 1 cycle

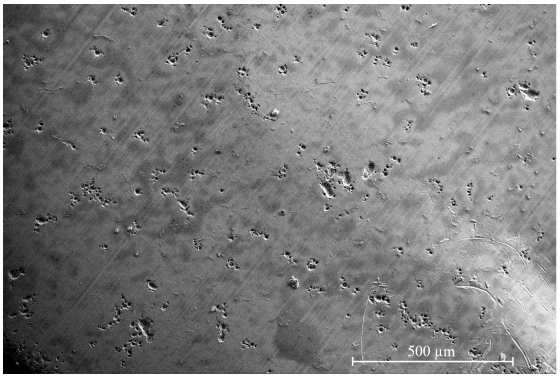

(d) LiFSI with 1000 ppm H_2O 6 cycles

Figure 4.14: SEM imaging of Al foils cycled for 1 and 6 cycles in electrolytes without FEC.

The SEM imaging of the FEC containing electrolyte is shown in Figure 4.15, where a) and b) shows the aluminium surface cycled in the LiFSI electrolyte with FEC for 1 and 6 cycles respectively. The surface cycled for one cycle, in Figure 4.15a, shows almost

no dark spots on the surface and little pitting compared to the aluminium cycled in the electrolytes without FEC. The aluminium cycled for six cycles, in Figure 4.15b, shows a similar degree of pitting corrosion on the surface as the surface cycled for one cycle. However, the amount of the darker layer covering the surface is much more prominent compared to the 1 cycle. In comparison to the darker spots on the Al surfaces of the cells cycled without FEC for 6 cycles, the darker area on the FEC containing electrolyte seems to be much more of a surface layer as both more cracks and deposits from the layer are observed on the surface.

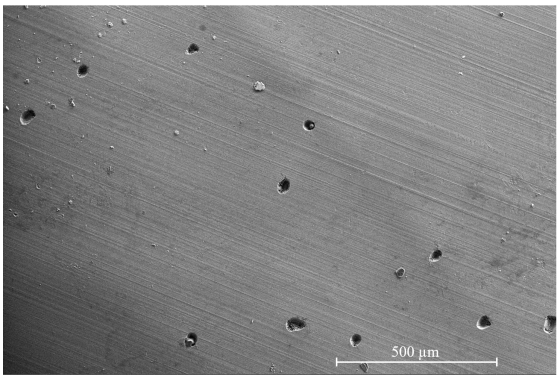

(a) LiFSI with FEC 1 cycle

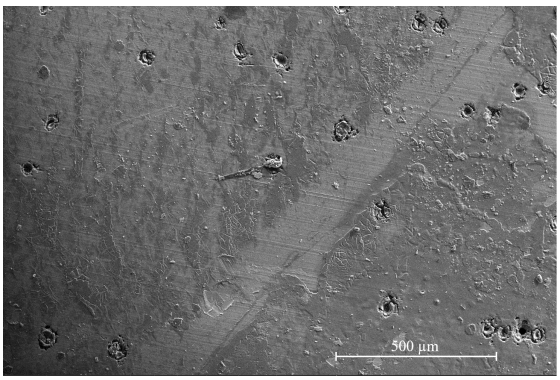

(b) LiFSI with FEC 6 cycles

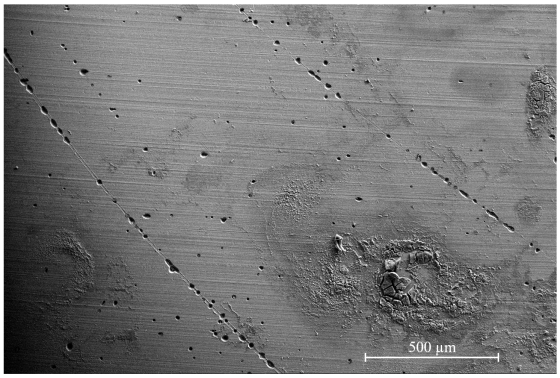

(c) LiFSI withFEC and 1000 ppm H_2O 1 cycle

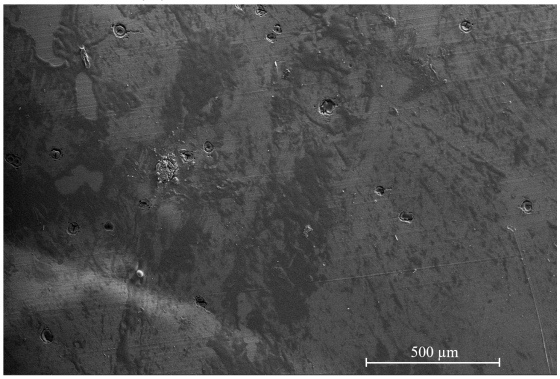

(d) LiFSI with FEC and 1000 ppm H_2O 6 cycles

Figure 4.15: SEM imaging of Al foils cycled for 1 and 6 cycles in electrolytes with FEC.

The aluminium surfaces that have been cycled in the FEC and water containing electrolyte for one and six cycled can be seen in Figure 4.15 c) and d). For the surface cycled once, in Figure 4.15c, a large deposit of some sort can be observed in addition to the pitting corrosion. Around the deposit, the same darker spots as

observed in the previous images can be observed to a larger extent than for the FEC containing electrolyte but quite similar to the water containing electrolyte. For the aluminium cycled for six cycles, in Figure 4.15d, in the FEC and water containing electrolyte the thicker darker layer on top of the aluminium surface as observed for the Al foil cycled for six cycles in the FEC containing electrolyte can be seen. In addition to some pitting corrosion and deposits, the amount of pits observed on this surface is quite small.

Comparing all the SEM imaged in Figure 4.14 and Figure 4.15 its clear to see that the FEC containing electrolytes create a much thicker surface layer compared to the non FEC containing electrolytes. For the electrolytes without FEC more pitting corrosion of the aluminium surface is observed, this correlates with the higher current densities observed for the electrolytes without FEC.

GDOES Analysis

This section provides the results obtained from the GDOES analysis. This measurement technique is normally done on hard samples, which is the reason for attaching them to the steel plate as shown in the experimental section. However, as the instruments creates the plasma the attachment was not sufficient causing some of the samples to get sucked into the chamber. This caused instabilities in the measurements, as can be seen on some of the curves. One of the samples, Al foil cycled in LiFSI electrolyte with 1000 ppm of H_2O, had serious instability issues, and its result is therefore not included. Some measurements irregularities in the peaks can be observed, this is a result of the samples not sticking properly to the substrate. For each measurement the peaks of the relevant elements are included, these are Aluminium, Lithium, Sulphur, Carbon, Oxygen, Chlorine, Hydrogen and Fluorine.

The GDOES measurements taken of a pristine Al foil are presented in Figure 4.16. No major peaks are observed for this sample, and the Al peak rises fairly quickly indicating no major surface layer on this. Smaller peaks for O, C and H are observed.

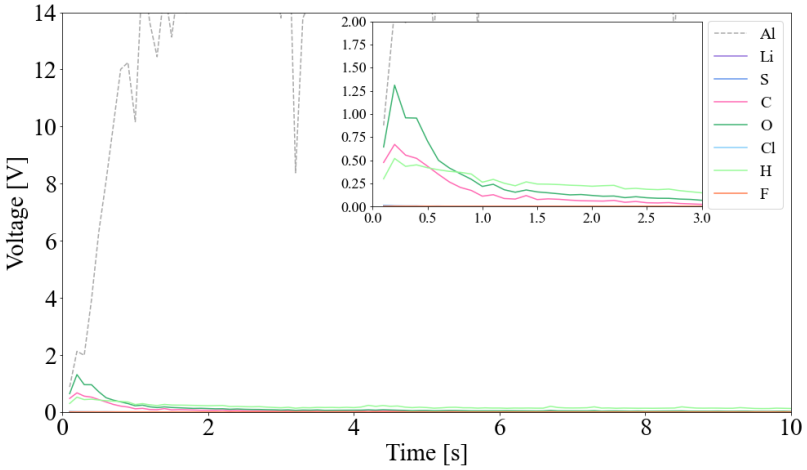

Figure 4.16: Pristine Al

GDOES results of Al foil cycled in $LiPF_6$ for 6 cycles are shown in Figure 4.17. A strong signal for Li is observed, however the signal is short, indicating that the element is mainly present at the outer surface and that the surface layer is thin. The smaller S peak is similar to the Li peak in shape, indicating that this element is also present only on the outer surface. The C, O and H shapes have a more gradual decrease in voltage, indicating that these are present further into the sample. The Al peaks show a steep incline, this could indicate that the film on the surface, most likely Al_2O_3, is very thin.

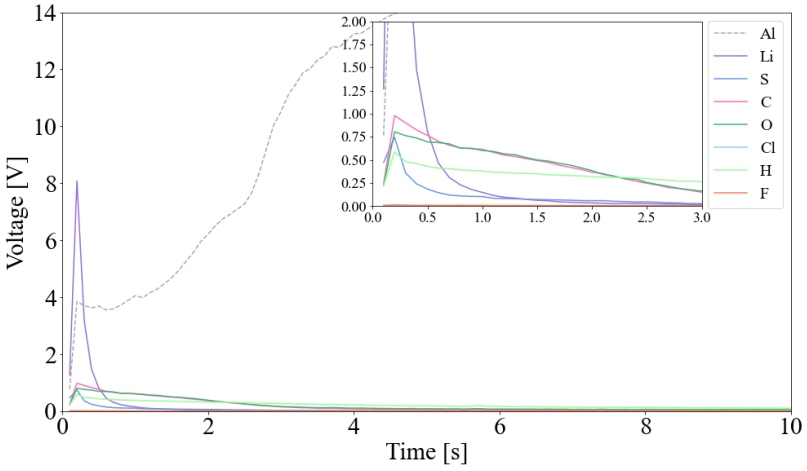

Figure 4.17: $LiPF_6$

The aluminium samples cycled in the LiFSI electrolyte are shown in Figure 4.18, where a) shows the 1 cycle sample and b) shows the 6 cycle sample. In Figure 4.18a the sample cycled only once shows a short but sharp peak for Li. For the S, C and H that have lower peaks the maximum voltage for the peak are observed at 0 s. This indicates that most of the products are present on the outermost surface, while only smaller amounts are present further into the sample. The O peak observed is wider, however the measurements taken are unstable as can be seen from the irregularities on the lines which makes it harder to say something about the thickness of the film. The sample cycled for 6 cycles, in Figure 4.18b, shows a more stable measurement. The Li peak on this sample is equal to that of the cell cycled once. The S peak observed is higher and wider than the Li peak, indicating that it is present both further into the sample and at a higher content than the Li. Wider more wavelike peaks are observed for O and C, this indicates that these are not present on the outer surface but further into the sample. The H levels are stable throughout the entire measurement, which could be the result of its presence in the air, as it does not disappear as the signal continues as the bulk Al is reached.

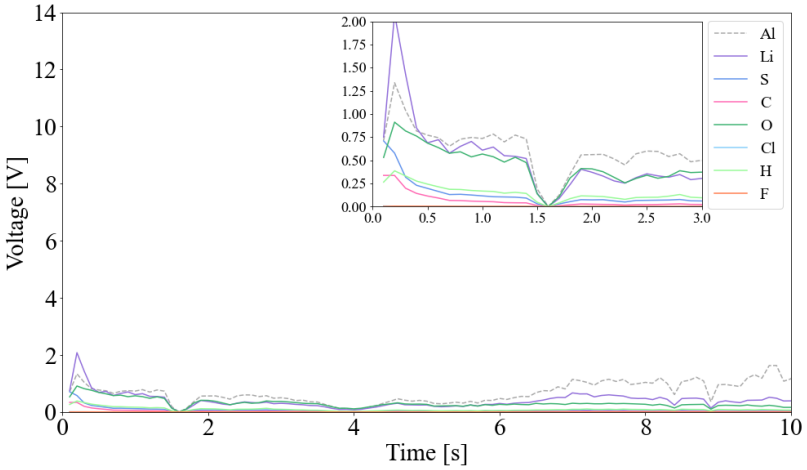

(a) LiFSI 1 cycle

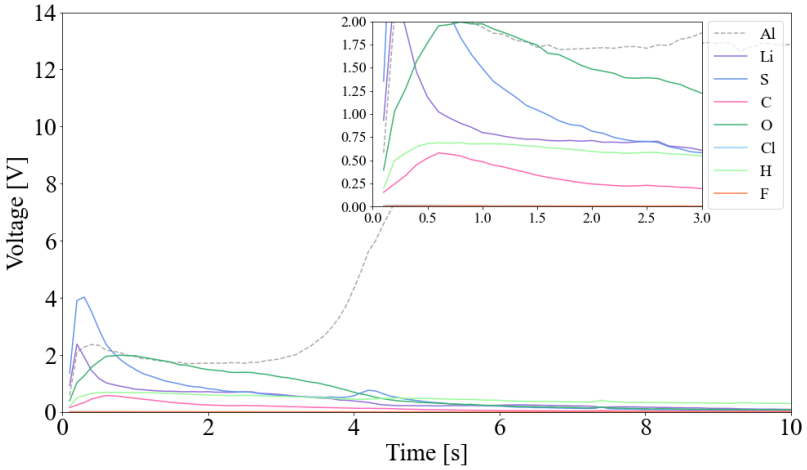

(b) LiFSI 6 cycles

Figure 4.18: GDOES analysis on Al foils cycled in LiFSI without FEC for 1 and 6 cycles.

For the aluminium surfaces cycled in the LiFSI electrolyte, more and higher signals are observed for the Al cycled for six cycles. This could indicate that the surface film mainly forms after the first cycle.

As mentioned for the samples cycled in LiFSI with 1000 ppm of H_2O only the Al foil cycled once was measured due to the poor attachment of the 6 cycle sample. Therefore, in Figure 4.19 only the 1 cycle sample is shown. The measurements are also for this sample unstable, as can be seen from the irregularities, especially for the Li measurement. From this analysis, larger Li and S peaks are observed indicating

their presence on the outer surface. Also more wavelike peaks of O, H and C are observed. However, their presence further into the sample is unknown as the voltages drop at 2 s. The oxygen peak is much larger than both the H and C peaks, meaning that the oxygen content is higher.

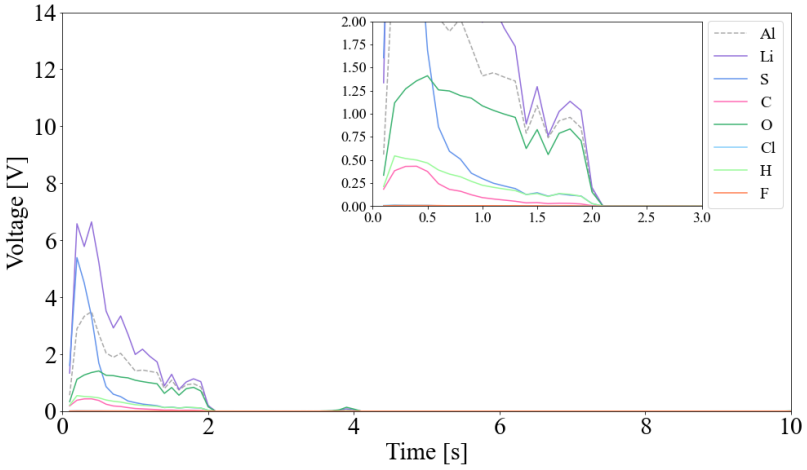

Figure 4.19: LiFSI with 1000 ppm H_2O 1 cycle

Since the GDOES analysis is only done for cycle 1, the difference between cycling once and six times cannot be compared for this electrolyte. However, comparing it with the analysis for the LiFSI electrolyte it was observed that the Li and S peak is much larger for the Al sample cycled in the water containing electrolyte. Similarly, the Li peak is larger than the S peak for both the samples cycled for one cycle.

The GDOES results for the aluminium samples cycled in the FEC containing electrolyte are shown in Figure 4.20, for a) 1 cycle and b) 6 cycles. For the sample cycled for one cycle, in Figure 4.20a, the measurements indicate the presence of Li and S at the surface with sharp peaks. The Li peak is higher than the S peak, and also has a flat area after its peak value which is not present at the S peak. This indicates that not only is the Li content higher, but the element is also present further in the sample. The wavelike O peaks show that the oxygen presence continues further into the sample. However, small instabilities are observed. C and H peaks are also observed, the peaks are not as sharp as the Li and S. However, the voltages decrease after a short time indicating that their presence is mainly on the surface

layer. Instabilities in the measurements are observed, mainly for the O and Al. For the sample cycled six times, in Figure 4.20b, the height of the peaks is relatively low. The highest peak is observed for S, with a slightly more rounded peak compared to previous measurements. The Li peak preserves its sharp peak, however the height of the peak is far lower. For the oxygen peak a decline in height can be observed continuously with the decline of the S peak, indicating that in addition to its presence throughout the sample, there is a higher presence at the outer surface layer as well. Small round peaks of C and H are also observed, these decline in voltage at the same time as all the other elements which could indicate the end of the surface layer.

For the samples cycled in the FEC electrolyte, the same trend can also be observed. For cycle 1 the Li signal is larger than the S, but for cycle 6 a switch has occurred and the S peak is larger than the Li. However, the O, C and H peaks show opposite trends for the LiFSI and FEC electrolytes as the contents all increase for LiFSI while they all decrease for the FEC electrolyte.

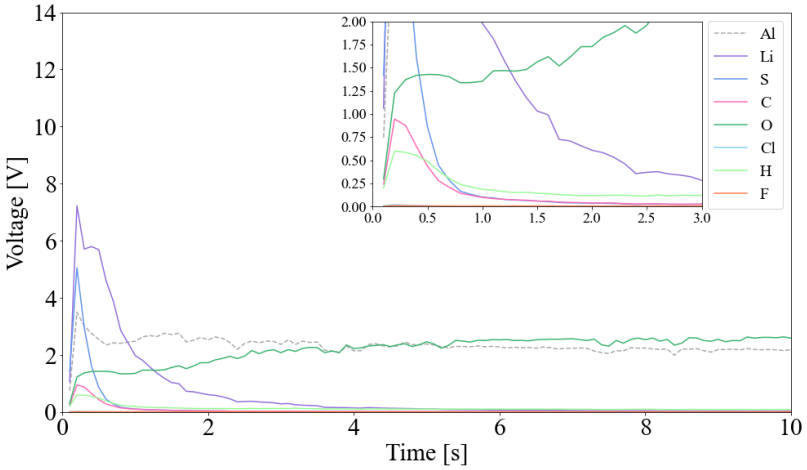

(a) LiFSI with FEC 1 cycle

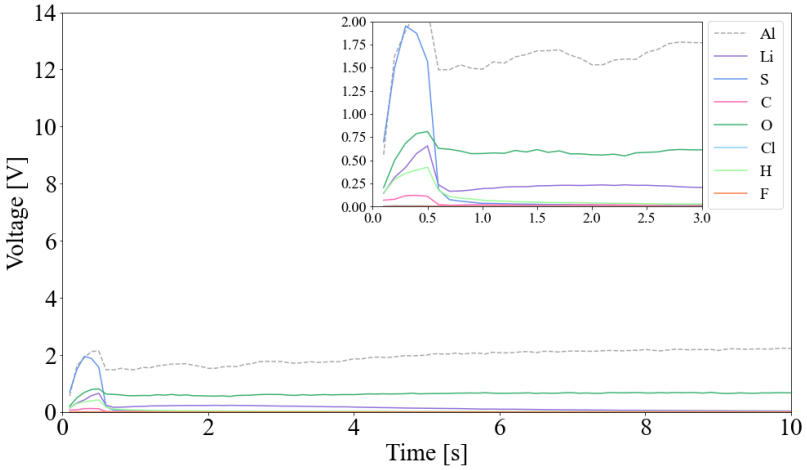

(b) LiFSI with FEC 6 cycles

Figure 4.20: GDOES results for Al foils cycled in LiFSI with FEC for 1 and 6 cycles

Lastly, the samples cycled FEC and 1000 ppm of H_2O containing electrolyte is shown in Figure 4.21, for a) 1 cycle and b) 6 cycles. The aluminium sample cycled for one cycle in Figure 4.21a shows a very large Li peak, much higher than the previous Li peaks. The peak is also quite wide, which could indicate a thicker surface film compared to the other samples. Also observed is a smaller but sharp peak for S. The O peak is quite stable throughout the entire measurement, indicating that its presence could be from the air. The C and H peaks increase similarly to the O peak, but they do decline as the time increases indicating that their main presence is at the

surface. For the six cycle sample in Figure 4.21b more wavelike peaks are observed. The presence of both Li and S for a larger timespan could indicate that the surface film has increased in thickness compared to the one cycle sample. The small O peak is stable throughout most of the measurement, indicating that its presence can come from the air. However, the S and C peaks are also quite stable so this could be due to the instabilities observed.

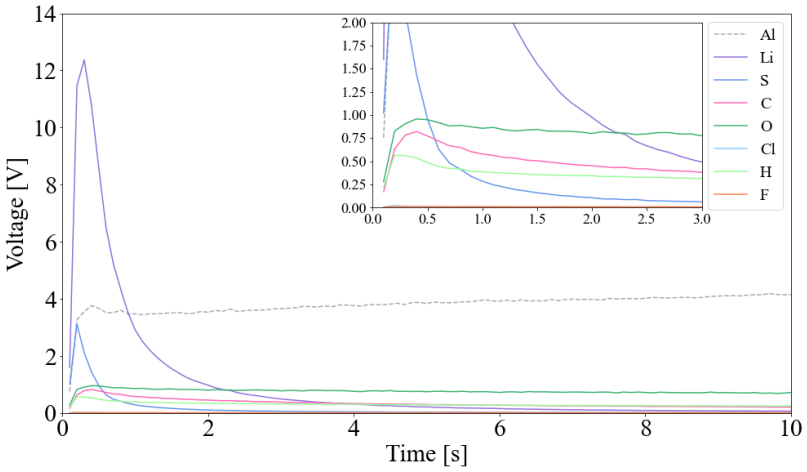

(a) LiFSI with FEC and 1000 ppm H_2O 1 cycle

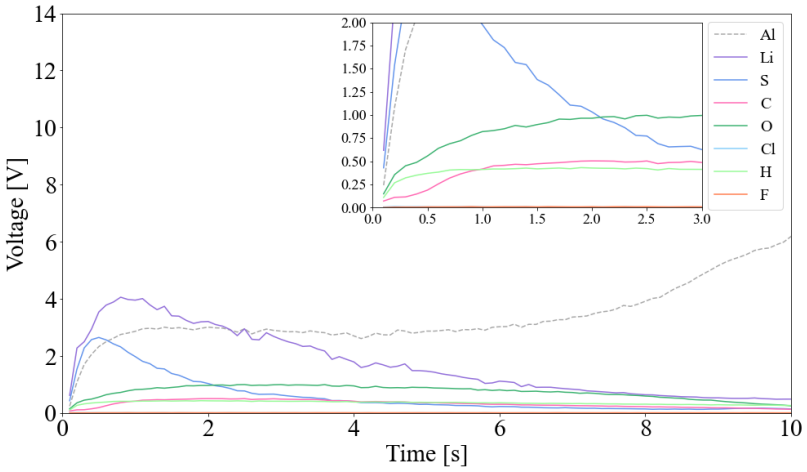

(b) LiFSI with FEC and 1000 ppm H_2O 6 cycles

Figure 4.21: GDOES results for Al foils cycled in LiFSi with FEC and 1000 ppm of water for 1 and 6 cycles

The samples cycled in the FEC and water electrolyte also show higher Li peaks

compared to the S peaks for cycle 1, the switch to a higher S peak is however not observed for cycle 6. The C and H peaks decline slightly and the O peak is fairly similar from one cycle to six cycles.

In summary, all of the samples show wavelike shaped peaks for O, C and H indicating that these elements are not only present on the outer surface of the samples but also further to the pure Al sample. In general, the Li and S peaks are indicators of the thickness of the surface film. However, due to the unknown surface component, no calibration of the measurements could be performed to determine the surface layer thickness. F was not observed for any of the samples. The Li and S presence could be due to salt remaining on the surface, however since there is no presence of F on the surface it is not likely that the Li and S are due to the LiFSI, but rather due to some decomposition products. To further analyse the composition of the surface, FTIR analysis is utilised.

FTIR Analysis

This section provides the FTIR results for all the Al samples cycled in the four electrolytes. From all the FTIR results background measurement of the pristine Al foil was retracted, the spectra of the pristine Al sample are included in Figure B.2 in Appendix B.2.

Figure 4.22 and 4.23 shows the measurements obtained for the aluminium surfaces cycled in electrolytes without FEC, LiFSI and LiFSI with 1000 ppm of H_2O, both for 1 and 6 cycles. The measurements are split into two wavelength ranges, where Figure 4.22 shows 2000 - 350 cm^{-1} and Figure 4.23 shows 4000 - 2000 cm^{-1}.

For the first wavelength range, in Figure 4.22, there are mainly three areas that contain peaks for the samples without FEC. However, the peaks observed are more wavelike causing it to be more difficult to distinguish the peaks. Peaks that can be found in all four samples are 570, 690, 1180, 1375, 1445 and 1660 cm^{-1}. In addition to these the following sections provide the additional peaks observed on the samples.

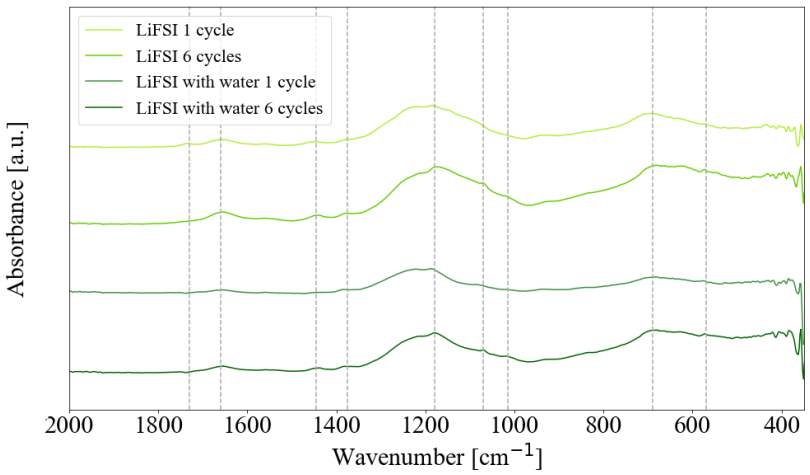

Figure 4.22: Wavenumber range 2000-350 cm^{-1}

The sample cycled in the LiFSI electrolyte for one cycle has one additional peaks at 1730 cm^{-1}. For the sample cycled for six cycles in the same LiFSI electrolyte peaks are found at 1015 and 1070 cm^{-1}. For the sample cycled for one cycle in the water containing electrolyte one additional peak is observed at 1070 cm^{-1}. Lastly, for the sample cycled for six cycles in the same electrolyte peaks are observed at 1015 and 1070 cm^{-1}.

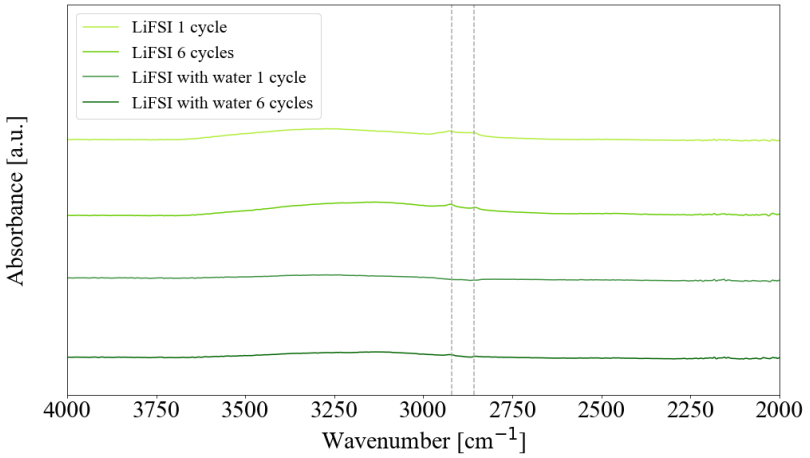

Figure 4.23: Wavenumber range 4000-2000 cm^{-1}

The FTIR results for the higher wavelength range for the samples cycled in the electrolytes without FEC is shown in Figure 4.23. Also for this range the peaks that

can be observed are small and more wavelike. However, two peaks are observed for both the samples cycled in the LiFSI electrolyte and the sample cycled six times in the water containing electrolyte at 2929 cm^{-1} and 2875 cm^{-1}. For the LiFSI samples a broad but more wavelike peak is observed from 3600 - 3000 cm^{-1}. For the sample cycled in the water containing electrolyte for one cycle no peaks are observed at this wavenumber range.

The FTIR results for the samples cycled in the FEC containing electrolytes are shown in Figure 4.24 and 4.25. The results include Al samples cycled in the FEC containing electrolyte and the FEC and 1000 ppm H_2O electrolyte, cycled for both one and six times. Figure 4.24 shows the wavelength range 2000 - 350 cm^{-1} and Figure 4.25 shows 4000 - 2000 cm^{-1}. Compared to the FTIR results for the electrolytes without FEC, the FEC containing electrolytes present several peaks and sharper peaks.

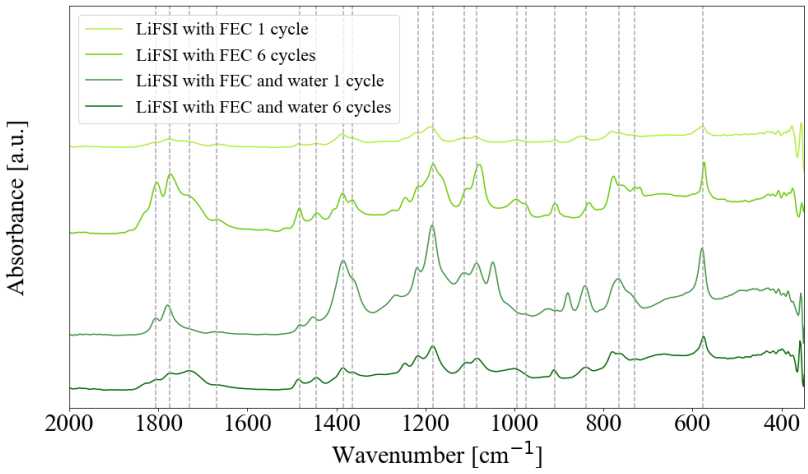

Figure 4.24: Wavenumber range 2000-350 cm^{-1}

For the first wavelength range, in Figure 4.24, a substantial amount of peaks are observed. Peaks that are observed for all four samples are 577, 730, 840/845, 910/920, 1113, 1183, 1217, 1365, 1385, 1445, 1483, 1670, 1730, 1775 and 1805 cm^{-1}. In addition, the following peaks are found in the individual samples. The sample cycled for one cycle in the FEC containing electrolyte shows peaks at 780, 995 and 1245 cm^{-1}. All peaks for this sample are much smaller compared to the peaks observed for the six cycle sample. The six cycle sample shows several peaks at 770, 870, 975, 995,

1080, 1245, 1269 and 1830 cm^{-1}. The peaks common for one and six cycles, 770/780, 995 and 1245 cm^{-1}, have increased intensity for the sample cycled six times. For the sample cycled for one cycle in the FEC and water containing electrolyte sharp peaks are observed at 765, 880, 975, 1050 and 1085 cm^{-1}. Comparatively, the sample cycled for six cycles shows peaks with less intensity at 765, 780, 995, 1085, 1245 and 1830 cm^{-1}. This electrolyte only has one common peak, in addition to peaks common for all FEC electrolytes, at 765 cm^{-1}. The increase in peaks from cycle 1 to cycle 6 for the FEC containing electrolyte could indicate a heavier presence of a surface layer on the aluminium sample cycled several times. For the samples in the FEC and water containing electrolyte both samples show similar amounts of peaks, however the intensity of the peaks is much larger for the sample cycled once.

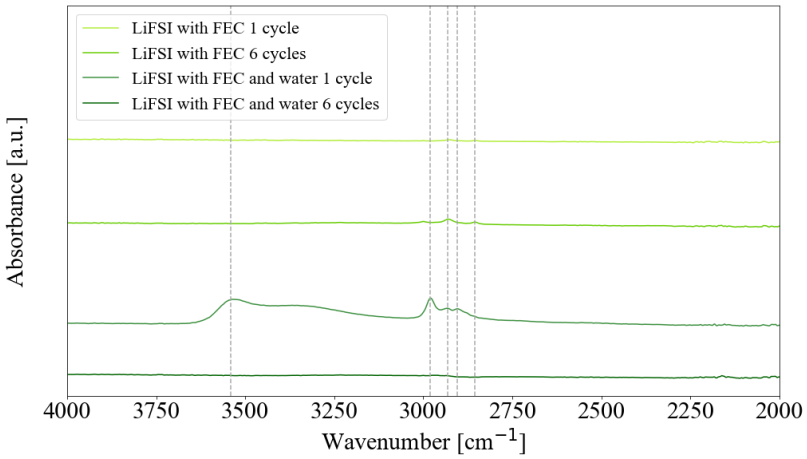

Figure 4.25: Wavenumber range 4000-2000 cm^{-1}

The higher wavenumber range for the samples cycled in the FEC containing electrolyte, shown in Figure 4.25, presents peaks with low intensity. For the one cycle sample in FEC and the six cycle sample in FEC and water, no peaks are observed. The sample cycled for six cycles in the FEC electrolyte three small peaks are observed at 2855, 2932 and 2990 cm^{-1}. For the sample cycled one time in the FEC and water containing electrolyte more peaks are observed. Peaks are observed at 2855, 2905, 2932 and 3540 cm^{-1}, in addition a broad more wavelike peak is observed from 3200 - 3600 cm^{-1} with the peak at 3540 cm^{-1} being its peak value.

The peaks from all eight samples are summarised in Table 4.4.

Table 4.4: Peaks from all eight samples analysed with FTIR.

LiFSI 1C	LiFSI 6C	W 1C	W 6C	FEC 1C	FEC 6C	F+W 1C	F+W 6C
570	570	570	570	577	577	577	577
690	690	690	690				
				730	730	730	730
					770	765	765
				780			780
				845	840	840	840
					870	880	
				910	910	920	910
					975	975	
				995	995		995
	1015		1015				
	1070	1070	1070			1050	
					1080	1085	1085
				1113	1110	1113	1113
1180	1180	1180	1180	1183	1183	1183	1183
				1217	1217	1217	1217
				1245	1245		1245
					1269	1269	
1375	1375	1375	1375	1365	1365	1365	1365
				1385	1385	1385	1385
1445	1445	1445	1445	1445	1445	1450	1445
				1483	1483	1483	1483
1660	1660	1660	1660	1670	1670	1670	1670
1730				1730	1730	1730	1730
				1775	1775	1775	1775
				1805	1805	1805	1805
					1830		1830
					2855	2855	
2875	2875		2875				
						2905	
2920	2920		2920				
					2932	2932	
					2990	2980	
						3540	

An analysis of the peaks for all samples analysed with FTIR is presented below, based on the peaks presented in Table 2.1 in the theory, Section 2.1. For peaks not presented in this section, no relevant components with similar peak values have been found. First, the peaks common for all samples are presented. First is 570 cm^{-1} for the samples without FEC or 577 cm^{-1} for the samples cycled in FEC. These peaks could indicate the presence of SO_2 which have peaks at 570 cm^{-1}, or Li_2O that show peaks at 609 cm^{-1}. Another common peak is observed at 1180 cm^{-1} for samples without FEC and 1183 cm^{-1} for the samples in FEC. This peak corresponds to one of the peaks found for LiFSI salt, at 1177 cm^{-1}. Other possibilities are polycarbonates present due to the polymerisation of the EC or DMC solvent, with a peak at 1190 cm^{-1}. SO_2 is another possibility as this component also has peaks reported at 1184 cm^{-1}. At 1445 another common peak for all samples is found. This peak could indicate the presence of Li_2CO_3 with a peak at 1435 cm^{-1} or CH_3 from the DMC solvent at 1454 cm^{-1}. In addition, $ROCO_2Li$ also show peaks around this area with peaks ranging from 1450-1400 cm^{-1}. At 1660 cm^{-1} for the samples without FEC and 1670 for the samples with FEC another common peak can be found. Around this value several C and O containing bonds are found, such as C=O at 1642 cm^{-1}, $ROCO_2Li$ at 1650 and 1668 cm^{-1}, aldehydes at 1650-1725 cm^{-1} and carboxylic acids at 1650-1725 cm^{-1}. At 1375 cm^{-1} for samples without FEC, and at 1365 for all FEC containing samples a peak is observed. This could correspond to the additional peak for the LiFSI salt found at 1365 cm^{-1}, indicating that these peaks could be due to the presence of LiFSI salt on the surface. SO_2 shows two peaks, at 1380 and 1360 cm^{-1}, which coincides with the 1365 and 1385 cm^{-1} peaks for the FEC containing samples. Common for the peaks at 570/577 cm^{-1}, 1180/1183 cm^{-1} and 1660/1670 cm^{-1} is that all the peaks are at a slightly higher wavenumber for the FEC containing samples compared to the samples cycled without FEC.

For the samples cycled without FEC much fewer and lower peaks are observed. In addition to the peaks already discussed, a few other peaks can also be relevant. At 1015 cm^{-1} peaks are observed for both six cycle samples, for these electrolytes and the one cycle water sample a peak at 1070 cm^{-1} is also observed. In this range several vibrations from C, H and O is found, such as C−O at 1060 cm^{-1}, C−O−H at 1050-1000 cm^{-1}, ROLi at 1100-1000 cm^{-1}, $ROCO_2Li$ at 1090 cm^{-1} and O−H at 1075-1050

cm^{-1}. These are all viable options for what these peaks could be for. At 2875 cm^{-1} and 2920 cm^{-1} peaks are also observed for the samples without FEC, except for the one cycle sample in the water containing electrolyte. These could indicate the presence of C−H from EC with a peak at 2928 cm^{-1} and $ROCO_2Li$ with a peak at 2900 cm^{-1}.

For the samples cycled in the FEC containing electrolytes, the following peaks could be relevant. Peaks are observed at 840 cm^{-1}, 845 cm^{-1} for one cycle FEC, these could indicate the presence of Li_2CO_3 with peaks at 857 cm^{-1} or $ROCO_2Li$ with peaks of both 800-840 and 855 cm^{-1}. In addition, S−F shows peaks at 827 cm^{-1}, which could coincide with the peaks observed at 840 cm^{-1}. Peaks are also observed at 910 cm^{-1}, 920 cm^{-1} for the one cycle sample in FEC and water electrolyte, these could indicate the presence of CH_{3O} which have peaks at 916 cm^{-1}. Peaks at 975 cm^{-1} for six cycles FEC and one cycle FEC and water are observed in addition to 995 cm^{-1} for all except one cycle FEC and water. For the one cycle FEC and water peaks are observed at 1050 cm^{-1} and 1085 cm^{-1}, the latter also present for six cycles FEC and six cycles FEC and water samples. These could indicate the presence of several C, H and O bonds such as C−O at 1060 cm^{-1}, C−O−H at 1050-1000 cm^{-1}, ROLi at 1100-1000 cm^{-1}, $ROCO_2Li$ at 1090 cm^{-1} and O−H at 1075-1050 cm^{-1} as previously discussed for the samples without FEC. The following peak at 1113 cm^{-1} is found for all the FEC containing samples, this peak could also indicate the presence of ROLi or $ROCO_2Li$. At 1217 cm^{-1} another common peak is observed, which is similar to one of the LiFSI peaks at 1209 cm^{-1}. Another option is SO_2 where references show peaks at 1211 cm^{-1}. In addition to the peaks at 1365 cm^{-1} that are previously discussed peaks are also found at 1385 cm^{-1} for the FEC containing samples. These could also indicate the LiFSI presence or SO_2 which has two peaks at these values, as mentioned previously. CH_2 from DMC show peaks at 1481 cm^{-1}, these correlate with peaks found at 1483 cm^{-1}. For all the FEC samples peaks are also found at 1730 cm^{-1} and 1775 cm^{-1}, these could indicate the presence of C=O from either EC at 1769 cm^{-1} or DMC at 1750 or possibly polycarbonates with peaks at 1765 cm^{-1}. Peaks are also found for all FEC samples at 1805 cm^{-1}, in addition to both the six cycle samples showing peaks at 1830 cm^{-1}. These could correspond to EC that shows peaks at 1810 cm^{-1}. Peaks are observed at 2855 cm^{-1} for the FEC cycled six times

and FEC and water cycled once, these could indicate the presence of C−H from EC that shows peaks at 2800-2900 cm^{-1}. A peak at 2905 is also visible for the FEC and water sample cycled once, this could also indicate the presence of C−H, or possibly the combination of CH_2 and CH_3 from EC and DMC with peaks at 3003-2850 cm^{-1} or $ROCO_2Li$ with reference peaks at 2900 cm^{-1}. Peaks are observed at 2932 cm^{-1}, except for the six cycle sample in FEC and water containing electrolyte, this could indicate the presence of C−H bonds from EC that have peaks at 2928 cm^{-1} or ROLi with reference peak at 2963 cm^{-1}. The final peaks around 3000 cm^{-1}, could indicate the presence of CH_2 or CH_3 at 3003 cm^{-1} or O−H at 3000-3800 cm^{-1}.

4.3 Degradation of FEC containing Electrolytes

The first parallels of the cells with the FEC containing electrolytes were made with electrolytes manufactured around 6 months before. Upon cell manufacture, the FEC and water electrolyte had turned slightly yellow, however not long after the electrolyte turned gradually darker and darker. Eventually, the electrolyte turned dark brown/black as illustrated in the image in Figure 4.26.

Figure 4.26: Picture taken of the FEC and water containing electrolyte

The colour change is a result of the FEC degrading and possibly reacting with water to produce HF in the electrolyte, which eventually causes the dark colour due to polymerisation. For the FEC containing electrolyte without additional water no change in colour was observed. Further, these FEC electrolytes are denoted as old FEC electrolytes.

4.3.1 Cell Performance during Galvanostatic Cycling

The coulombic efficiency and discharge capacities of the NMC_{111} cathodes cycled in the old FEC containing electrolytes are shown in Figure 4.27. The plots have been divided into voltage ranges for 4.2, 4.3 and 4.4 V from left to right. The two initial cycles are cycled at a c-rate of C/10, while all others are cycled at 1C. Also included is the reference cell cycled in $LiPF_6$.

The coulombic efficiencies in Figure 4.27a show relatively stable values for both the cells, at least for the 4.2 and 4.3 V ranges. For the initial cycles, the FEC and water containing electrolyte show an efficiency similar to the reference cell of 88.13 %, while the FEC containing electrolyte shows a slightly lower efficiency at 84.68 %. The same trend can be seen for cycle 2, with efficiencies of 96.58 % and 99.63 % for the FEC and FEC with water electrolytes respectively. In cycle 3 both cells show similar efficiencies at 90.54 % for FEC and 90.68 % for FEC and water. The subsequent cycles at the 4.2 V range for the FEC containing electrolyte are stable at around 99.6 % before a drop is observed for cycles 18 to 90.77 %. For the FEC and water containing electrolyte, there are no large devitations during the 4.2 V range, with values averaging around 100 %. For the initial cycle of the 4.3 V range, no drops are observed for either of the old FEC electrolytes. For the FEC electrolyte two drops are observed at the 4.3 V range at cycle 26 and cycle 37 down to 92.96 % and 91.57 %, respectively. As the FEC electrolyte cell enters the 4.4 V range the cells' coulombic efficiencies variate majorly, with the minimum value of 90.77 % at cycle 59. For the FEC and water electrolyte cell there are no drops until cycle 38 at the 4.3 V range down to 96.86 %. However, after this drop the variable efficiencies set in for this cell as well. The minimum efficiency is found at cycle 51 with an efficiency of 85.30 %. However, compared to the instabilities observed for the efficiencies for the cell with the new FEC electrolyte these instabilities of the old FEC are much smaller. As these cells have minimum values of 2-5 %.

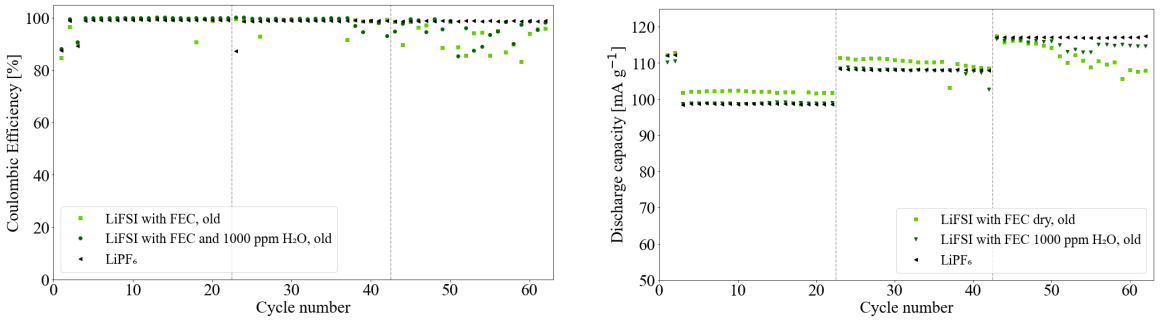

(a) Coloumbic efficiency

(b) Discharge capacity

Figure 4.27: Coloumbic efficiency and discharge capacity for NMC_{111} cycled in the old FEC containing electrolytes.

The discharge capacities of the old FEC electrolytes in Figure 4.27b show steady capacities for the first voltage range for both the electrolytes. For the two initial cycles the FEC electrolyte show similar capacities as the $LiPF_6$ reference cycles with values of 112 mA g^{-1} for cycle 1 and 2. As the c-rate increases to 1C, the discharge capacities lie around 102 mA g^{-1} for cycles 3 to 22, which is larger than for the $LiPF_6$ reference. However, a drop is observed at cycle 18 to similar values as the reference and the FEC and water containing electrolyte at 98.61 mA g^{-1}. Comparatively, the FEC and water containing electrolyte have discharge capacities of 110 mA g^{-1} for cycles 1 and 2. While its average capacities for the higher c-rate is similar to that of the $LiPF_6$ reference at 99 mA g^{-1}. As the voltage range increases so do the capacities of the cells. For the FEC electrolyte, a larger capacity fade can be observed as the capacity of cycle 23 is 111.70 mA g^{-1} goes down to 108.92 mA g^{-1} for cycle 42. In addition, a large drop is observed for cycle 37 down to 103.24 mA g^{-1}. As the voltage range increases to 4.4 V for the FEC containing electrolyte the capacity fade is even larger, with a difference of 9.47 mA g^{-1} of this voltage range compared with the drop of 2.78 mA g^{-1} from the previous voltage range. In addition, the capacity values become more unstable, with the minimum capacity found at cycle 59 at 83.26 mA g^{-1}. The 4.3 V for the FEC and water containing electrolyte shows a more stable capacity value, although the values are also lower. The average capacities lie around the reference cell at 99.6 mA g^{-1}. Drops are also observed for this electrolyte, with a small drop to 94.69 mA g^{-1} at cycle 39 and a larger one to 93.19 mA g^{-1} at cycle

42. At the largest voltage range the fade is much smaller for the FEC and water containing electrolyte, however a fade of 2.00 mAh g^{-1} is observed from cycles 43 to 62. A drop is observed for cycles 51 to 55, with the minimum value at cycle 53 at 87.62 mA g^{-1}.

4.3.2 Potential profiles from Galvanostatic Cycling

The potential profiles obtained from the galvanostatic cycling of the old FEC containing electrolytes are shown in Figure 4.28, for a) old FEC and b) old FEC with water electrolytes. The NMC_{111} cathode cycled in the old FEC electrolyte completed the cycling program in 142 h, with average cycling times of 18.45 h and 1.75 h for the C/10 and 1C cycles respectively. The cell cycled in the old FEC and water electrolyte completed the cycling in slightly longer, 145 h, also leading to slightly longer average cycling times. Where the C/10 cycles had an average time of 19.15 h and the 1C cycles had an average of 1.78 h. For both of the potential profiles, there are no areas with visible delays in charging or discharging.

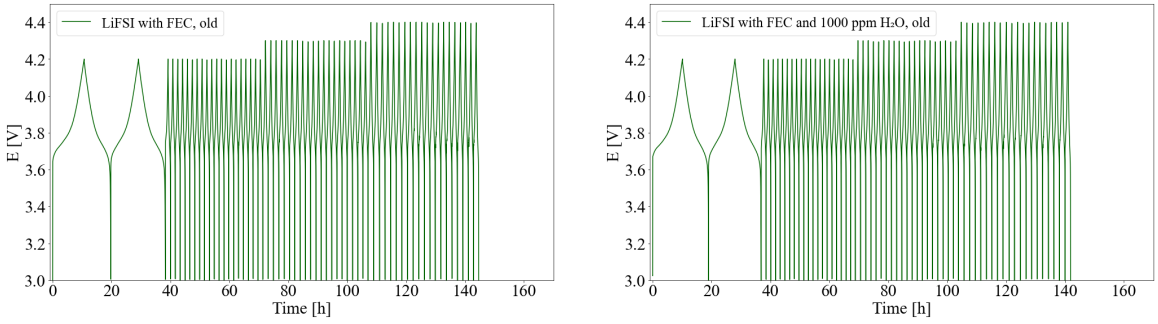

(a) LiFSi with FEC (old)

(b) LiFSI with FEC and 1000 ppm of H_2O (old)

Figure 4.28: Galvanostatic cycling of NMC_{111} in the old FEC containing electrolytes.

4.3.3 Cyclic Voltammograms of Al foils

Figure 4.29 shows the results from the cyclic voltammetry measurements done with the electrolyte made under the project work. From the figure, the maximum current densities of the cycling can be found. For the old FEC electrolyte the maximum current density is 0.113 mA cm^{-2}, and 0.103 mA cm^{-2} for the old FEC and water

electrolyte. The onset potentials, defined as the potential where the current density surpasses 0.001 mA cm^{-2}, are 4.270 V and 4.260 V for the electrolyte without and with additional water.

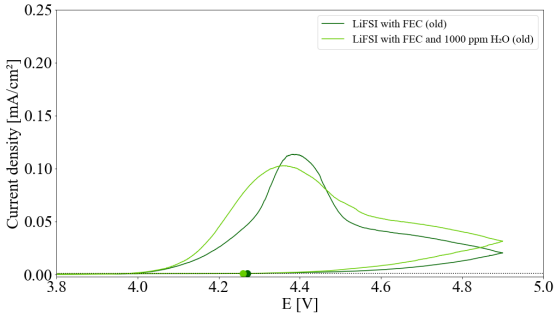

Figure 4.29: Cyclic voltammetry of Al foils cycled in old FEC containing electrolytes

These cyclic voltammograms can be compared to the current potential profiles obtained from cyclic voltammetry from the project work. These can be seen in Figure D.1 in Appendix D.1. Their maximum current densities and onset potentials are shown in Table D.1. It is clear to see that the degradation caused a decrease in maximum current densities, as the maximum current densities of the FEC electrolytes were 0.136 mA cm^{-2} and 0.291 mA cm^{-2} for the FEC and FEC with water electrolytes, respectively. However, the decrease for the FEC containing is small compared to that of the FEC and water containing electrolyte. The onset potentials show similar values of 4.276 V and 4.244 V for FEC and FEC with water, respectively.

Table 4.5: Onset potential and the maximum current density of Al foils cycled in the different electrolytes for 1 cycle.

Electrolyte	Onset potential [V]	Current density
LiFSI FEC, old	4.27006	0.11347
LiFSI FEC+H_2O, old	4.26004	0.10274

4.3.4 Post Mortem Characterisation

SEM Imaging

Figure 4.30 shows the SEM imaging of NMC_{111} cathodes cycled in a) old FEC and b) old FEC and water electrolyte. Both surfaces show lighter spheres with a more porous background. Not many differences from the other cathode surfaces are observed. However, on the NMC_{111} surface cycled in the FEC and water containing electrolyte darker spots are observed in the middle of the image.

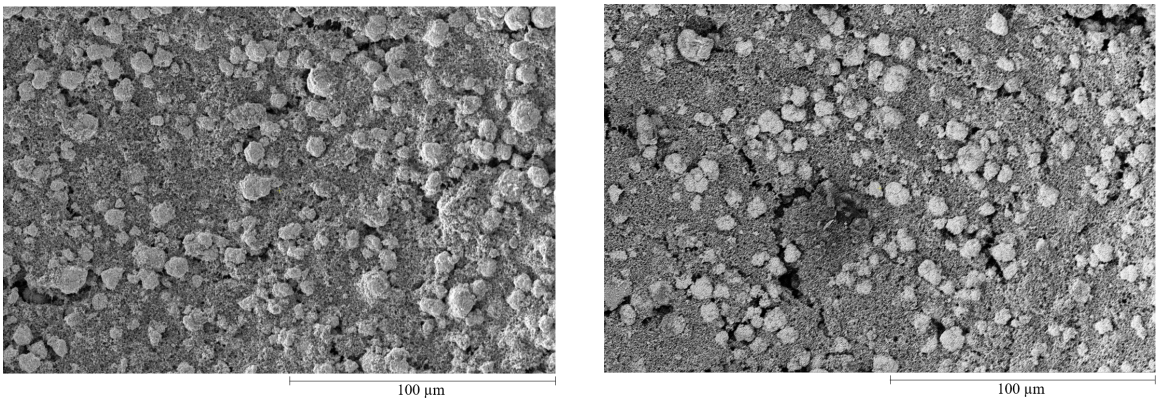

(a) LiFSi with FEC (old)

(b) LiFSI with FEC and 1000 ppm of H_2O (old)

Figure 4.30: Galvanostatic cycling of NMC_{111} in the old FEC containing electrolytes.

EDS analysis of these cathode surfaces was also performed. However, similarly to the other EDS analysis these showed no distinct differences compared to a pristine NMC cathode surface and are therefore included in Appendix C.3.

Chapter 5

Discussion

5.1 Effect of FEC

5.1.1 Effect on Aluminium Corrosion

From Figures 4.10a, 4.11a and 4.13 the cyclic voltammograms of the aluminium samples cycled in LiFSI and FEC electrolytes are shown. Together these figures represent the effect of the FEC additive on the corrosion of the aluminium current collector in the Li ion batteries. It is clear that the addition of FEC decreases the oxidative currents. It can also be seen that the anodic currents are not reversible, i.e. do not follow the same path as the voltage decreases down to 3 V again. This confirms that the increase in current density causes an irreversible process, such as electrolyte decomposition, aluminium corrosion or passivation of the Al surface [73].

The maximum current densities are much lower for the FEC containing cell, with values of 0.127, 0.177 and 0.132 mA cm^{-1} for the LiFSI compared to 0.08, 0.07 and 0.08 mA cm^{-1} for FEC. Using average values for these shows that the LiFSI sample has current densities that are 1.9 times larger than the FEC. The smaller oxidative currents indicate that FEC has a passivating effect on the corrosion of the aluminium current collector. Successful passivation is confirmed by the observed decrease of current densities as the cycle number increases [73]. Earlier studies have stated that the addition of FEC in the electrolyte could increase the threshold voltage for Al from 4.0 to 5.5 V [111]. These results suggest that the addition of FEC does not result in this large increase of threshold voltage. The results for the onset potential, defined as the voltage where the current density exceeds 0.001 mA cm^{-1}, indicate that only a small increase of 0.02 V occurs due to the addition of FEC. As the LiFSI shows an

average onset potential of 4.262 V, while the FEC shows an average of 4.282 V.

At higher applied potentials, the FEC containing cells have lower current densities. At a certain potential, an increase in the slope of the current densities can be observed for the LiFSI cells, causing a more rapid increase in the current densities. This occurs at 4.15, 4.50 and 4.35 V for the cells cycled six times, one time and the additional one cycle in the appendix. With an average potential of 4.3 V, this indicates that the FEC effectively represses the oxidative currents on the aluminium at higher potentials [2]. This is not observed for the electrolytes without FEC as these show high current densities at higher potentials.

The passivating properties of FEC can be seen in the SEM imaging, as the amount of pitting corrosion observed for the LiFSI samples in Figures 4.14a and 4.14b are higher compared to the FEC samples in Figures 4.15a and 4.15b. From the images, it is also clear that most of the corrosion occurs in the first cycle, as the amount of pits does not increase substantially from cycle 1 to cycle 6. It is clear that between these cycles a surface layer has appeared on both the LiFSI and FEC samples. However, to a much larger extent on the aluminium surface has been cycled in a FEC containing electrolyte. As previously discussed, since the current density of each cycle decreases, this layer results in passivating properties, if not the current would have increased continuously [2]. The appearance of the layers formed in the LiFSI and the FEC containing electrolyte differ. On the LiFSI 6 cycles sample in Figure 4.14b, the layer appears more as discolourations on the surface, as the surface structure of the polished Al is also visible at the dark spots. This is not the case for the FEC 6 cycle sample in Figure 4.15b, where no structure is observed through the layer. This indicates that the layer formed on the surface is thicker. However, the layer is unevenly present over the Al surface and contains cracks and deposits.

5.1.2 Effect on Surface Composition

The composition of the layers was analysed by GDOES presented in Figures 4.18 and 4.20, and FTIR presented in Figures 4.24 and 4.25. The SEM imaging indicated that the FEC layer is thicker as the texture of the aluminium surface polishing is not observed through, however from the GDOES measurement the time interval of the

Li and S peaks are relatively equal for the 6 cycles in the LiFSI and FEC samples. Which would suggest that the layers are of similar thickness. However, the major difference is that the SEM images are taken at the edges of the foil samples as this is the area where the most surface film forms. The GDOES measurements had to be taken in the middle of the foil, due to the instrument set up. This could cause the deviations observed for film thickness from these two analysis techniques. The intensity or height of the peaks is also smaller for the FEC 6 cycle sample, for all of the peaks. This might indicate that there is a lower presence of the elements on the surface. However, the GDOES measurements for the first cycle show that the peaks on the FEC samples are both higher and over a larger time interval, indicating a higher surface concentration and a thicker layer. This does not concur with what is observed with the SEM imaging as the FEC sample has no visible surface layer, while the LiFSI sample has some indications of darker areas on the surface. In general, the GDOES measurements show that the surface layer consists of mostly Li and S together with smaller amounts of O, C and H. The bonds of these elements can be distinguished from the FTIR measurements.

Also clear, is that the addition of FEC affects the number of components on the surface that can be detected by FTIR analysis. Some components are detected on all samples, these are SO_2, LiFSI, polycarbonates from EC/DMC, Li_2CO_3, $ROCO_2Li$ and C=O. In addition to these, only a few more components are found on the LiFSI samples, containing C−O, C−O−H, ROLi, O−H and C-H. However, all of these are also found for the FEC electrolyte, but at different wavenumbers. For the FEC samples, there are mainly two compounds found that are not present in the other samples, S−F and CH_3O. This could indicate that these compounds contribute to the thicker surface layer formation. Another possibility is that the thickness is a result of a higher concentration of the surface elements, due to the decomposition of FEC. This would also coincide with previous studies, as it reported that polycarbonates, Li_2CO_3 and LiF have the main impact on the surface layer [55]. The latter, LiF, is undetectable with the analysis used [85]. However, the FTIR analysis technique cannot determine surface concentrations with certainty as the signals could increase just by pressing the sample harder towards the crystal.

5.1.3 Effect on Discharge Capacity

The FEC addition results in improved capacity retention for anode materials [30, 50]. This is not necessarily the case for cathode materials. It has been shown previously that if an appropriate amount is added it could lead improved capacity retention for the NMC_{111} cathodes [29, 49].

From Figures 4.1a and 4.1b it can be seen that the FEC containing cell has much more variation in capacity values. Also clearly observed, is that the discharge capacities are lower for the FEC containing cell for all voltage ranges, compared to the LiFSI cell. With average values of 114, 101, 111 and 119 mA g^{-1} for C/10 at 4.2 V, 1C at 4.2 V, 1C at 4.3 V and 1C at 4.4 V range for the LiFSI cell. The FEC cell shows average values of 107, 96, 103 and 109 mA g^{-1} for the same ranges. These capacities show that an average decline of 7.5 mA g^{-1} can be seen as a result of the addition of 10 wt% FEC to the electrolyte. Capacity fades are observed for both cells at the 4.4 V range, with fades of 2.83 mA g^{-1} for LiFSI and 3.87 mA g^{-1} for FEC. In addition, the FEC cell shows a capacity fade for the 4.3 V range of 1.83 mA g^{-1} from cycle 23 to 42. The FEC containing cell shows large drops at certain cycles with a minimum value of 57 mA g^{-1}. However, the LiFSI shows no drop in discharge capacities. A positive effect on the discharge capacity due to FEC has been reported for NMC_{111} cathodes [61]. This could be attributed to trace amounts of HF in the system, contributing to passivating the Al foil which could improve the capacity retention. However, this was the result of the addition of only 2 wt% FEC. These results suggest that the amount of FEC added to this electrolyte was too large. The reason for this could be that the remaining FEC in the system decomposes and forms additional HF which contributes to transition metal dissolution, and thereby poorer capacity [53]. However, it is also reported that the additional FEC forms polycarbonates and LiF which both supposedly contribute to the stabilisation of the cathode electrolyte interface layer which should be beneficial for the cell performance. This is not observed from the SEM imaging or EDS analysis of the cathode surfaces.

5.1.4 Effect on Coulombic Efficiency

For anodes the addition of FEC generally increases the stability of the electrolyte interface layer, resulting in a higher coulombic efficiency [46, 47, 48] From Figures 4.2a and 4.2b a clear decline in the stability of the coulombic efficiencies for the FEC cell can be seen compared to the LiFSI cells. The FEC containing cell shows large deviations from the reference cell values with a minimum efficiency of 5.19 %, this drop is colossal compared to the minimum value of LiFSI at 81.17 %. These results show that the FEC results in poor coulombic efficiency for NMC_{111} cathodes. This could be a result of the passivating layer forming on the Al surface, which could contribute to a degradation of the cell performance. For both cells drops at cycle 1, cycle 3 and cycle 23 are observed. These drops are expected as they occur in connection with increases in the c-rate or voltage range and the increase Li pulled out from the cathode during charging. However, it is not observed for 4.4 V which could be related to the 4.3 V limitation of the NMC_{111} cathodes, i.e. changing to a higher voltage will not allow for more charging. Fades of the efficiencies of 1.03 % are observed at the 4.4 V range for the LiFSI cell, however the efficiencies for the FEC cell vary too much, and cannot be determined.

5.1.5 Effect on Cycling

The FEC containing cells all exhibit poor cycling stability. Several slow charges are observed, eventually causing failure to complete the cycling program. As observed from the number of cells that stopped cycling in Table A.1. This is related to leak currents occurring inside the batteries. This has not been further researched in this thesis, so no conclusions on where this current goes can be drawn. But a suggestion could be that it is used on Li dendrite formations. No deposits or black discolourations, from the cathodes, were observed on the separator. What was observed, is the black discolouration appearing on the Li counter electrode from the NMC_{111} cathode. A possible hypothesis could be that this layer is thicker in cells with FEC containing electrolytes, which could contribute to faster Li dendrite growth on the surface. This again could cause the major issues with leak currents for the FEC containing electrolytes, which supports the suggestion that the FEC content was too high.

5.2 Effect of Water

5.2.1 Effect on Corrosion

Figures 4.10a, 4.10b and 4.13 present the effect of the additional water has on the corrosion of aluminium in LiFSI based electrolytes. The water content, of 1000 ppm, slightly lowers the oxidative currents on the current collectors. Both the LiFSI and the water containing electrolyte result in the odd shape of the first cycle. Interesting is that this shape only occurs on the first cycle and that the subsequent cycles have the expected shape similar to the FEC electrolytes. However, this still indicates irreversible reactions occurring, such as aluminium corrosion or surface passivation [73].

The addition of water does not improve the onset potential. The water containing electrolytes show average onset potentials of 4.205 V, while the pure LiFSI electrolyte shows averages at 4.262 V. The water represses the current density at higher potentials, compared to LiFSI. This can be seen as the slope increases more rapidly for the LiFSI than the water containing cells at 4.65, 4.65 and 4.55 V for the cells cycled six times and the two parallels of one cycle. This results in an average of 4.62 V and indicates that the water shows a repressing effect on the oxidative currents on the aluminium current collector above this voltage. As seen in previous studies, water is reported to have similar decomposition products as the FEC electrolyte, which is what could contribute to the passivation of the aluminium corrosion [112].

As mentioned, the current densities show a slight reduction as a result of the water addition. The maximum current densities of the water containing cells are 0.113, 0.106 and 0.094 mA cm^{-2} compared to 0.127, 0.177 and 0.132 mA cm^{-1} of the LiFSI, i.e. an average decline of 0.041 mA cm^{-2}. As a result of the water addition, a decline can be observed for the second cycle of the sample cycled for six cycles. This is notable as this does not occur for any of the other cells where an increase in current density is observed. This could indicate a more rapid passivation effect on the aluminium surface. This coincides with what is observed at the SEM imaging in Figure 4.14c and 4.14d. The surface film forms faster, as it can be seen to a larger extent in the first cycle compared to the LiFSI. This corresponds to the lower amount of pitting

corrosion observed for both the one cycle and the six cycles. The surface layer formed does not appear thick or dense, as the polished aluminium surface is visible through the layer, indicating that only a thin surface film has formed.

5.2.2 Effect on Surface Composition

The GDOES measurements for the water containing electrolytes, in Figure 4.19, only show the measurements taken for one cycle. This makes it harder to assert the effect water has on the surface film. However, by comparing the one cycle measurements to that of the LiFSI sample it is clear that the addition of water causes a much larger response of the surface elements. With large peaks of both Li and S, in addition to the smaller C, H and O peaks similar to what's seen for the FEC samples. This argues that the decomposition products formed in water containing electrolytes are similar to the FEC containing electrolytes.

The water containing electrolyte contains the same compounds as observed in all samples, with the addition of compounds containing bonds such as C−O, C−O−H, ROLi, $ROCO_2Li$, O−H and C−H, which are also found at the FEC containing samples but at different wavenumbers. This indicates that the water does not affect the surface elements to a large extent and that the number of peaks found in the FTIR spectra is similar to the LiFSI with their low intensity.

5.2.3 Effect on Discharge Capacity

Figure 4.1a shows that the addition of water causes a slight decline in discharge capacity. However, the values are still higher than the $LiPF_6$ reference cell. The average discharge capacities are 113, 100, 111 and 119 mA g^{-1} for C/10 at 4.2 V, 1C at 4.2, 1C at 4.3 and 1C at 4.4 V respectively. The water also reduces the capacity fade observed at 4.4 V. The fade is still present, with a fade of 0.86 mA g^{-1}, but is smaller than for the LiFSI electrolyte which has a drop of 2.83 mA g^{-1}. This indicates that the presence of water stabilises the discharge capacity at higher potentials. This coincides with previous studies, where Young et al. reported a 17 % enhancement in capacity retention due to the addition of 1000 ppm of water [112].

Young et al. compared these effects to be equal to the effect of adding 10 wt% FEC to the electrolyte. However, the results of this thesis show that the water addition far exceeds the properties obtained from the FEC addition, as the FEC addition shows poorer properties than just the LiFSI. However, cells produced for this thesis only included Li metal as counter electrode and no research was done for full cells.

Suggested mechanisms that cause these improvements in cycling performance are that the water contributes to the SEI layer. By OH^- from the water reacting with the carbonates in the EC solvent due to the anode potential contributing to water splitting. This reaction causes the formation of polymers that are a beneficial influence on the SEI layer [112]. This is presumed to also have a positive effect on the Li metal counter electrodes. The reaction also contributes to CO_2 formation inside the batteries, which has shown to enhance the cycling performance of silicon anodes [112].

5.2.4 Effect on Coulombic Efficiency

From Figure 4.2a it can be seen that the addition of water has a positive effect on the coulombic efficiency. Most importantly the elimination of the capacity fade at 4.4 V. In addition the initial drop of the 4.3 V region is reduced. This coincides with what has been reported recently for NMC_{111} cathodes. Burns et al. reported that the addition of 1000 ppm of water was beneficial for the coulombic efficiency [113]. Only one negative effect of the water content was reported, swelling [114, 113]. However, in this research the mechanical stress on the cells is reduced by the use of pouch cells due to their increased flexibility.

5.2.5 Effect on Cycling

The cycling of the water containing electrolyte, in Figure 4.4b, shows that the addition of water does not affect the cycling negatively as the cell shows similar stable cycling as the LiFSI electrolyte. This could be due to the water forming HF inside the cell, which reduces the Al corrosion and thus retains the cycling stability. This coincides with the smaller current densities obtained for the aluminium cycled in the water containing electrolyte.

5.3 Combined Effect of FEC and Water

5.3.1 Effect on Corrosion

In Figures 4.10a, 4.11b and 4.13 the oxidative currents on the aluminium current collectors are shown, for the LiFSI electrolyte and the FEC and water electrolyte. Together these present the combined effect of FEC and water in a LiFSI based electrolyte. It is clear that the addition of both 1000 ppm of H_2O and 10 wt % FEC to the electrolyte decreases the oxidative currents on the aluminium current collector. Also observed, similar to the FEC electrolyte, is that irreversible reactions occur on the surface due to the dissimilar shape as the voltage increases and decreases.

The negative effect of the water addition on the onset potential can also be seen for the FEC and water containing electrolyte, with average onset potentials of 4.220 V However, an increase in onset potentials is observed due to the FEC addition compared to the water containing electrolytes.

From Figure 4.11b, the FEC and water containing electrolyte have the lowest current densities of all four electrolytes. The same can be observed for the average maximum current densities of the two parallels cycled for only one cycle. The addition of FEC to the electrolyte causes the first cycle to have a similar shape as the subsequent cycles. However, a slight increase is observed from cycles 1 to 2, which was not seen in the sample containing only water. Clearly observed is the positive effect the FEC and water addition has on repressing the oxidative current on the aluminium at higher potentials. The FEC and water containing cells show the lowest current densities at high potentials in all parallels. This indicates that the addition of both FEC and water to the electrolyte has better passivating properties than the FEC and water by themselves, even though the additives are reported to produce similar reduction products inside the batteries [112]. Similar to the water containing cell the SEM for cycle 1 in Figure 4.15c shows the beginning of the surface film formation, which does not occur for cycle 1 of the FEC containing cell. After six cycles, Figure 4.15d, more surface film formation has occurred. This film shows more similarities with the FEC cells rather than the water containing cells, as it appears thicker and no texture is observed through the layer. The film does not homogeneous cover the surface but

does however, appear more even at the places it does occur compared to the pure FEC. Also, fewer deposits and cracking are observed, which could indicate that the presence of water in addition to the FEC creates a more stable surface layer.

5.3.2 Effect on Surface Composition

The compositions of the surface layers of the samples cycled in the FEC and water containing electrolyte for one and six cycles are shown in Figures 4.21a and 4.21b, respectively. These show that the time interval of the peaks is much larger for the sample cycled for six cycles, compared to the sample cycled once. The Li peak on the one cycle sample is much higher than for the six cycle sample. While the peaks for S, C, H and O are around the same height. However, due to the large differences in time intervals the lower peaks do not necessarily indicate a lower content but that the content has spread over a thicker film. Since the S content is relatively similar in height but has a larger time interval, this suggests that the S content has increased from one to six cycles. The layers are thicker which is consistent with what's observed in the SEM imaging. This could indicate that, unlike the FEC samples, more of a surface layer has formed in the middle of the sample which is where the GDOES measurements are taken.

The FTIR measurements for the FEC and water containing samples show the same surface components as the FEC sample. Where the main difference compared to the non FEC samples is the presence of S−F and CH_3O.

5.3.3 Effect on Discharge Capacity

From Figure 4.1b it can be observed that the addition of water to the FEC electrolyte causes a large increase in discharge capacities for NMC_{111} cathodes. Average values of 115, 103, 111 and 119 mA g^{-1} for the different ranges of C/10 at 4.2 V, 1C at 4.2 V, 1C at 4.3 V and 1C at 4.4 V, respectively. These values are the highest discharge capacities of all cells tested, indicating that the combined effect of FEC and water has a positive impact on the discharge capacity. The capacity fades of 1.02 mA g^{-1} for 4.3 V and 2.69 mA g^{-1} for 4.4 V, show a decrease in fade compared to the cells

only containing FEC. As the water containing cell shows the smallest capacity face, this suggests that the water has a positive impact on capacity retention.

5.3.4 Effect on Coulombic Efficiency

In Figure 4.2b it is clear that the addition of water to the FEC electrolyte has a positive effect on the stability of the coulombic efficiency for NMC_{111} cathodes. However, compared to the LiFSI and water electrolytes, the efficiencies have a high variation. The values start slightly above the $LiPF_6$ reference cell, but after a small fade of 0.63 % at the 4.4 V range, end up at equal values to the reference cell. Even though the addition of water has a stabilising effect on the coulombic efficiency, this cell still has the lowest efficiency value of 2.91 %. Generally, it can be observed that the addition of water to the FEC electrolyte causes fewer drops in the coulombic efficiency, but the drops that do occur are slightly larger than for the FEC electrolyte.

5.3.5 Effect on Cycling

The cycling of NMC_{111} cathodes in the FEC and water containing electrolyte, in Figure 4.5b, shows that the cycling stability has not improved compared to the FEC electrolyte. Indicating that the improvement in discharge capacity does not impact the cycling stability to a large extent, as the coulombic efficiency of the cell is still quite poor. The leak currents, previously discussed in the FEC section, still occur for the FEC and water electrolyte. This indicates that the addition of water together with the rather large FEC content does not improve the Li dendrite formation on the Li counter electrode.

5.4 Effect of FEC Degradation on Battery Performance

The degradation of FEC in electrolytes containing additional water is clearly observed from the discolouration observed in Figure 4.26 for the 10 wt% FEC and 1000 ppm H_2O electrolyte created around 6 months before. The FEC defluorises and reacts with the hydrogen from the water, causing HF formation. However, HF is colourless.

A possible reason for the colour change could be polymerisation No visible changes for the old FEC electrolyte, this only contains 100 ppm of H_2O, so reactions causing HF formation are likely less. A previous study by Shin et al. shows that the addition of 5 wt% of FEC causes an increase in HF formation during storage compared to no FEC addition [115]. However, this was done at elevated temperatures of 55-60 °C which are higher than the storage temperatures of these FEC electrolytes. For these electrolytes a higher FEC concentration is used, this could possibly generate more HF in the system, but this is uncertain.

Figure 4.29 shows the cyclic voltammetry results for the old FEC electrolytes. Resulting from the FEC degradation a decrease in current densities, compared to the FEC electrolytes when they were new, can be observed. The FEC electrolyte only shows a slight decrease, while the water content causes a reduction to almost a third of the original current density. The degradation does not affect the onset potentials largely as these are fairly similar to what was reported for the FEC electrolytes when they were new. This indicates that the passivating properties of the FEC are improved as a result of the degradation. This could be due to the HF presence, which is what causes the passivation in $LiPF_6$ electrolytes. However, the presence of HF in the electrolyte undermines the objective of exchanging from $LiPF_6$ based electrolytes to LiFSI based ones. The main problem with these electrolytes is that the HF causes flammability and safety issues [3].

From Figures 4.27a and 4.1b an increase in both coulombic efficiency stability and the discharge capacities can be observed for the degraded electrolytes, compared to the cell performance of the FEC electrolytes produced for this thesis. An increase in cycling stability can also be observed as a result of the degradation, as no slow charges are observed for the cell and both completed the cycling program. Previous studies have shown that the additional FEC leading to HF formation causes transition metal dissolution and reduces the capacity of the cell [53]. This does not coincide with the results obtained in this thesis, where the degradation caused increased cell performance and cycling stability. This could be because there are only trace amounts of HF present, which results in the majority being used for passivation of the aluminium current collector and not degradation of the cathode material.

Chapter 6

Conclusion

The effect of FEC and water additives on aluminium corrosion and NMC_{111} cathodes has been investigated. The aim was to see if the addition of 10 wt% FEC and 1000 ppm H_2O, on their own or combined, could reduce the corrosion of the current collector and retain cell performance during cycling in LiFSI based electrolytes. Four electrolyte compositions were compared based on oxidative currents, surface composition and cell performance. Cyclic voltammetry measurements showed that the addition of 10 wt% of FEC and 1000 ppm of H_2O both reduced the oxidative currents on the aluminium current collector. Most effective was the combined electrolyte with both FEC and water. SEM imaging showed that the FEC addition had the largest impact on the surface layer formation, forming thicker surface layers On the aluminium. GDOES and FTIR analysis showed that the composition of the surface layers are similar, suggesting that FEC and water form similar decomposition products in LiFSI electrolytes. Components crucial for the cathode electrolyte interface layers, Li_2CO_3 and polycarbonates, were observed in all samples. LiF was undetectable with the chosen analysis methods. The main distinction resulting from the FEC additive was the additional S−F and CH_3O components. Galvanostatic cycling showed that the FEC additive had a detrimental effect on the NMC_{111} cathodes, leading to poor discharge capacities and coulombic efficiencies, suggesting that the FEC content was too large. The addition of water to the FEC electrolyte improved the discharge capacity and coulombic efficiency to such an extent that the combined electrolyte showed the highest discharge capacities. However, poor coulombic efficiencies and slow charges were still observed. Slow charging was observed for all electrolytes containing additives, due to leak currents in the batteries.

Chapter 7

Further Work

FEC and water containing electrolytes show great discharge capacities combined with a high ability to repress oxidative currents on the aluminium current collector. This suggests that further investigations should be performed on these LiFSI based electrolytes, to find optimal FEC and water contents. As discussed in this thesis, the results indicate that the addition of 10 wt% of FEC was too large. Further work on testing smaller FEC contents together with the 1000 ppm of H_2O should be performed, to see if this could improve the coulombic efficiencies and the cycling stability. Previous research has shown that 2 wt% FEC has shown positive effects on cathode performance [61]. Suggesting that the addition of 1000 ppm H_2O to a FEC content of 2 wt% could be a good starting point, then increasing the FEC content at intervals up to 10 wt%. For any electrolyte composition, full cell configuration should be investigated. Since all components of the batteries have to be compatible, the effect of the FEC content together with the water content on the anode is of great importance, and should be identified. Further analysis of the leak currents produced should also be performed, as the arguments provided in this thesis are only suggestions based on observations during battery disassembly.

Further surface analysis of the passivating layer occurring on the aluminium current collector should be performed, as one of the reported crucial surface elements was not detectable with FTIR. The suggested analysis technique is x-ray photoelectron spectroscopy (XPS) analysis, which was not performed due to the time limitations of this thesis. It is hard to determine whether it's the cathode or the aluminium component that leads to the failure of the batteries. This could be further investigated by carefully removing the cathode coating, exposing the aluminium current collector to observe how the Al underneath appears after the cycling.

Bibliography

[1] J.-M. Tarascon, "Key challenges in future Li-battery research," *The Royal Society Publishing*, vol. 368, no. 28, pp. 3227–3241, 2010.

[2] W. J. Zhang, "A review of the electrochemical performance of alloy anodes for lithium-ion batteries," *Journal of Power Sources*, vol. 196, pp. 13–24, 1 2011.

[3] D. Deng, "Li-ion batteries: Basics, progress, and challenges," *Energy Science and Engineering*, vol. 3, pp. 385–418, 9 2015.

[4] W. R. Bennett, "Considerations for Estimating Electrode Performance in Li-Ion Cells," 2012.

[5] S. T. Myung, Y. Hitoshi, and Y. K. Sun, "Electrochemical behavior and passivation of current collectors in lithium-ion batteries," 7 2011.

[6] J. Foropoulos and D. D. Desmarteau, "Synthesis, properties, and reactions of bis((trifluoromethyl)sulfonyl) imide CF3CO2)2NH," *Inorganic Chemistry*, vol. 23, no. 23, pp. 3720–3723, 1984.

[7] X. Wu and Z. Du, "Study of the corrosion behavior of LiFSI based electrolyte for Li-ion cells," *Electrochemistry Communications*, vol. 129, 8 2021.

[8] L. J. Krause, W. Lamanna, J. Summerfield, M. Engle, G. Korba, R. Loch, and R. Atanasoski, "Corrosion of aluminum at high voltages in non-aqueous electrolytes containing perfluoroalkylsulfonyl imides; new lithium salts for lithium-ion cells," *Journal of Power Sources*, vol. 68, pp. 320–325, 10 1997.

[9] L. Li, S. Zhou, H. Han, H. Li, J. Nie, M. Armand, Z. Zhou, and X. Huang,

"Transport and Electrochemical Properties and Spectral Features of Non-Aqueous Electrolytes Containing LiFSI in Linear Carbonate Solvents," *Journal of The Electrochemical Society*, vol. 158, p. A74, 12 2011.

[10] A. M. Haregewoin, A. S. Wotango, and B. J. Hwang, "Electrolyte additives for lithium ion battery electrodes: progress and perspectives," *Energy & Environmental Science*, vol. 9, pp. 1955–1988, 6 2016.

[11] K. Xu, "Electrolytes and Interphases in Li-Ion Batteries and Beyond," *Chemical Reviews*, vol. 114, pp. 11503–11618, 12 2014.

[12] C. Julien, A. Mauger, A. Vijh, and K. Zaghib, "Lithium Batteries," *Lithium Batteries*, pp. 29–68, 2016.

[13] C. A. Lundgren, K. Xu, T. R. Jow, J. Allen, and S. S. Zhang, "Lithium-ion batteries and materials," *Springer Handbooks*, vol. 15, no. 1, pp. 449–494, 2017.

[14] J. Goodenough and K.-S. Park, "The Li-Ion Rechargeable Battery: A Perspective," *Journal of the American Chemical Society (JACS)*, vol. 135, no. 4, pp. 1167–1176, 2013.

[15] S. Goriparti, E. Miele, F. De Angelis, E. Di Fabrizio, R. Proietti Zaccaria, and C. Capiglia, "Review on recent progress of nanostructured anode materials for Li-ion batteries," *Journal of Power Sources*, vol. 257, pp. 421–443, 7 2014.

[16] M. Osiak, H. Geaney, E. Armstrong, and C. O'Dwyer, "Structuring materials for lithium-ion batteries: advancements in nanomaterial structure, composition, and defined assembly on cell performance," *Journal of Materials Chemistry A*, vol. 2, pp. 9433–9460, 6 2014.

[17] M. T. McDowell, S. Woo Lee, C. Wang, and Y. Cui, "The effect of metallic coatings and crystallinity on the volume expansion of silicon during electrochemical lithiation/delithiation," *Nano Energy*, vol. 1, pp. 401–410, 5 2012.

[18] M. S. Whittingham, "Lithium Batteries and Cathode Materials," *Chemical Reviews*, vol. 104, pp. 4271–4301, 10 2004.

[19] A. S. Hameed, "Introduction to Li-ion Batteries," pp. 1–30, 2016.

[20] N. Yabuuchi and T. Ohzuku, "Novel lithium insertion material of LiCo1/3Ni1/3Mn1/3O2 for advanced lithium-ion batteries," *Journal of Power Sources*, vol. 119-121, pp. 171–174, 6 2003.

[21] Z. Li, N. A. Chernova, M. Roppolo, S. Upreti, C. Petersburg, F. M. Alamgir, and M. S. Whittingham, "Comparative Study of the Capacity and Rate Capability of LiNiyMnyCo1–2yO2 (y = 0.5, 0.45, 0.4, 0.33)," *Journal of The Electrochemical Society*, vol. 158, p. A516, 3 2011.

[22] T. Ohzuku, K. Ariyoshi, Y. Makimura, N. Yabuuchi, and K. Sawai, "Materials Strategy for Advanced Lithium-Ion (Shuttlecock) Batteries: Lithium Nickel Manganese Oxides with or without Cobalt," *Electrochemistry*, vol. 73, pp. 2–11, 1 2005.

[23] Z. Liu, A. Yu, and J. Y. Lee, "Synthesis and characterization of LiNi1xyCoxMnyO2 as the cathode materials of secondary lithium batteries," *Journal of Power Sources*, vol. 81-82, pp. 416–419, 9 1999.

[24] C. Tian, F. Lin, and M. M. Doeff, "Electrochemical Characteristics of Layered Transition Metal Oxide Cathode Materials for Lithium Ion Batteries: Surface, Bulk Behavior, and Thermal Properties," *Accounts of chemical research*, vol. 51, pp. 89–96, 1 2018.

[25] I. A. Shkrob, J. A. Gilbert, P. J. Phillips, R. Klie, R. T. Haasch, J. Bareño, and D. P. Abraham, "Chemical Weathering of Layered Ni-Rich Oxide Electrode Materials: Evidence for Cation Exchange," *Journal of The Electrochemical Society*, vol. 164, pp. A1489–A1498, 5 2017.

[26] L. Kong, C. Li, J. Jiang, and M. G. Pecht, "Li-Ion Battery Fire Hazards and Safety Strategies,"

[27] A. L. Lipson, J. L. Durham, M. Leresche, I. Abu-Baker, M. J. Murphy, T. T. Fister, L. Wang, F. Zhou, L. Liu, K. Kim, and D. Johnson, "Improving the Thermal Stability of NMC 622 Li-Ion Battery Cathodes through Doping during Coprecipitation," *ACS Applied Materials and Interfaces*, vol. 12, pp. 18512–18518, 4 2020.

[28] K. Xu, "Nonaqueous Liquid Electrolytes for Lithium-Based Rechargeable Batteries," *Chemical Reviews*, vol. 104, pp. 4303–4417, 2004.

[29] S. E. Trask, K. Z. Pupek, J. A. Gilbert, M. Klett, B. J. Polzin, A. N. Jansen, and D. P. Abraham, "Performance of Full Cells Containing Carbonate-Based LiFSI Electrolytes and Silicon-Graphite Negative Electrodes," *Journal of The Electrochemical Society*, vol. 163, pp. A345–A350, 12 2016.

[30] Z. Xu, J. Yang, H. Li, Y. Nuli, and J. Wang, "Electrolytes for advanced lithium ion batteries using silicon-based anodes," *Journal of Materials Chemistry A*, vol. 7, no. 16, pp. 9432–9446, 2019.

[31] J. B. Goodenough and Y. Kim, "Challenges for rechargeable batteries," *Journal of Power Sources*, vol. 196, pp. 6688–6694, 8 2011.

[32] R. W. Schmitz, P. Murmann, R. Schmitz, R. Müller, L. Krämer, J. Kasnatscheew, P. Isken, P. Niehoff, S. Nowak, G. V. Röschenthaler, N. Ignatiev, P. Sartori, S. Passerini, M. Kunze, A. Lex-Balducci, C. Schreiner, I. Cekic-Laskovic, and M. Winter, "Investigations on novel electrolytes, solvents and SEI additives for use in lithium-ion batteries: Systematic electrochemical characterization and detailed analysis by spectroscopic methods," *Progress in Solid State Chemistry*, vol. 42, pp. 65–84, 12 2014.

[33] K. M. Abraham, J. L. Goldman, and D. I. Natwig, "Characterization of Ether Electrolytes for Rechargeable Lithium Cells," tech. rep.

[34] F. W. Dampier, "Insoluble sulfide positive electrodes for organic electrolyte lithium secondary batteries," *C. R. Walk and J. S. Gore, This Journal*, vol. 128, p. 1, 1980.

[35] J. M. Tarascon and D. Guyomard, "New electrolyte compositions stable over the 0 to 5 V voltage range and compatible with the Li1+xMn2O4/carbon Li-ion cells," *Solid State Ionics*, vol. 69, pp. 293–305, 8 1994.

[36] J. Wang, Y. Yamada, K. Sodeyama, C. H. Chiang, Y. Tateyama, and A. Yamada, "Superconcentrated electrolytes for a high-voltage lithium-ion battery," *Nature Communications*, vol. 7, 6 2016.

[37] T. Richard, J. K. Xu, O. Borodin, and M. Ue, *Electrolytes for Lithium and Lithium-Ion Batteries*. Springer, 2014.

[38] J. Cha, J. G. Han, J. Hwang, J. Cho, and N. S. Choi, "Mechanisms for electrochemical performance enhancement by the salt-type electrolyte additive, lithium difluoro(oxalato)borate, in high-voltage lithium-ion batteries," *Journal of Power Sources*, vol. 357, pp. 97–106, 7 2017.

[39] Y. Yamada, C. H. Chiang, K. Sodeyama, J. Wang, Y. Tateyama, and A. Yamada, "Corrosion Prevention Mechanism of Aluminum Metal in Superconcentrated Electrolytes," *ChemElectroChem*, vol. 2, pp. 1687–1694, 11 2015.

[40] K. Kanamura, T. Okagawa, and Z. i. Takehara, "Electrochemical oxidation of propylene carbonate (containing various salts) on aluminium electrodes," *Journal of Power Sources*, vol. 57, pp. 119–123, 9 1995.

[41] K. Hirata, T. Kawase, and Y. Sumida, "Passivation Behavior of Aluminum in a Carbonate-Free Electrolyte Based on Lithium Bis(fluorosulfonyl)imide and Sulfolane," *Journal of The Electrochemical Society*, vol. 167, p. 140534, 11 2020.

[42] C. Campion, W. Li, and B. L. Lutch, "Thermal Decomposition of LiPF 6-Based Electrolytes for Lithium-Ion Batteries," 2005.

[43] H. Yang, G. V. Zhuang, and P. N. Ross, "Thermal stability of LiPF6 salt and Li-ion battery electrolytes containing LiPF6," *Journal of Power Sources*, vol. 161, pp. 573–579, 10 2006.

[44] G. H. Newman, R. W. Francis, L. H. Gaines, and B. M. Rao, "Hazard investigations of LiClO4 / Dioxolane Electrolyte," Tech. Rep. 9, 1980.

[45] K.-i. Takata, M. Morita, and Y. Matsuda, "Cycling Characteristics of Secondary Li Electrode in LiBF 4 / Mixed Ether Electrolytes," tech. rep., 1985.

[46] F. Lindgren, C. Xu, L. Niedzicki, M. Marcinek, T. Gustafsson, F. Björefors, K. Edström, and R. Younesi, "SEI Formation and Interfacial Stability of a Si Electrode in a LiTDI-Salt Based Electrolyte with FEC and VC Additives for Li-

Ion Batteries," *ACS Applied Materials and Interfaces*, vol. 8, pp. 15758–15766, 6 2016.

[47] M. Sina, J. Alvarado, H. Shobukawa, C. Alexander, V. Manichev, L. Feldman, T. Gustafsson, K. J. Stevenson, and Y. S. Meng, "Direct Visualization of the Solid Electrolyte Interphase and Its Effects on Silicon Electrochemical Performance," *Advanced Materials Interfaces*, vol. 3, pp. 1600438–1600438, 10 2016.

[48] G. M. Veith, M. Doucet, R. L. Sacci, B. Vacaliuc, J. K. Baldwin, and J. F. Browning, "Determination of the Solid Electrolyte Interphase Structure Grown on a Silicon Electrode Using a Fluoroethylene Carbonate Additive," *Scientific Reports*, vol. 7, 12 2017.

[49] J. C. Burns, A. Kassam, N. N. Sinha, L. E. Downie, L. Solnickova, B. Way, and J. R. Dahn, "Predicting and Extending the Lifetime of Li-Ion Batteries," *Journal of The Electrochemical Society*, vol. 160, pp. A1451–A1456, 7 2013.

[50] N. S. Choi, K. H. Yew, K. Y. Lee, M. Sung, H. Kim, and S. S. Kim, "Effect of fluoroethylene carbonate additive on interfacial properties of silicon thin-film electrode," *Journal of Power Sources*, vol. 161, pp. 1254–1259, 10 2006.

[51] Y. Li, F. Lian, L. Ma, C. Liu, L. Yang, X. Sun, and K. Chou, "Fluoroethylene Carbonate as Electrolyte Additive for Improving the electrochemical performances of High-Capacity Li1.16[Mn0.75Ni0.25]0.84O2 Material," *Electrochimica Acta*, vol. 168, pp. 261–270, 6 2015.

[52] I. A. Shkrob, K. Z. Pupek, and D. P. Abraham, "Allotropic Control: How Certain Fluorinated Carbonate Electrolytes Protect Aluminum Current Collectors by Promoting the Formation of Insoluble Coordination Polymers," *Journal of Physical Chemistry C*, vol. 120, pp. 18435–18444, 8 2016.

[53] K. Kim, I. Park, S. Y. Ha, Y. Kim, M. H. Woo, M. H. Jeong, W. C. Shin, M. Ue, S. Y. Hong, and N. S. Choi, "Understanding the thermal instability of fluoroethylene carbonate in LiPF6-based electrolytes for lithium ion batteries," *Electrochimica Acta*, vol. 225, pp. 358–368, 1 2017.

[54] A. L. Michan, B. S. Parimalam, M. Leskes, R. N. Kerber, T. Yoon, C. P. Grey,

and B. L. Lucht, "Fluoroethylene carbonate and vinylene carbonate reduction: Understanding lithium-ion battery electrolyte additives and solid electrolyte interphase formation," *Chemistry of Materials*, vol. 28, pp. 8149–8159, 11 2016.

[55] C. C. Nguyen and B. L. Lucht, "Comparative Study of Fluoroethylene Carbonate and Vinylene Carbonate for Silicon Anodes in Lithium Ion Batteries," *Journal of The Electrochemical Society*, vol. 161, pp. A1933–A1938, 9 2014.

[56] T. Jaumann, J. Balach, U. Langklotz, V. Sauchuk, M. Fritsch, A. Michaelis, V. Teltevskij, D. Mikhailova, S. Oswald, M. Klose, G. Stephani, R. Hauser, J. Eckert, and L. Giebeler, "Lifetime vs. rate capability: Understanding the role of FEC and VC in high-energy Li-ion batteries with nano-silicon anodes," *Energy Storage Materials*, vol. 6, pp. 26–35, 1 2017.

[57] V. Etacheri, R. Marom, R. Elazari, G. Salitra, and D. Aurbach, "Challenges in the development of advanced Li-ion batteries: a review," *Energy & Environmental Science*, vol. 4, pp. 3243–3262, 8 2011.

[58] J. Pan, Y. T. Cheng, and Y. Qi, "General method to predict voltage-dependent ionic conduction in a solid electrolyte coating on electrodes," *Physical Review B - Condensed Matter and Materials Physics*, vol. 91, 4 2015.

[59] J. S. Kim, K. Kim, W. Cho, W. H. Shin, R. Kanno, and J. W. Choi, "A truncated manganese spinel cathode for excellent power and lifetime in lithium-ion batteries," *Nano Letters*, vol. 12, pp. 6358–6365, 12 2012.

[60] R. Petibon, N. N. Sinha, J. C. Burns, C. P. Aiken, H. Ye, C. M. Vanelzen, G. Jain, S. Trussler, and J. R. Dahn, "Comparative study of electrolyte additives using electrochemical impedance spectroscopy on symmetric cells," *Journal of Power Sources*, vol. 251, pp. 187–194, 4 2014.

[61] Y. Qian, P. Niehoff, M. Börner, M. Grützke, X. Mönnighoff, P. Behrends, S. Nowak, M. Winter, and F. M. Schappacher, "Influence of electrolyte additives on the cathode electrolyte interphase (CEI) formation on LiNi1/3Mn1/3Co1/3O2 in half cells with Li metal counter electrode," *Journal of Power Sources*, vol. 329, pp. 31–40, 10 2016.

[62] L. Ellis, I. Hill, K. Gering, and J. Dahn, "Synergistic Effect of LiPF 6 and LiBF 4 as Electrolyte Salts in Lithium-Ion Cells," *Journal of The Electrochemical Society*, pp. A2426–A2433, 2017.

[63] W. Zhao, L. Zou, J. Zheng, H. Jia, J. Song, M. H. Engelhard, C. Wang, W. Xu, Y. Yang, and J. G. Zhang, "Simultaneous Stabilization of LiNi0.76Mn0.14Co0.10O2 Cathode and Lithium Metal Anode by Lithium Bis(oxalato)borate as Additive," *ChemSusChem*, vol. 11, pp. 2211–2220, 7 2018.

[64] P. Niehoff and M. Winter, "Composition and growth behavior of the surface and electrolyte decomposition layer of/on a commercial lithium ion battery LixNi 1/3Mn1/3Co1/3O2 cathode determined by sputter depth profile X-ray photoelectron spectroscopy," *Langmuir*, vol. 29, pp. 15813–15821, 12 2013.

[65] Y. Lu, Z. Tu, and L. A. Archer, "Stable lithium electrodeposition in liquid and nanoporous solid electrolytes," *Nature Materials*, 2014.

[66] J. Zheng, X. Wu, and Y. Yang, "Improved electrochemical performance of Li[Li0.2Mn 0.54Ni0.13Co0.13]O2 cathode material by fluorine incorporation," *Electrochimica Acta*, vol. 105, pp. 200–208, 2013.

[67] A. Heist and S.-H. Lee, " Improved Stability and Rate Capability of Ionic Liquid Electrolyte with High Concentration of LiFSI ," *Journal of The Electrochemical Society*, vol. 166, pp. A1860–A1866, 6 2019.

[68] X. Fan, L. Chen, X. Ji, T. Deng, S. Hou, J. Chen, J. Zheng, F. Wang, J. Jiang, K. Xu, and C. Wang, "Highly Fluorinated Interphases Enable High-Voltage Li-Metal Batteries," *Chem*, vol. 4, pp. 174–185, 1 2018.

[69] J. Li, L. Baggetto, S. K. Martha, G. M. Veith, J. Nanda, C. Liang, N. J. Dudney, J. Li, L. Baggetto, S. K. Martha, G. M. Veith, J. Nanda, N. J. Dudney, and C. Liang, "An Artificial Solid Electrolyte Interphase Enables the Use of a LiNi0.5 Mn1.5 O4 5 V Cathode with Conventional Electrolytes," *Advanced Energy Materials*, vol. 3, pp. 1275–1278, 10 2013.

[70] Q. Wu, W. Lu, M. Miranda, T. K. Honaker-Schroeder, K. Y. Lakhsassi, and D. Dees, "Effects of lithium difluoro(oxalate)borate on the performance of Li-

rich composite cathode in Li-ion battery," *Electrochemistry Communications*, vol. 24, pp. 78–81, 10 2012.

[71] W. Zhao, J. Zheng, L. Zou, H. Jia, B. Liu, H. Wang, M. H. Engelhard, C. Wang, W. Xu, Y. Yang, and J.-G. Zhang, "High Voltage Operation of Ni-Rich NMC Cathodes Enabled by Stable Electrode/Electrolyte Interphases," *Advanced Energy Materials*, vol. 8, p. 1800297, 7 2018.

[72] S. S. Zhang and T. R. Jow, "Aluminum corrosion in electrolyte of Li-ion battery,"

[73] A. Hofmann, M. Schulz, V. Winkler, and T. Hanemann, "Anodic Aluminum Dissolution in Conducting Salt Containing Electrolytes for Lithium-Ion Batteries," *Journal of The Electrochemical Society*, vol. 161, no. 3, pp. A431–A438, 2014.

[74] X. Zhang and T. Devine, "Identity of Passive Film Formed on Aluminum in Li-Ion Battery Electrolytes with LiPF6," *Journal of The Electrochemical Society*, vol. 153, no. 9, pp. B344–B351, 2006.

[75] R. Greef, R. Peat, L. Peter, J. Robinson, and D. Pletcher, *Instrumental methods in electrochemistry*. Ellis Horwood Limited, 1990.

[76] A. J. Bard and L. R. Faulkner, *Electrochemical Methods: Fundamentals and Applications*. 2nd ed., 2001.

[77] J. Hjelen, *Scanning elektron-mikroskopi*. Trondheim: SINTEF, 8 1989.

[78] W. Zhou and Z. Lin Wang, *Scanning Microscopy for Nanotechnology*. Springer, 1st ed., 2007.

[79] A. Garratt-Reed and D. Bell, *Energy-Dispersive X-ray Analysis in the Electron Microscope*. 2003.

[80] T. Nelis and R. Payling, *Glow discharge optical emission spectroscopy: a practical guide*. The Royal Society of Chemistry, 2003.

[81] P. Chapon, A. Tempez, and C. Tauzirde, "Glow Discharge Spectrometry," tech. rep.

[82] B. Smith, *Fundamentals of Fourier Transform Infrared Spectroscopy.* CRC press, 2nd ed.

[83] E. Moore, *Fourier Transform Infrared Spectroscopy (FTIR) : Methods, Analysis, and Reseach Insights.* New York: Nova Science Publishers, 2016.

[84] N. Abidi, *FTIR Microspectroscopy.* Springer International Publishing, 1 ed., 2021.

[85] K. Edström, M. Herstedt, and D. P. Abraham, "A new look at the solid electrolyte interphase on graphite anodes in Li-ion batteries," *Journal of Power Sources*, vol. 153, pp. 380–384, 2 2006.

[86] H. W. Thompson and P. Torkington, "The vibrational spectra of esters and ketones," *Journal of the Chemical Society*, pp. 640–645, 1945.

[87] N. Sheppard and D. M. Simpson, "The infra-red and Raman spectra of hydrocarbons. Part II. Paraffins," *Quarterly Reviews, Chemical Society*, vol. 7, no. 1, pp. 19–55, 1953.

[88] B. Fortunato, P. Mirone, and G. Fini, "Infrared and Raman spectra and vibrational assignment of ethylene carbonate," *Spectrochimica Acta Part A: Molecular Spectroscopy*, vol. 27, pp. 1917–1927, 9 1971.

[89] J. Fox and A. Martin, "Investigations of Infra-Red Spectra ($2 \cdot 5$-$7 \cdot 5\ \mu$). Absorption of Water on JSTOR," *Mathematical and Physical Sciences*, vol. 174, no. 957, pp. 234–262, 1940.

[90] J. Yang, N. Solomatin, A. Kraytsberg, Y. Ein-Eli, J. Yang, N. Solomatin, A. Kraytsberg, and Y. Ein-Eli, "In-Situ Spectro–electrochemical Insight Revealing Distinctive Silicon Anode Solid Electrolyte Interphase Formation in a Lithium–ion Battery," *ChemistrySelect*, vol. 1, pp. 572–576, 3 2016.

[91] Y. Ikezawa and H. Nishi, "In situ FTIR study of the Cu electrode/ethylene carbonate + dimethyl carbonate solution interface," *Electrochimica Acta*, vol. 53, no. 10, pp. 3663–3669, 2008.

[92] J. E. Katon And, M. D. Cohen, and J. E. Katon, "The Vibrational Spectra and

Structure of Dimethyl Carbonate and its Conformational Behavior," *Canadian Journal of Chemistry*, vol. 53, no. 9, pp. 1378–1386, 1975.

[93] T. Pirzada, S. A. Arvidson, C. D. Saquing, S. S. Shah, and S. A. Khan, "Hybrid carbon silica nanofibers through sol-gel electrospinning," *Langmuir*, vol. 30, pp. 15504–15513, 12 2014.

[94] R. S. Rasmussen, D. D. Tunnicliff, and R. Robert Brattain, "Infrared and Ultraviolet Spectroscopic Studies on Ketones," *Journal of the American Chemical Society*, vol. 71, pp. 1068–1072, 3 1949.

[95] B. M. Gatehouse, S. E. Livingstone, and R. S. Nyholm, "The infrared spectra of some simple and complex carbonates," *Journal of the Chemical Society*, pp. 3137–3142, 1958.

[96] N. Delpuech, D. Mazouzi, N. Dupré, P. Moreau, M. Cerbelaud, J. S. Bridel, J. C. Badot, E. De Vito, D. Guyomard, B. Lestriez, and B. Humbert, "Critical role of silicon nanoparticles surface on lithium cell electrochemical performance analyzed by FTIR, Raman, EELS, XPS, NMR, and BDS spectroscopies," *Journal of Physical Chemistry C*, vol. 118, pp. 17318–17331, 8 2014.

[97] V. Etacheri, U. Geiger, Y. Gofer, G. A. Roberts, I. C. Stefan, R. Fasching, and D. Aurbach, "Exceptional electrochemical performance of Si-nanowires in 1,3-dioxolane solutions: A surface chemical investigation," *Langmuir*, vol. 28, pp. 6175–6184, 4 2012.

[98] K. I. Morigaki and A. Ohta, "Analysis of the surface of lithium in organic electrolyte by atomic force microscopy, Fourier transform infrared spectroscopy and scanning auger electron microscopy," *Journal of Power Sources*, vol. 76, pp. 159–166, 12 1998.

[99] D. Aurbach, B. Markovsky, A. Shechter, Y. Ein-Eli, and H. Cohen, "A Comparative Study of Synthetic Graphite and Li Electrodes in Electrolyte Solutions Based on Ethylene Carbonate-Dimethyl Carbonate Mixtures," *Journal of The Electrochemical Society*, vol. 143, pp. 3809–3820, 12 1996.

[100] N. R. Mulder, "The Effect of LiFSI Salt Concentration and Electrolyte Additives on the Performance of Silicon Anodes for Lithium-Ion Batteries," 2018.

[101] S. Dalavi, P. Guduru, and B. L. Lucht, "Performance Enhancing Electrolyte Additives for Lithium Ion Batteries with Silicon Anodes," *Journal of The Electrochemical Society*, vol. 159, no. 5, pp. A642–A646, 2012.

[102] R. Barnes, U. Liddel, and V. Williams, "Infrared Spectroscopy. Industrial Applications," *Analytical Chemistry*, vol. 15, no. 11, pp. 659–709, 1943.

[103] D. Aurbach, Y. Gofer, M. Ben-Zion, and P. Aped, "The behaviour of lithium electrodes in propylene and ethylene carbonate: Te major factors that influence Li cycling efficiency," *Journal of Electroanalytical Chemistry*, vol. 339, pp. 451–471, 11 1992.

[104] D. Aurbach, M. D. Levi, E. Levi, and A. Schechter, "Failure and stabilization mechanisms of graphite electrodes," *Journal of Physical Chemistry B*, vol. 101, pp. 2195–2206, 3 1997.

[105] D. Aurbach, Y. Gofer, and J. Langzam, "The Correlation Between Surface Chemistry, Surface Morphology, and Cycling Efficiency of Lithium Electrodes in a Few Polar Aprotic Systems," *Journal of The Electrochemical Society*, vol. 136, pp. 3198–3205, 11 1989.

[106] M. A. Mohamed, J. Jaafar, A. F. Ismail, M. H. Othman, and M. A. Rahman, "Fourier Transform Infrared (FTIR) Spectroscopy," *Membrane Characterization*, pp. 3–29, 2 2017.

[107] K. Fujil, S. Seki, S. Fukuda, R. Kanzaki, T. Takamuku, Y. Umebayashi, and S. I. Ishiguro, "Anion conformation of low-viscosity room-temperature ionic liquid 1-ethyl-3-methylimidazolium bis(fluorosulfonyl) imide," *Journal of Physical Chemistry B*, vol. 111, pp. 12829–12833, 11 2007.

[108] S. Gatto, O. Palumbo, S. Caramazza, F. Trequattrini, P. Postorino, G. B. Appetecchi, and A. Paolone, "The infrared spectrum of bis(fluorosulfonyl)imide revisited: Attractive performances of the PBE0/6-31G** model," *Vibrational Spectroscopy*, vol. 82, pp. 16–21, 1 2016.

[109] J. Huang and A. F. Hollenkamp, "Thermal behavior of ionic liquids containing the FSI anion and the Li + cation," *Journal of Physical Chemistry C*, vol. 114, pp. 21840–21847, 12 2010.

[110] M. Kerner, N. Plylahan, J. Scheers, and P. Johansson, "Thermal stability and decomposition of lithium bis(fluorosulfonyl)imide (LiFSI) salts," *RSC Advances*, vol. 6, no. 28, pp. 23327–23334, 2016.

[111] I. A. Shkrob, K. Z. Pupek, and D. P. Abraham, "Allotropic Control: How Certain Fluorinated Carbonate Electrolytes Protect Aluminum Current Collectors by Promoting the Formation of Insoluble Coordination Polymers," *Journal of Physical Chemistry C*, vol. 120, pp. 18435–18444, 8 2016.

[112] R. S. Young, H. Yu, and M. N. Obrovac, "Enhancing NMC/silicon alloy full cell cycling by adding water to the electrolyte," *Journal of Applied Electrochemistry*, vol. 51, pp. 1501–1507, 10 2021.

[113] J. C. Burns, N. N. Sinha, G. Jain, H. Ye, C. M. VanElzen, E. Scott, A. Xiao, W. M. Lamanna, and J. R. Dahn, "The Impact of Intentionally Added Water to the Electrolyte of Li-ion Cells: I. Cells with Graphite Negative Electrodes," *Journal of The Electrochemical Society*, vol. 160, p. A2281, 10 2013.

[114] D. J. Xiong, R. Petibon, L. Madec, D. S. Hall, and J. R. Dahn, " Some Effects of Intentionally Added Water on LiCoO 2 /Graphite Pouch Cells ," *Journal of The Electrochemical Society*, vol. 163, pp. A1678–A1685, 6 2016.

[115] H. Shin, J. Park, A. M. Sastry, and W. Lu, "Effects of Fluoroethylene Carbonate (FEC) on Anode and Cathode Interfaces at Elevated Temperatures," *Journal of The Electrochemical Society*, vol. 162, pp. A1683–A1692, 6 2015.

Appendices

Appendix A

Additional plots for NMC Cathodes

Table A.1 shows all cells made with NMC cathodes for this thesis. Indicated is if the cells worked (w), meaning if they completed the cycling program or if they stopped (s). If the cells stopped the cycle they stopped on is also noted with CX, where X indicates the cycle number from 1 to 62. The parallels included in the the result section is parallel 1, while parallel 2 is the additional parallel added to calculate the averages in the appendices.

Table A.1: Overview of all cells cycled in the different electrolytes with NMC cathodes.

LiFSI	LiFSI with H_2O	LiFSI with FEC	LiFSI with FEC and H_2O
1 (w)	1 (w)	*old FEC electrolytes*	
2 (w)	2 (w)	1 (w)	1 (w)
3 (-)	3 (s:c7)	2 (s:c42)	2 (w)
	4 (s:c18)	3 (-)	3 (s:c19)
	5 (s:c17)	*new FEC electrolytes*	
	6 (s:c12)	1 (w)	1 (s:c54)
	7 (s:c29)	2 (s:c19)	2 (s:c37)
		3 (s:c26)	3 (s:c23)
		4 (s:c3)	
		5 (s:c3)	
		6 (-)	

A.1 Cell Performance during Galvanostatic Cycling

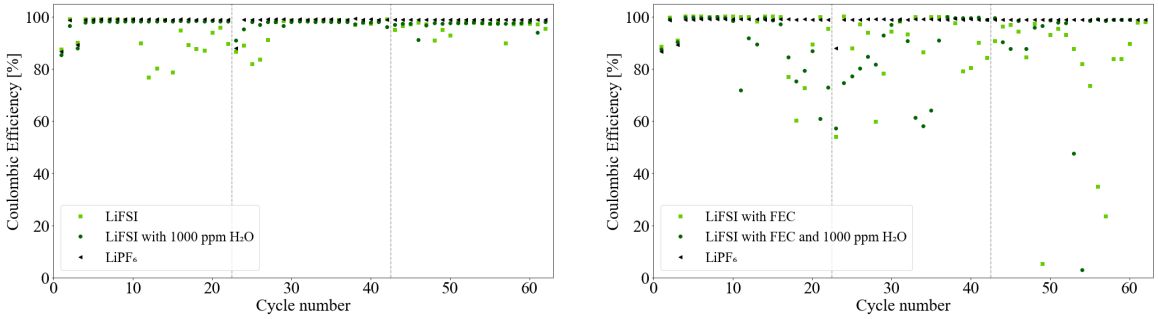

(a) Coloumbic efficiency without FEC

(b) Coloumbic efficiency with FEC

Figure A.1: Calculated average of the coulombic efficiencies for two parallels with NMC_{111} cycled electrolytes a) without FEC and b) with FEC.

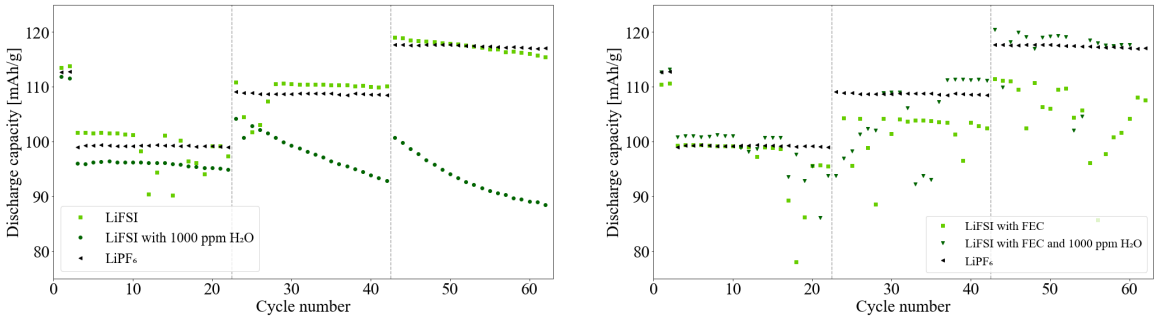

(a) Discharge capacity without FEC

(b) Discharge capacity with FEC

Figure A.2: Calculated average of the discharge capacities for two parallels with NMC_{111} cycled electrolytes a) without FEC and b) with FEC.

A.2 Potential Profiles from Galvanostatic Cycling

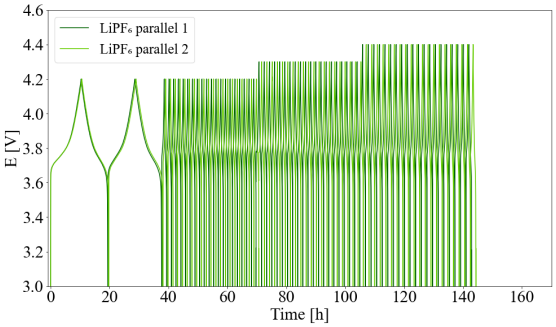

Figure A.3: Additional parallel of the galvanic cycling of NMC_{111} in $LiPF_6$

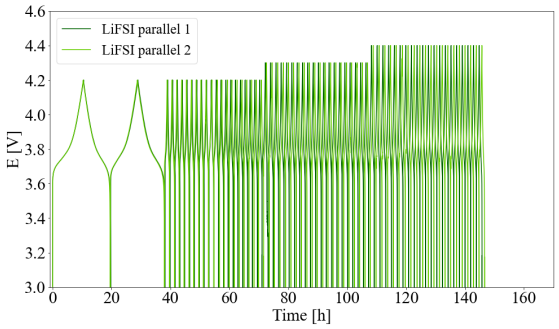

(a) LiFSI

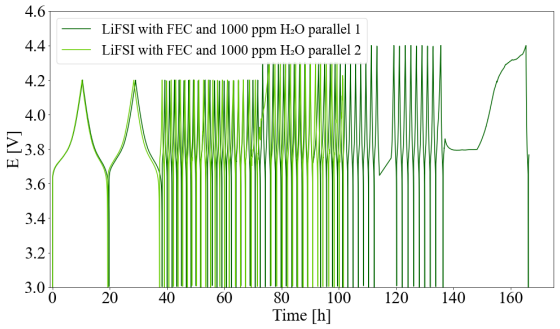

(b) LiFSI with 1000 ppm H_2O

Figure A.4: Additional parallels of the galvanic cycling of NMC_{111} in electrolytes without FEC

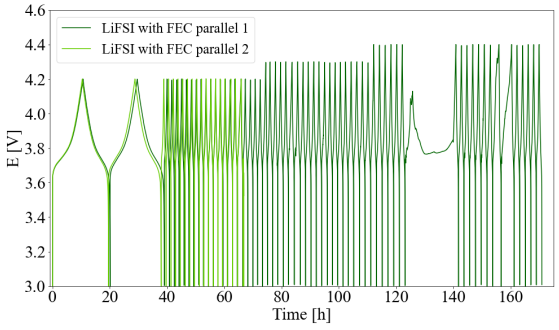

(a) LiFSI with FEC

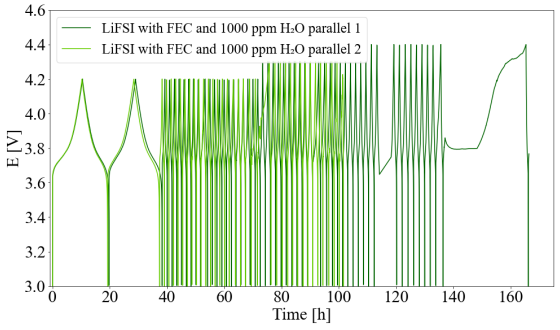

(b) LiFSI with FEC and 1000 ppm H_2O

Figure A.5: Additional parallels of the galvanic cycling of NMC_{111} in electrolytes with FEC

A.3 EDS Analysis of NMC Cathodes

For the cathode surface cycled in the LiFSI electrolyte the EDS analysis is shown in Figure A.6.

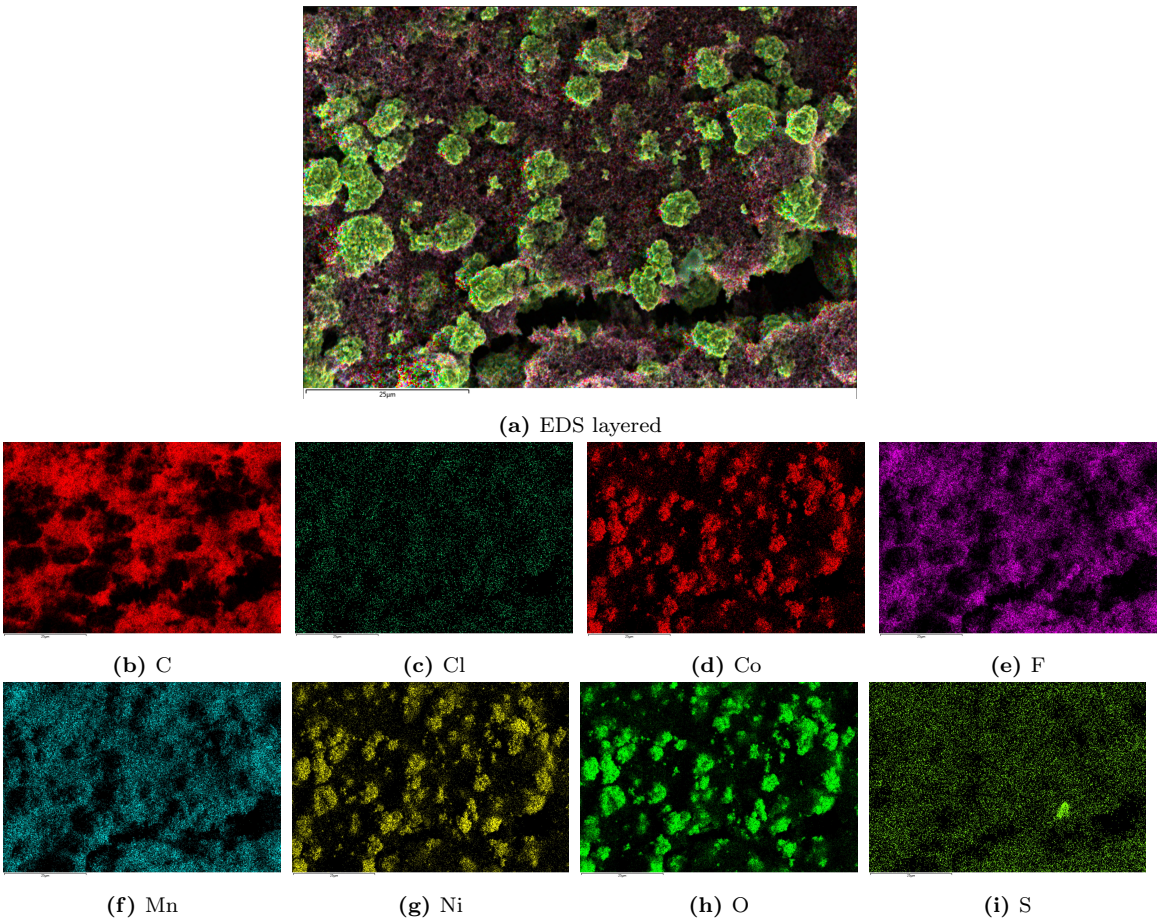

(a) EDS layered

(b) C **(c)** Cl **(d)** Co **(e)** F

(f) Mn **(g)** Ni **(h)** O **(i)** S

Figure A.6: EDS analysis of NMC_{111} cathodes cycled in LiFSI electrolyte.

The white spheres previously mentioned from the SEM images consist of Co, Mn, Ni and Oxygen as can be seen from the distributions in Figure A.6 d), f), g) and h). These elements correlate with the active material as previously mentioned. The Mn content can also be observed in the background together with C, Cl, F and S, as for the pristine cathode.

The EDS analysis for cathode surface cycled in the water containing electrolyte can be seen in Figure A.7. The same composition as for the previous cathode surfaces is observed, with the Co, Mn, Ni and O containing spheres and the C, F, Cl, Mn and S background.

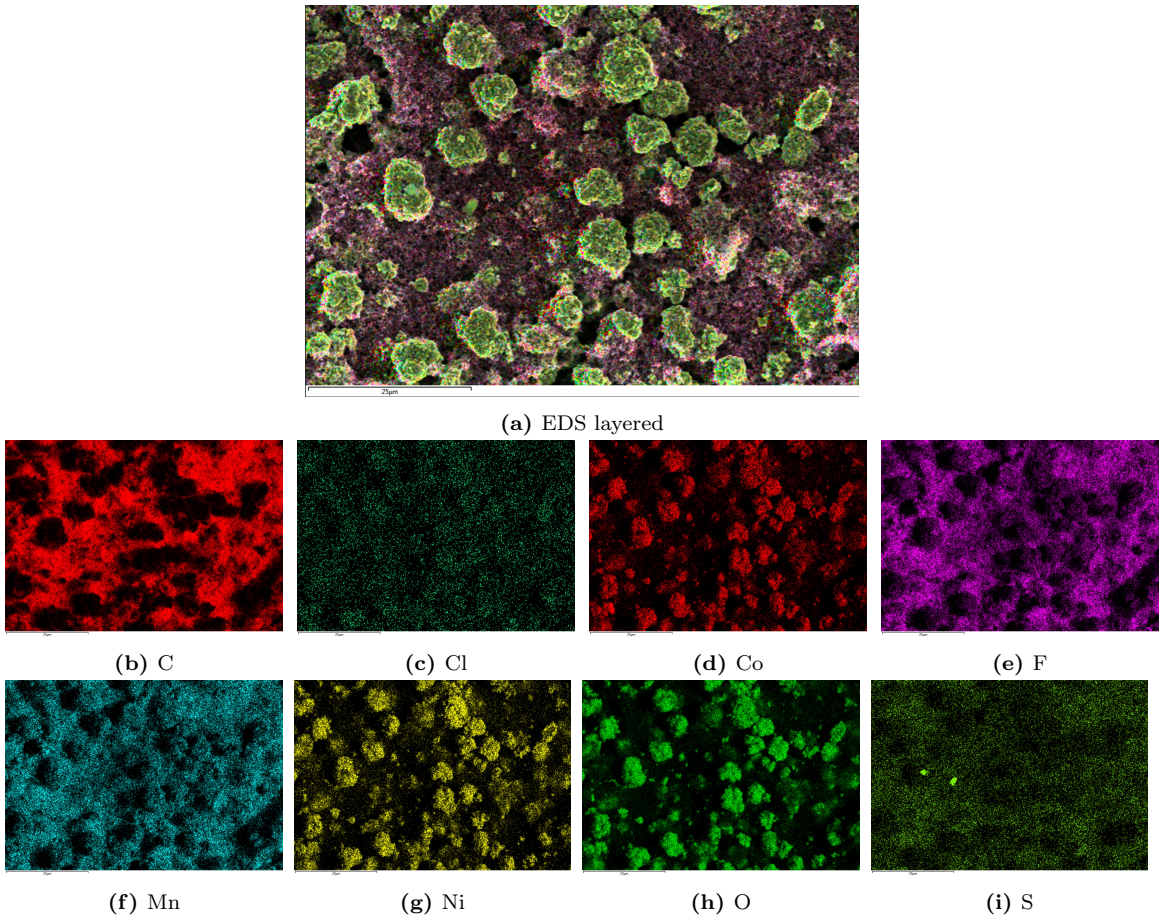

(a) EDS layered

(b) C **(c)** Cl **(d)** Co **(e)** F

(f) Mn **(g)** Ni **(h)** O **(i)** S

Figure A.7: EDS analysis of NMC_{111} cathodes cycled in LiFSI electrolyte with 1000 ppm of H_2O.

The EDS analysis for the NMC_{111} cycled in the FEC containing electrolytes are shown in the two following figures. Compared to the EDS analysis of the pristine cathode and the cathodes cycled in the LiFSI electrolyte the signals of all the elements are weaker for these cathodes. This is the result of the parameters not being set to the optimal values that were used for the three previous EDS analyses, as the working distance was not changed to 10 mm and the 4 mm from the SEM imaging was used.

In Figure A.8 the EDS analysis results for a NMC_{111} cathode cycled in the FEC containing LiFSI electrolyte is presented. The same phenomenon observed in the previous analyses can also be seen here. Co, Mn, Ni and O containing spheres and mainly C and F in the porous background. Smaller amounts of Cl is observed on the entire surface. S and Mn is observed on the entire surface, with the exception of the craters. In the bottom right corner in Figure A.8 i) a small area with a very high S concentration can be observed.

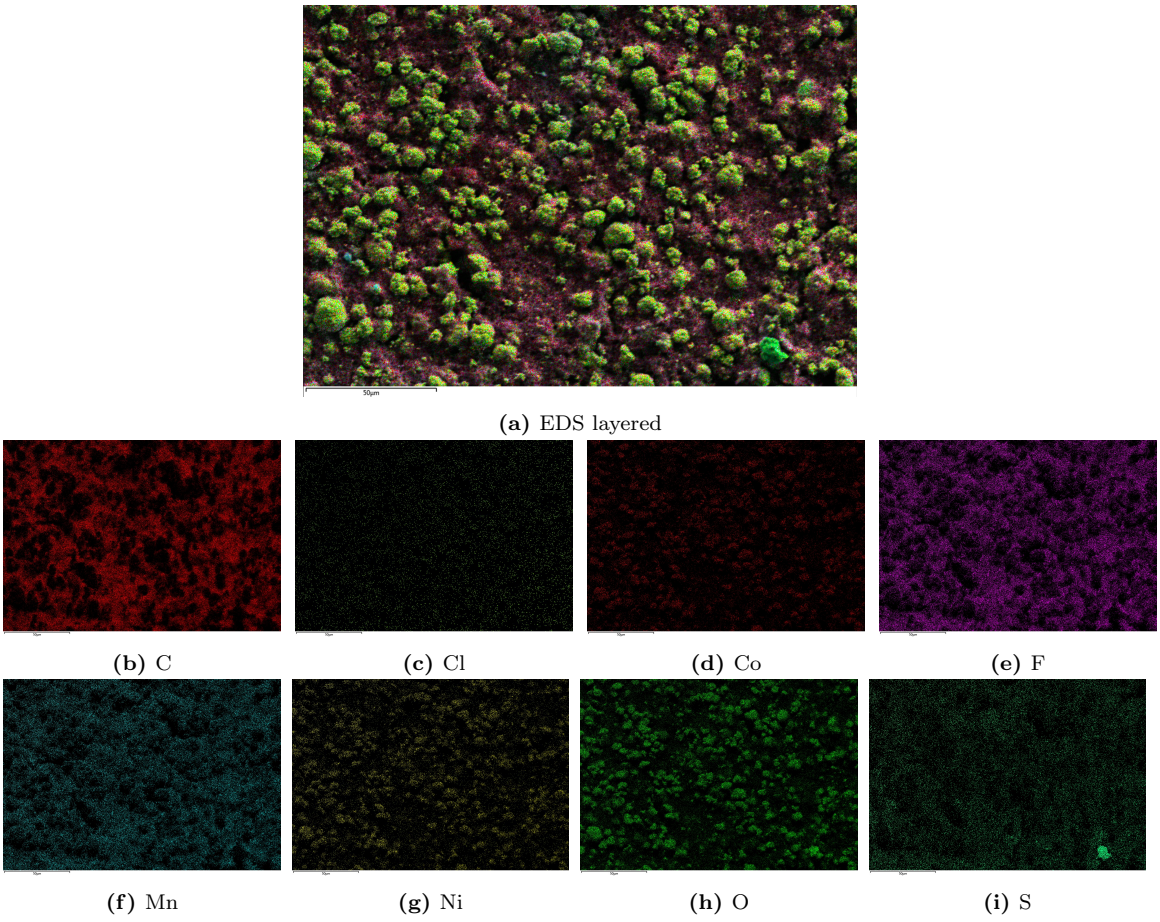

(a) EDS layered

(b) C **(c)** Cl **(d)** Co **(e)** F

(f) Mn **(g)** Ni **(h)** O **(i)** S

Figure A.8: EDS analysis of NMC_{111} cathodes cycled in the FEC containing LiFSI electrolyte.

The EDS analysis of a NMC_{111} cathode cycled in the LiFSI electrolyte with FEC and 1000 ppm of H_2O is presented. The trend with Co, Mn, Ni and O containing spheres and a background consisting of mainly C and F can also be seen for this cathode surface. For this cathode surface the Mn can also be seen on the entire surface, together with small amounts of Cl of S.

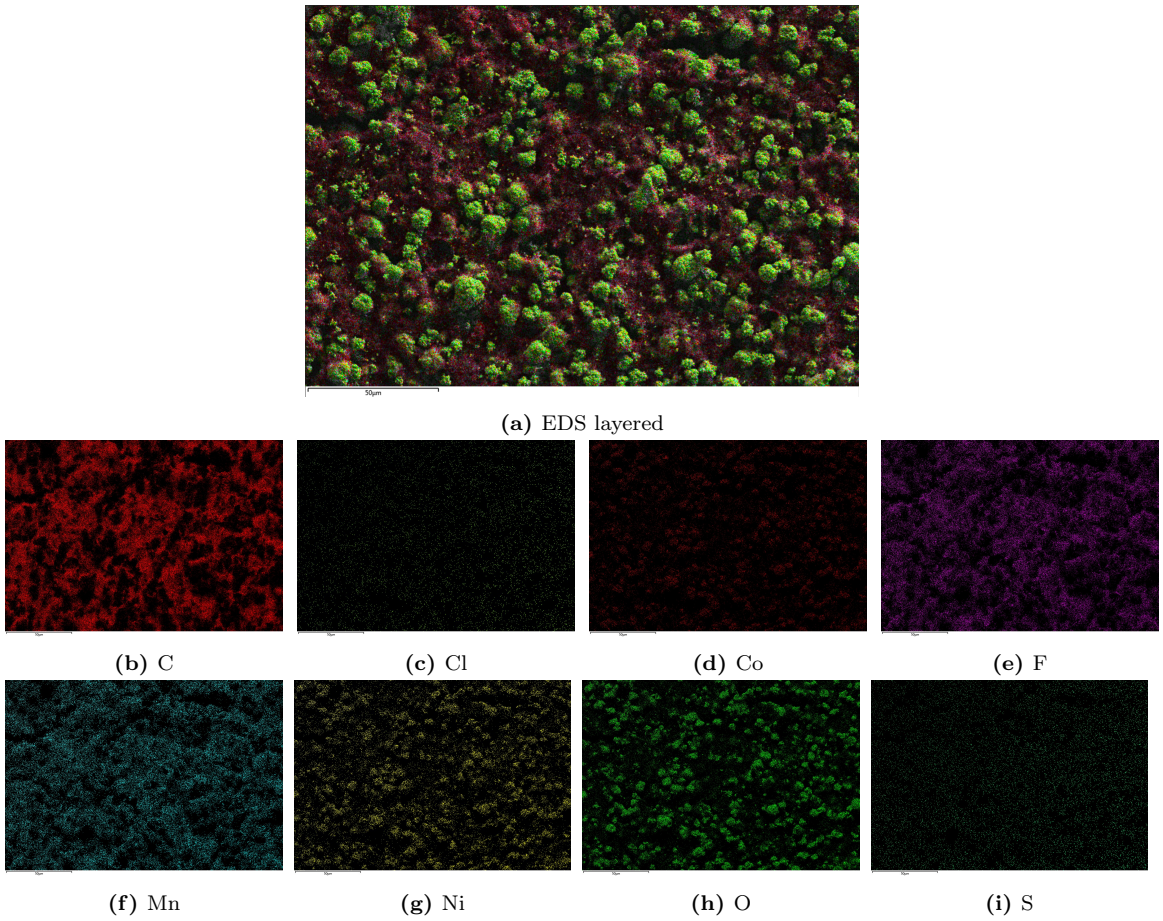

(a) EDS layered

(b) C **(c)** Cl **(d)** Co **(e)** F

(f) Mn **(g)** Ni **(h)** O **(i)** S

Figure A.9: EDS analysis of NMC_{111} cathodes cycled in LiFSI electrolyte with FEC and 1000 ppm of H_2O.

Appendix B

Additional plots for Al foils

B.1 Cyclic Voltammograms of Al foils

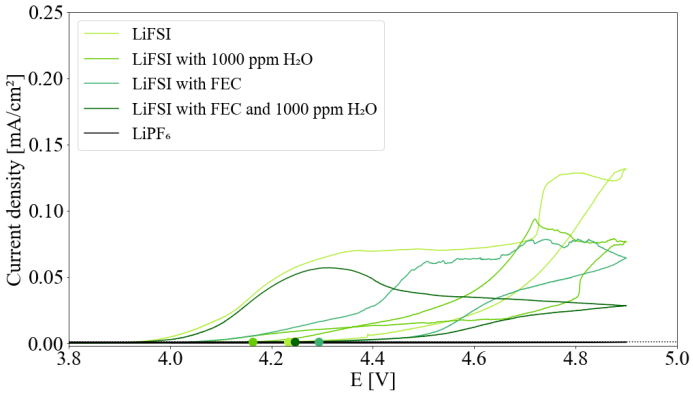

Figure B.1: Additional parallel of Al foil cycled for one cycle in the different LiFSI electrolytes.

B.2 FTIR Al pristine

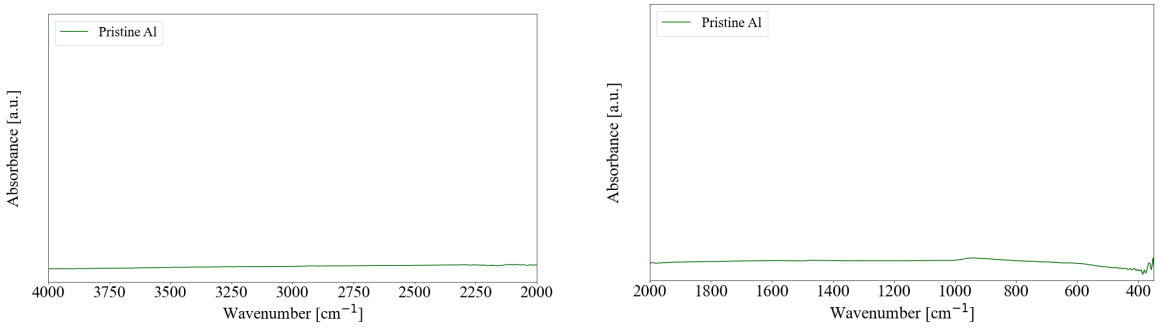

(a) Wavenumber range 4000 - 2000 cm^{-1}

(b) Wavenumber range 2000 - 350 cm^{-1}

Figure B.2: Measurement of pristine Al foil that are retracted from the FTIR sample measurements.

Appendix C

Additional plots for old FEC

C.1 Potential profiles from Galvanostatic cycling

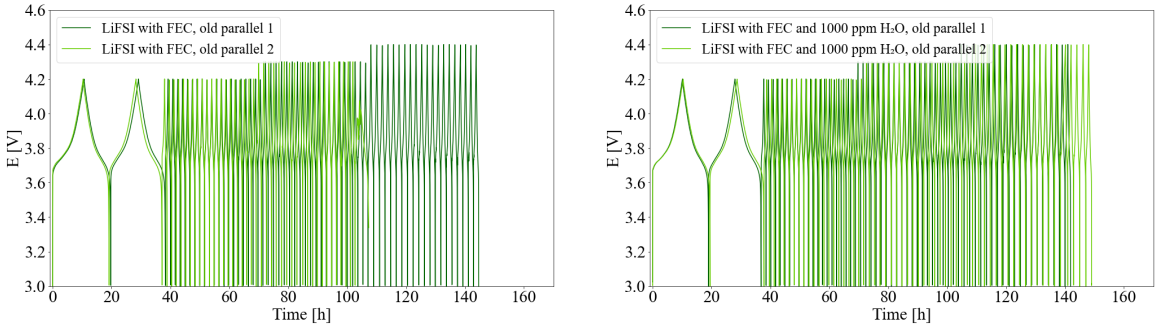

(a) LiFSi with FEC (old)

(b) LiFSI with FEC and 1000 ppm of H_2O (old)

Figure C.1: Additional parallels of the galvanostatic cycling of NMC_{111} in the old FEC containing electrolytes.

C.2 Cell Performance

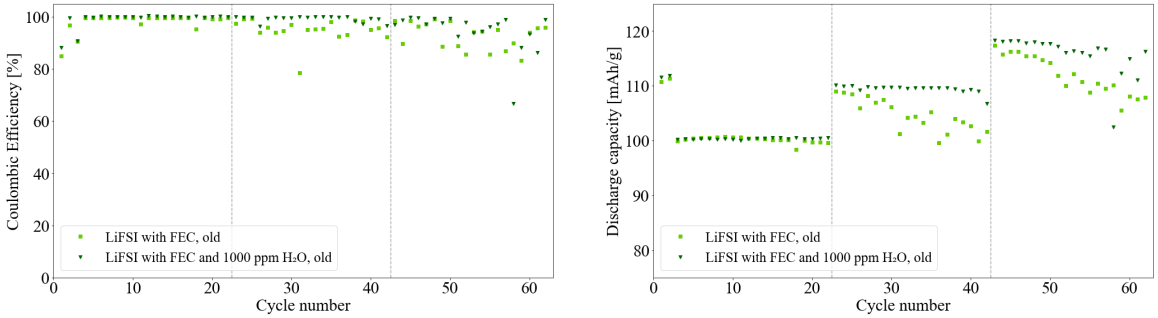

(a) Coulombic efficiency

(b) Discharge capacity

Figure C.2: Calculated average for the coulombic efficiencies and discharge capacities of two parallels of NMC_{111} cycled in the old FEC containing electrolytes.

C.3 EDS Analysis

To determine the composition of the NMC_{111} surfaces EDS analysis was performed for the following elements b) Carbon, c) Chlorine, d) Cobalt, e) Fluorine, f) Manganese, g) Nickel, h) Oxygen and i) Sulpher. In addition, Figure a) shows the SEM image with the EDS images layered on top.

Figure C.3 shows the EDS results for the NMC_{111} cathode surface cycled in the old LiFSI electrolyte with FEC.

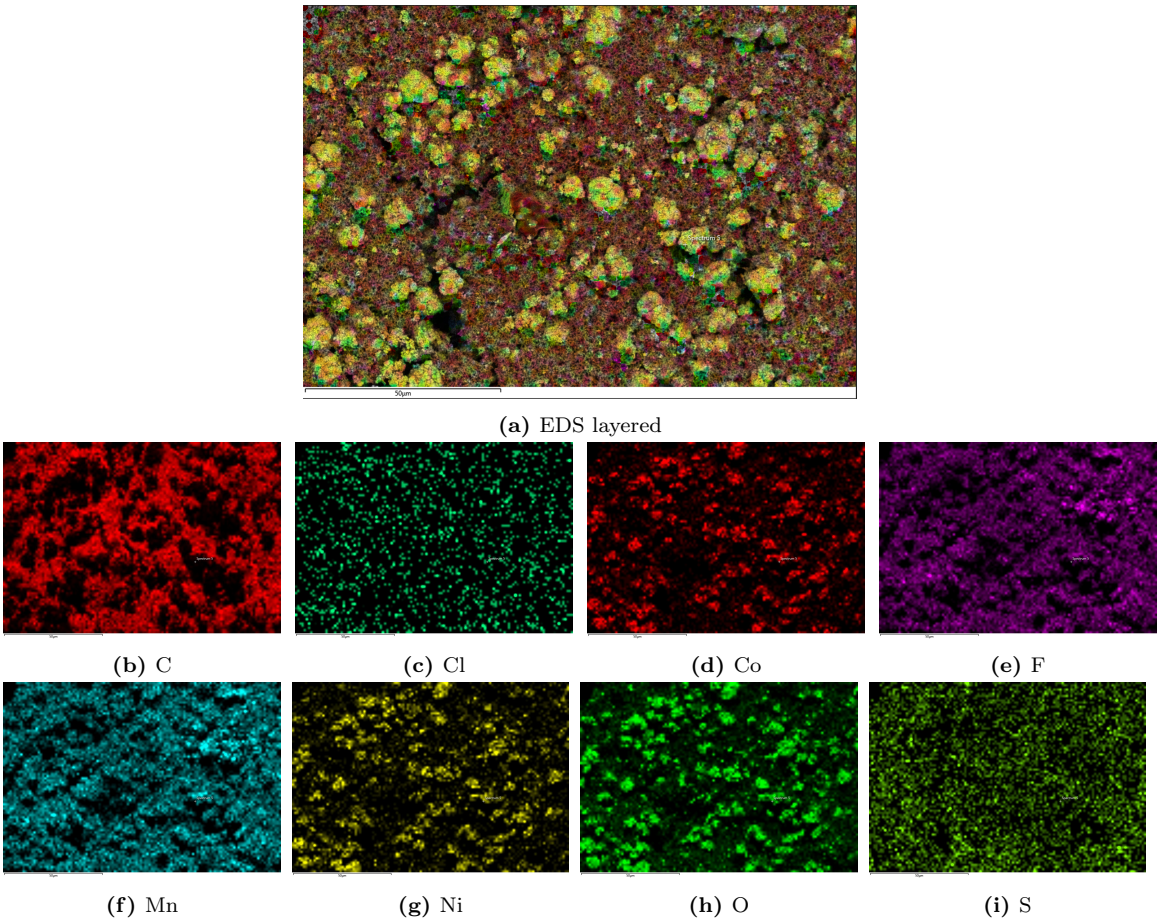

(a) EDS layered

(b) C **(c)** Cl **(d)** Co **(e)** F

(f) Mn **(g)** Ni **(h)** O **(i)** S

Figure C.3: SEM with EDS NMC_{111} cathode in old FEC electrolyte

The analysis show that the lighter spheres are made up of Co, Mn and Ni and O from Figures C.3 d), f), g) and h). As discussed in the previous EDS section, this is the composition of the cathode material $LiNi_xMn_yCo_zO_2$. Lithium is not included as it

cannot be detected by the EDS instrument. The porous background consist mainly of C, F and Mn as seen from Figures C.3 b), e) and f). The C and F are constitutes of the binder solution, which is a mix of carbon black and PVDF. Both Cl and S can be observed sporadically over the entire cathode surface form Figures C.3 c) and i).

The EDS analysis of the NMC_{111} cathode is shown in Figure C.4.

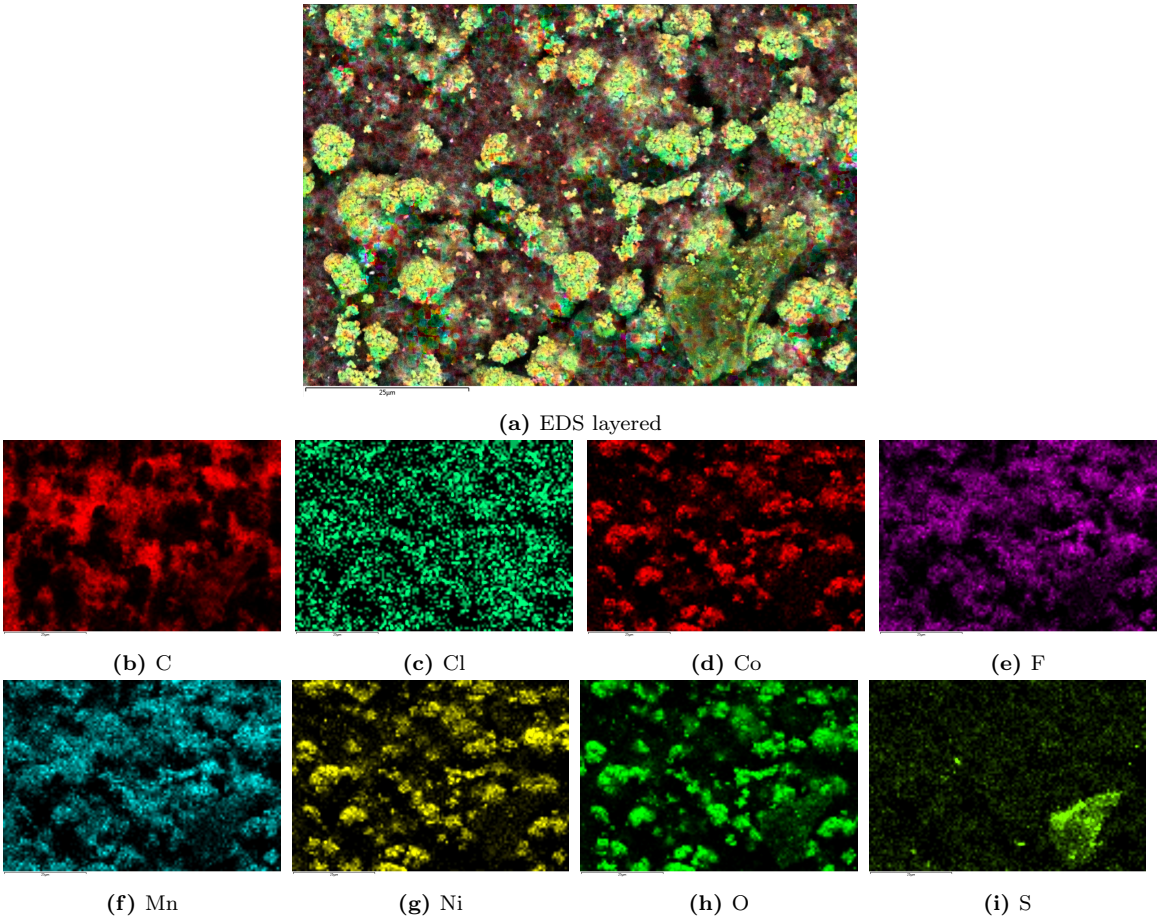

(a) EDS layered

(b) C **(c)** Cl **(d)** Co **(e)** F

(f) Mn **(g)** Ni **(h)** O **(i)** S

Figure C.4: SEM with EDS NMC_{111} cathode in old FEC and water containing electrolyte

Similar to the other cathode surfaces its evident that the spheres on this surface also consist of Co, Mn, Ni and O from Figures C.4 d), f), g) and h). The main constituents of the background is also C, F and Mn for this cathode surface from Figure C.4 b), e) and f). The chlorine content of this cathode is heavily spread over the entire surface area, shown in Figure C.4 c). However, the darker spot discussed in the SEM imaging of this cathode surface has a high presence of S, as seen in Figure C.4 i).

Appendix D

Plots from Project Thesis

D.1 Cyclic Voltammetry of old FEC Electrolytes from Project Thesis

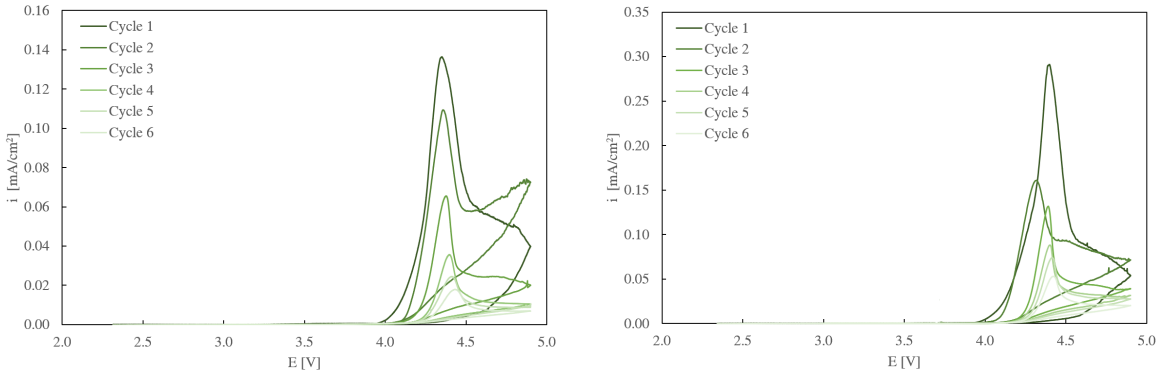

(a) LiFSI with FEC

(b) LiiFSI with FEC and water

Figure D.1: Voltammograms of the old FEC electrolytes from the project work, when they were not old.

Table D.1: Maximum current densities and onset potential of the old FEC electrolyte from when they were not old.

Electrolyte	Onset potential [V]	Current density [mA cm^{-2}]
LiFSI FEC, old	4.276	0.136
LiFSI FEC+H_2O	4.244	0.291

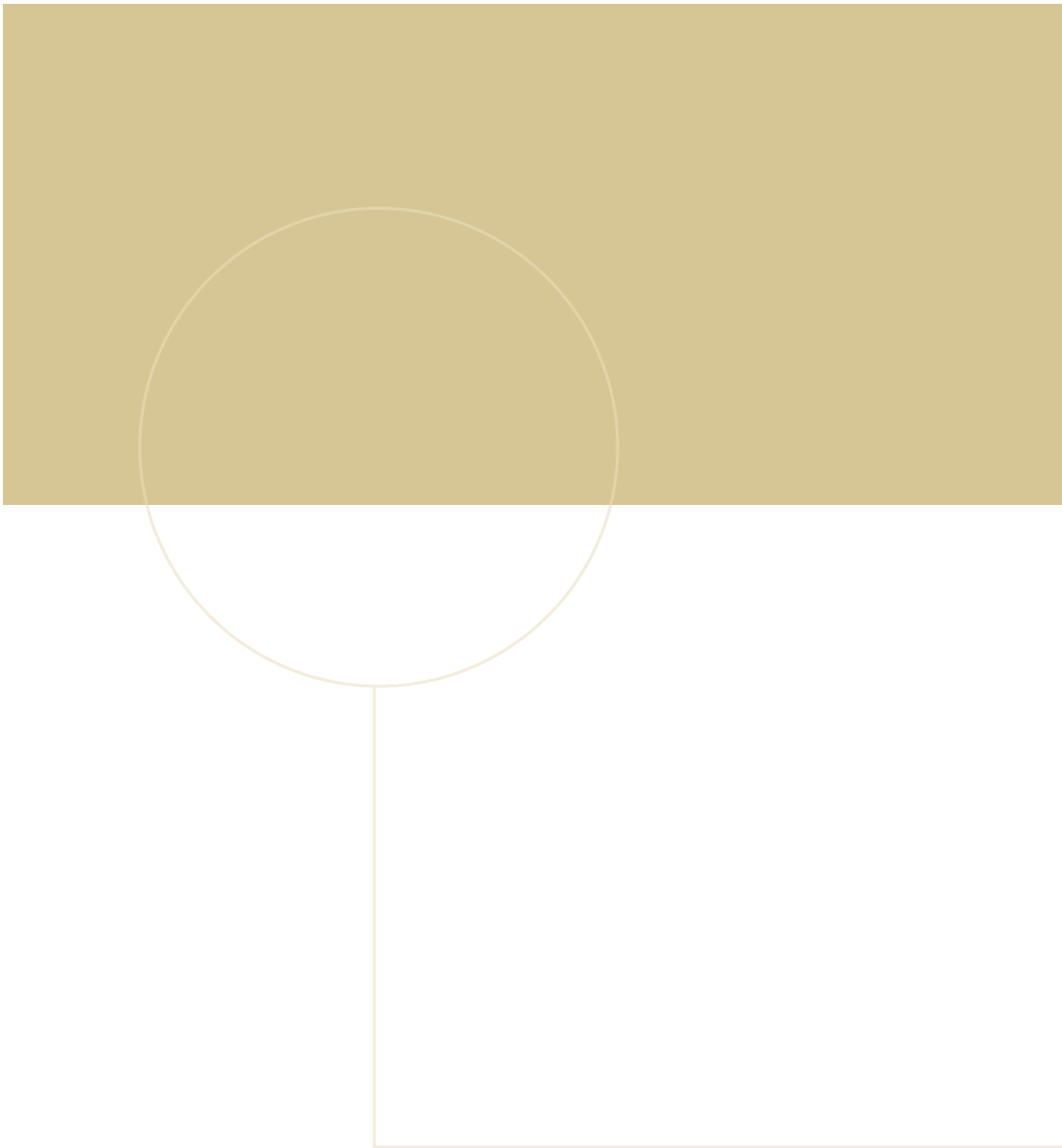

NTNU

Norwegian University of
Science and Technology